Development of a Parallel Hybrid Energy Management Strategy with Consideration of Drive Quality and State of Charge Dynamics

Thomas David Legg

Thesis submitted to the Faculty of the

Virginia Polytechnic Institute and State University

in partial fulfillment of the requirements for the degree of

Master of Science

in

Mechanical Engineering

Douglas J. Nelson, Chair

John B. Ferris

Steve C. Southward

May 6, 2021

Blacksburg, Virginia

Keywords: hybrid, vehicle, simulation, drive quality, battery management

Development of a Parallel Hybrid Energy Management Strategy with Consideration of Drive Quality and State of Charge Dynamics

Thomas David Legg

(ABSTRACT)

The development of a rule-based hybrid energy management strategy for a parallel P4 full hybrid without access to a functional prototype is presented. A simulation model is developed using component bench data and validated using EPA-reported fuel economy test data, including a proposal for complete criteria for valid test results using EPA speed error and SAE J2951 parameters. A combined Willans line model is proposed for the engine and transmission, with control modes based on efficiency-derived power thresholds. Algorithms are proposed for battery state of charge (SOC) management including engine loading and one pedal strategies. Vehicle drive quality with the hybrid control strategy is analyzed, with acceleration and jerk managed through axle torque rate limits and filters. The simulated control strategy for the hybrid vehicle has an energy consumption reduction of 20% for the Hot 505, 3.6% for the HWFET, and 12% for the US06 compared to the stock vehicle. For standard drive cycles, battery SOC is maintained within 20% to 80% safe limits, with charge balanced behavior achieved. Jerk contributions of the hybrid powertrain are generally kept below a 10 m/s^3 tolerable limit, with peaks of 15 m/s^3 tuned for vehicle launch drive quality. The complete energy management strategy proposed improves fuel economy compared to baseline data while maintaining vehicle drive quality and is considered well-rounded and ready for in-vehicle testing and implementation.

Development of a Parallel Hybrid Energy Management Strategy with Consideration of Drive Quality and State of Charge Dynamics

Thomas David Legg

(GENERAL AUDIENCE ABSTRACT)

A hybrid electric vehicle with an engine on the front axle and an electric motor on the rear axle is analyzed. A control strategy is developed based on a set of rules with different modes depending on the vehicle speed and accelerator pedal position, switching between using only the electric motor, only the engine, and a combination of both. The control strategy increases fuel economy while maintaining the charge level of the hybrid battery pack and providing a smooth and enjoyable driving experience.

Contents

List of Figures viii

List of Tables xii

1 Scope 1

2 Introduction 2

2.1 Hybrid vehicles 3

2.1.1 Hybrid architecture selection 6

2.1.2 Hybrid Blazer comparison 9

3 Methods of energy management 13

3.1 Offline optimization 13

3.2 Rule-based strategies 15

3.3 Online optimization 16

4 System Modeling 18

4.1 Glider physics 18

4.2 Engine and transmission model 21

4.2.1 Modeling methods 22

4.2.2 Engine auxiliary load 24

4.3 Model evaluation criteria 25

4.3.1 Drive cycle speed error criteria 27

4.3.2 SAE J2951 evaluation criteria 31

4.3.3 Energy consumption validation 35

4.4 Motor and battery models 37

4.4.1 Motor model 37

4.4.2 Battery model 39

4.5 Total powertrain capability 40

5 Rule Formulations **43**

5.1 Willans Line estimation method 43

5.1.1 Engine Willans Line 43

5.1.2 Transmission Willans Line 44

5.1.3 Combined Willans Line 44

5.1.4 Estimation boundaries 46

5.2 Hybrid rules definition 49

5.3 Battery energy management 55

5.3.1 SOC function for speed 55

5.3.2 SOC function for power 57

5.3.3 One pedal regenerative braking 59

5.3.4 Charge and discharge safety limits 61

6 Drive quality **62**

6.1 Drive quality criteria 64

6.2 Drive quality algorithms 66

6.2.1 Mode transition algorithm 67

6.2.2 Pedal tip-in algorithm 68

6.3 Drive quality evaluation 69

6.3.1 Launch control 69

6.3.2 Steady-state tip-in 74

6.3.3 Acceleration let-off 76

6.3.4 Deceleration tip-in 77

7 Energy consumption simulation **80**

7.1 Simulation results 81

7.1.1 FTP Phase 3 82

7.1.2 US06 84

7.1.3 HWFET 86

7.2 Sensitivity analysis 88

7.2.1 Engine lower efficiency 88

7.2.2 Engine Only speed 89

8 Conclusion **91**

8.1 Future work 92

References **93**

Appendices **101**

Appendix A Auxiliary load **102**

Appendix B Drive cycle 100 Hz smoothing **103**

Appendix C Motor torque rate limit **106**

Appendix D Launch scenario speed plot **107**

Appendix E Additional drive quality plots **108**

List of Figures

2.1 Series and Power-Split hybrid powertrain configurations 4

2.2 Parallel hybrid motor configuration classifications 6

2.3 Modified Chevrolet Blazer hybrid architecture 9

2.4 EPA drive cycle torque demand for hybrid Blazer with motor torque limit outline 12

4.1 Free-body diagram of a vehicle 19

4.2 2.5L Chevrolet engine efficiency map derived from EPA dynamometer data [40] 22

4.3 Operating point relative error for the smoothed 2.5 L engine fuel map 23

4.4 Example of rising edge drive cycle allowable range [46] 27

4.5 US06 model validation simulation results 29

4.6 Hot 505 model validation simulation results 29

4.7 HWFET model validation simulation results 30

4.8 HWFET 2019 EPA test car list data reported SAE criteria 34

4.9 US06 2019 EPA test car list data reported SAE criteria 34

4.10 Simulated drive cycle engine operating points 36

4.11 High-voltage motor manufacturer-supplied efficiency map coverage 37

4.12 High-voltage motor smooth efficiency map contour plot 38

4.13 High-voltage energy storage system battery cell voltage curve 39

4.14 Engine axle torque envelope overlaid on the maximum torque in each gear . 41

4.15 High-voltage motor positive and negative axle torque envelope 41

4.16 Total powertrain axle torque envelope 42

5.1 Willans line for the hybrid Blazer for data from 0 to 60kW 44

5.2 Willans line for the hybrid Blazer 9-speed transmission 45

5.3 Combined Willans line for the vehicle front powertrain 46

5.4 Region of predictable engine efficient operation 47

5.5 Engine operating points from Figure 4.10 with 60 kW engine estimation limit overlaid 49

5.6 Regions of powertrain operation, with powertrain torque limits marked . . . 50

5.7 Regions of powertrain operation as a function of power 54

5.8 Road load axle torque overlaid on rule regions 54

5.9 Engine Load threshold plot over rules, with hysteresis region marked 56

5.10 Engine Load threshold as a function of speed 57

5.11 Engine Load hysteresis plot over rules 58

5.12 Engine Load re-engagement hysteresis from Regenerative Braking 58

5.13 Engine Load hysteresis function 59

5.14 Zero accelerator pedal input axle torque request 60

5.15 Zero accelerator pedal input deceleration 60

5.16 Zero accelerator pedal input deceleration 61

6.1 Competition-required pedal torque response 63

6.2 Highlighted mode transitions which require crossfading torque 63

6.3 Constant speed mode transitions commanded axle torque crossfade 67

6.4 Accelerator and brake pedal inputs for launch simulations 69

6.5 Target acceleration curve simulation with torque smoothing 70

6.6 Target acceleration curve simulation without smoothing 71

6.7 Simulated vehicle response for varying pedal inputs at launch with smoothing 72

6.8 Simulated vehicle response for varying pedal inputs at launch without smoothing 73

6.9 Accelerator pedal tip-in after achieving steady speed 75

6.10 Accelerator pedal let-off to 0% from a constant pedal acceleration 76

6.11 Accelerator and brake pedal inputs for deceleration to tip-in simulations . . 78

6.12 Vehicle velocity profiles for deceleration to tip-in simulations 78

6.13 Varying deceleration to tip-in scenario simulation results 79

7.1 Hot 505 drive cycle operating points overlaid on Rule Regions 82

7.2 Hot 505 drive cycle simulation results 83

7.3 US06 drive cycle operating points overlaid on Rule Regions 84

7.4 US06 drive cycle speed trace 85

7.5 HWFET drive cycle operating points overlaid on Rule Regions 86

7.6 HWFET drive cycle speed trace 87

7.7 Engine lower efficiency sensitivity analysis power output 89

A.1 Stock Blazer RS hot start and idle measured alternator 12 V current 102

B.1 Comparison of linear and pchip interpolated US06 at 100 Hz 104

B.2 Error between EPA-defined linear interpolation and pchip interpolation methods 105

C.1 Simulink code implementation of motor and total axle torque rate limit . . . 106

D.1 Speed profile during vehicle launch scenarios 107

E.1 Accelerator pedal let-off to 5% from a constant pedal acceleration 108

E.2 Accelerator pedal let-off to 10% from a constant pedal acceleration 109

E.3 Accelerator pedal let-off to 15% from a constant pedal acceleration 110

E.4 Accelerator pedal let-off to 20% from a constant pedal acceleration 111

List of Tables

2.1 Hybridization level functionality comparison [1] 3

2.2 Hybrid Blazer high-voltage e-axle parameters 8

2.3 Hybrid Blazer high-voltage battery parameters 8

2.4 Comparable full hybrid crossover vehicles 10

3.1 Overview of methods (−/+: dis-/advantage) [5] 17

4.1 EPA dynamometer parameters for the 2019 Chevrolet Blazer RS AWD [38] . 20

4.2 Mass-scaled hybrid Blazer glider model parameters 21

4.3 Auxiliary 12V load on engine 25

4.4 Simulation PI controller driver model gain values 30

4.5 SAE drive cycle metrics [47] 32

4.6 EPA and simulated drive cycle metrics 32

4.7 Blazer 2.5 L validation glider parameters [38] 35

4.8 EPA Tier 2 Cert Gasoline properties [49] 35

4.9 Validation simulation results for the Blazer 2.5 L 36

6.1 Competition-defined jerk from launch limits 65

6.2 Peak and sustained jerk limits 66

6.3 ISO 15622:2018 acceleration and jerk operational limits [61] 66

6.4 Torque surge and overshoot targets 66

6.5 Pedal tip-in axle torque rate of change limits 68

6.6 Simulated peak jerk during launch simulations 70

6.7 Varying accelerator pedal let-off scenario simulation results 77

7.1 Important parameters for the vehicle simulation model [38] 80

7.2 Comparison of stock Blazer RS and simulated hybrid energy consumption . 81

7.3 Sensitivity analysis for engine lower efficiency boundary 88

7.4 Sensitivity analysis for Engine Only operation speed 89

Chapter 1

Scope

The vehicle under analysis is a Chevrolet Blazer RS modified to be a full hybrid electric vehicle in a P4 parallel configuration with custom adaptive cruise control and lane centering systems. A standard rule-based hybrid vehicle control strategy based on a combined conventional powertrain Willans Line is proposed and evaluated.

The vehicle control system discussed in this paper is specifically developed for a human driver, with cruise control drivers considered out of scope. Clutch control is also considered out of scope, with the engine and motor considered to always be engaged. Battery state of charge management and drive quality are explored as they relate to the energy management strategy given human driver accelerator and brake pedal inputs, with a detailed discussion of vehicle modeling and simulation.

The contributions of this paper include in-depth discussion of validation criteria for the simulation model, mathematical derivation of control rules, battery state of charge management techniques, and control and evaluation methods for drive quality of the completed energy management strategy.

Chapter 2

Introduction

The looming threat of global climate change has pushed mankind to develop cleaner methods for manufacturing, energy production, and transportation. In addition to regulating existing industry, a focus has been placed on educating the next generation of engineers in advanced technology to usher in the new eco-friendly era.

In a collaboration between the public and private automotive sectors, the EcoCAR Moblity Challenge is a university engineering design competition with the goal of designing, building, and tuning a hybrid vehicle based on the 2019 Chevrolet Blazer RS platform. As a part of this challenge, the Hybrid Electric Vehicle Team (HEVT) at Virginia Tech has spent the first three years of the four year competition cycle designing and constructing the hybrid Blazer, providing dozens of undergraduate engineering students hands-on design experience with industry-standard tools and methods.

The goal of this paper is to present the hybrid propulsion control strategy, specifically the energy consumption management strategy, developed for the HEVT EcoCAR hybrid architecture. Due to project delays and testing restrictions as a result of COVID-19, on-vehicle test data is limited, so a validation and evaluation process is proposed within a simulation environment to prepare the control strategy for in-vehicle use without the ability to test on actual hardware. Viability of the control strategy on the vehicle is of key importance, so battery energy management along with acceleration and jerk control are explored.

2.1 Hybrid vehicles

A hybrid vehicle is defined by the use of more than one source of energy to propel the vehicle. While hybrid vehicles of many types have been marketed and sold, the most common consumer hybrid vehicles use gasoline and electric power, with or without the ability to charge the electric battery pack from external grid power [1, 2]. Typically, the primary goal of powertrain hybridization is energy efficiency improvements, usually realized through engine downsizing or engine downspeeding, allowing the engine to operate within regions of higher efficiency [3]. However, there are many possible areas of improvement for vehicles when adding an additional source of tractive power, including but not limited to optimizing performance [4], reducing energy consumption [4, 5, 6], and increasing the lifespan of powertrain components [7].

Hybrid electric vehicles can be categorized depending on the level of functionality achieved, with the basic categories for the level of hybridization laid out in Table 2.1, including micro, mild, full, and plug-in hybrids.

Table 2.1: Hybridization level functionality comparison [1]

Function or component parameter	Types of HEV			
	Micro	Mild	Full	Plug-In
Idle Start/Stop	•	•	•	•
Electric Torque Assistance		•	•	•
Energy Recuperation		•	•	•
Electric Drive			•	•
Battery Charging (during driving)			•	•
Battery Charging (from Grid)				•
Battery Voltage Range (V)	12	48-160	200-300	300-400
Electric Machine Power (kW)	2-3	10-15	30-50	60-100
EV Mode Range (km)	0	0	5-10	>10

In addition to categories for degree of hybridization, there are three primary powertrain configurations for hybrid vehicles based on the location of the high-voltage motor in relation to the engine:

Series: A hybrid vehicle that uses an electric motor as the sole source of tractive power, while the engine is connected to a generator, as shown in Figure 2.1. The engine is not mechanically coupled to the driveline but can be considered electrically coupled. This type of hybrid typically operates as an electric vehicle for short range travel, with the option to engage the engine for extended range. A production example of a series hybrid is the BMW i3 hybrid.

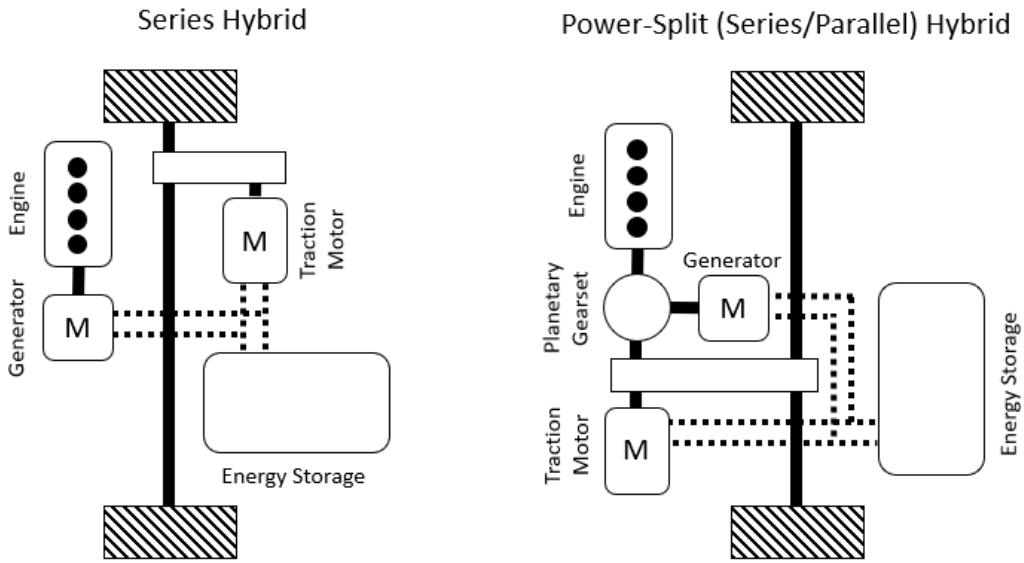

Figure 2.1: Series and Power-Split hybrid powertrain configurations

Power-Split: A type of hybrid vehicle otherwise known as a series-parallel hybrid that has the ability to either operate as a series hybrid, with the engine only operating as a generator, or as a parallel hybrid, with the engine and electric drive simultaneously providing tractive power, as also shown in Figure 2.1. In this way, the engine is both electrically and

mechanically coupled to the driveline. The engine is typically connected through an eCVT planetary gearset (electronic continuously variable transmission), where the generator can be controlled to determine the amount of power used to charge the battery pack the amount to send to the tires directly [8]. Examples of power-split hybrids include the Chevy Volt and Toyota Prius.

Parallel: A hybrid vehicle that uses a combination of engine and motor power to propel the vehicle, with varying levels of functionality depending upon motor placement on the vehicle driveline, as shown in Figure 2.2.

The P0 location is located on a belted accessory drive, with an electric motor typically about the size of an alternator, while the P1 location is referred to as an integrated starter generator (ISG) and is typically a smaller motor mounted directly to the crankshaft of the engine. P0 and P1 configurations are typically used in micro or mild hybrid configurations, with the primary focus being start-stop and torque assist functionality [1].

The P2 location is on the engine side of the transmission, but is different from a P1 in that a clutch is placed between the engine and electric motor. The primary benefit of this architecture is flexibility: the high voltage motor can take advantage of the torque multiplication of the multi-speed transmission, the vehicle can operate in an EV-Only mode by disengaging the clutch between the engine and motor, and the motor can charge the battery pack by loading the engine with the transmission in neutral [1, 9]. Examples of P2 hybrids include the Volkswagen Passat hybrid and Hyundai Sonata hybrid.

The P3 location is post-transmission on the same axle driven by the engine. Electric motors used in a P3 configuration require higher torque capabilities, as the motor does not take advantage of the transmission for torque multiplication. HEVT has explored hybrid architectures using the P3 motor location in previous EcoCAR competitions [10].

The P4 mounting location is mounted on a different axle than the engine, and is typically seen as either a hub motor or an e-axle, a motor-gearbox-differential packaged unit. While the P4 motor location is not mechanically coupled to the engine, it is considered ”coupled through the road.” A P4 motor is typically not used alone, but rather, in combination with another motor mounted in the P0, P1, or P2 parallel locations or in a power-split configuration [1].

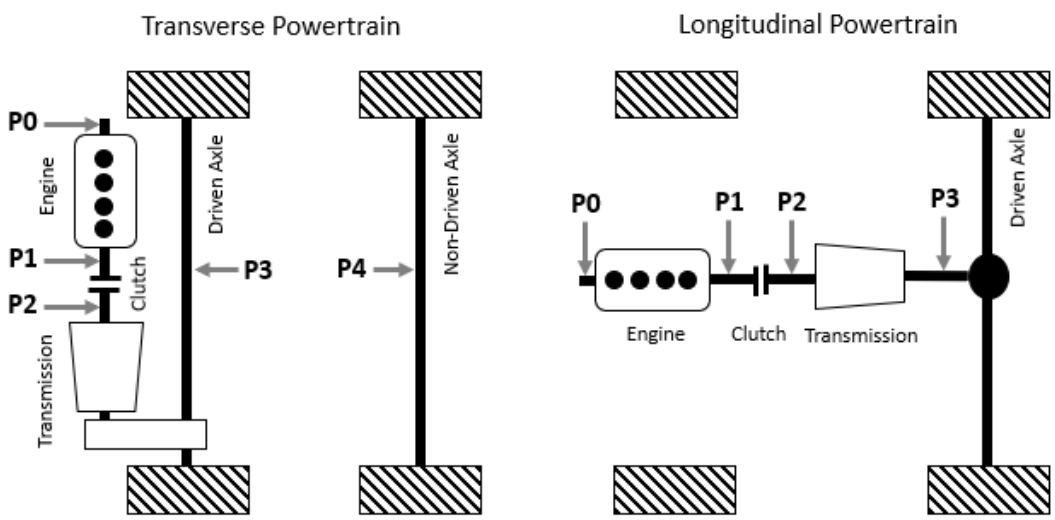

Figure 2.2: Parallel hybrid motor configuration classifications

2.1.1 Hybrid architecture selection

As a part of the EcoCAR Moblity Challenge competition, each team is tasked with converting a 2019 Chevrolet Blazer RS into a hybrid electric vehicle. The conversion process involves downsizing the stock 3.6 L six-cylinder engine as well as integrating a high-voltage electric powertrain.

One stipulation of the engine selection process was a limited pool of possible choices that would be officially supported by competition sponsors. These engines included combinations of 2.5 L NA (naturally aspirated), 2.0 L Turbo, and 1.5 L Turbo engines, each paired with 9-speed transmissions in a transverse, FWD configuration. The engine and transmission

are considered a paired packaged ”powercube” which should not be split, and as a result, the options for hybrid architectures was limited to parallel hybrids not including P1 and P2 configurations. Additionally, due to restrictions involved with integrating a motor on the front axle with the available engine and transmission options, P3 configurations were not considered.

In the first year of competition, HEVT analyzed each engine option, and decided that the 2.5 L NA engine was the best available choice due to the high marginal efficiency compared to the turbocharged alternatives. The increasing absolute efficiency with increased load is especially useful for a hybrid vehicle, which has greater control authority over the engine operating regions compared to conventional vehicles [11].

For the high voltage motor, the competition did not provide any officially supported options, but rather, presented multiple off-the-shelf products sold by sponsoring companies which were available to competition teams, including P0 and P4 motor options, with and without included gearboxes. Each competition-presented motor option was analyzed by HEVT, but due to either difficulty integrating the motor into the Blazer or due to underwhelming simulated vehicle energy consumption savings, outside options were explored. HEVT found an external company willing to provide a few different high-voltage motors with integrated single-speed transmissions which could be physically integrated into the rear subframe of the Blazer in a parallel P4 configuration without significant structural modification. Two options were considered including an 80 kW, 250 Nm e-axle and a 50 kW, 200 Nm e-axle. After energy consumption simulation analysis, the 80 kW, 250 Nm motor was chosen [11], with parameters listed in Table 2.2.

Additionally, the competition provided a limited selection of high-voltage energy storage systems, with the single option being a 54 kW, 1.5 kWh (0.45 kWh usable) battery pack from a production full hybrid vehicle. Additionally, the competition dictated that teams

Table 2.2: Hybrid Blazer high-voltage e-axle parameters

Parameter	Value	Units
mass	78.5	kg
V_{nom}	350	V
T_{max}	250	Nm
P_{max}	80	kW
G_{ratio}	11.59	

building an energy storage system themselves was out of scope. In search of other options, multiple competition teams found a company capable and willing to produce a small number of custom high-voltage energy storage systems for use by competition teams. The 90 kW, 5.0 kWh (2.0 kWh usable) battery pack was selected by HEVT along with three other competition schools [11], with parameters listed in Table 2.3.

Table 2.3: Hybrid Blazer high-voltage battery parameters

Parameter	Value	Units
mass	93.5	kg
V_{nom}	345.6	V
P_{max}	90	kW
I_{max}	300	A
P_{min}	-45	kW
I_{min}	-150	A
E_{cap}	5.0	kWh
E_{usable}	2.0	kWh
R_{int}	0.2	Ω

The chosen 80 kW, 250 Nm motor, which paired well with the available 90 kW, 5.0 kWh battery pack and 2.5 L NA engine, became the hybrid architecture for the Virginia Tech team, as shown in Figure 2.3. Further discussion of the specific selection process for powertrain components is available [11].

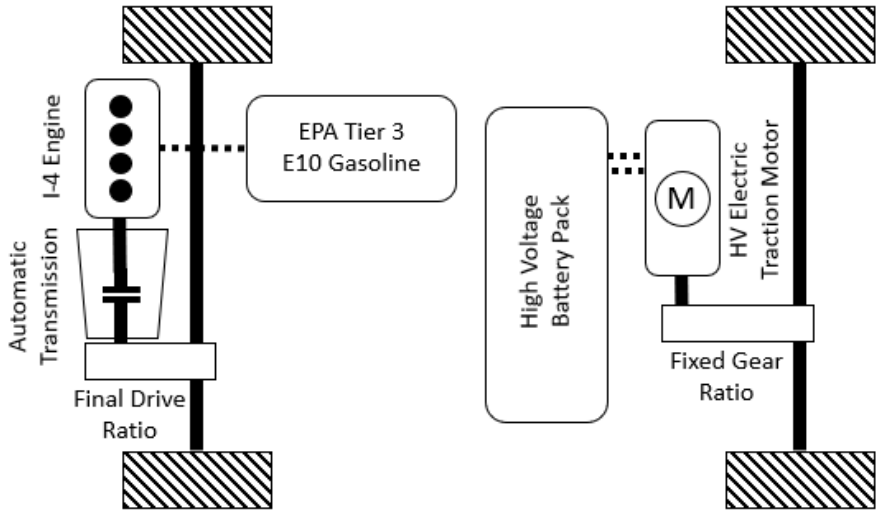

Figure 2.3: Modified Chevrolet Blazer hybrid architecture

2.1.2 Hybrid Blazer comparison

To better understand how the chosen hybrid architecture compares to existing production hybrid options, a select list of comparable full hybrid vehicles for sale in the United States is provided in Table 2.4. The criteria for selection is availability on or about the 2020 model year, similar crossover styling/market segment targeting, non-plug-in hybrid functionality, and a high-voltage full hybrid powertrain. The hybrid type classification is listed for each vehicle, along with the engine for the given trim level, the total powertrain peak power, the curb weight rounded to the nearest 250 lb, and the high-voltage battery usable energy capacity.

Based on the selection of full hybrid crossovers currently on the market, some general comparisons can be made. The most obvious difference is hybrid powertrain configuration, as the HEVT Blazer is the only option without an electric motor on the engine axle, with each other architecture having a P2 of Power-Split system. Also, although the HEVT Blazer has a similar displacement engine to many hybrids, it has a higher power output; this is due to

Table 2.4: Comparable full hybrid crossover vehicles

Hybrid Make/Model	Metrics				
	Hybrid Configuration	Engine Specification	Total PT	Curb Weight	Battery Capacity
HEVT Blazer	P4	2.5L I4 (200 hp)	305 hp	4500 lb	2.0 kWh
2021 Toyota Venza [12]	Power-Split + P4	2.5L I4 (176 hp)	219 hp	4000 lb	0.9 kWh
2020 Ford Escape SE [13]	Power-Split	2.5L I4 (165 hp)	198 hp	3500 lb	1.1 kWh
2020 Acura MDX Sport [14, 15]	P2 + P4	3.0L V6 (257 hp)	321 hp	4500 lb	1.3 kWh
2020 Honda CR-V LX [16, 17]	Power-Split	2.0L I4 (143 hp)	212 hp	3750 lb	1.4 kWh
2021 Kia Sorento [18, 19]	P2	1.6L I4 (177 hp)	227 hp	4000 lb	1.5 kWh
2021 Lexus RX450h AWD [20, 21]	Power-Split + P4	3.5L V6 (259 hp)	308 hp	4750 kg	1.9 kWh

the HEVT Blazer using an engine from a conventional vehicle, while other hybrids typically use purpose-built Atkinson cycle engines with lower power output but higher fuel efficiency. Additionally, despite the higher powertrain capability, the extra power does not necessarily equate to greater performance due to the increased mass which typically leads to modest acceleration performance.

Due to the hybrid architecture differences, many of the features or capabilities common among production and academic hybrid architecture control systems are missing from the hybrid vehicle under analysis. The specific features which make energy management difficult are discussed below.

Engine clutch control: Control of the engine clutch allows the energy management strategy to disengage and turn off the engine when not in use, saving fuel from idle and drag, allowing researchers to assume the engine is off when not in use [5]. While physically possible, disengaging the transmission clutch to put the engine in neutral is not practical for the hybrid architecture under analysis, as the difficulty of implementing running starts after E-Launch on an engine not originally designed for use in a hybrid vehicle is prohibitive. As a result, except due to idle start-stop, the engine is always on while the vehicle is on, resulting in a mix of engine idle fuel consumption and DFCO (decel fuel cut-off) slowing the vehicle.

Motor clutch control: A permanent magnet motor produces drag on the driveline even when not in use. Many e-axles have clutches which allow the control system to disengage the motor when not in use, with studies showing a positive effect on energy consumption [6]; however, the e-axle used in the HEVT Blazer does not have such capability.

P4 motor configuration: A significant portion of research into hybrid control strategies has been focused on series, power-split, and P0/P1 parallel hybrid architectures due to the high level of control over engine operating points in a pre-transmission motor location [4, 5, 6, 22, 23, 24, 25]. Additionally, most comparable hybrid vehicles have at least one motor connected to the engine, as shown in Table 2.4. Hybrid configurations which allow both manipulation of engine operating points as well as the ability to charge the battery at idle mean these architectures are robust, flexible, and favored by industry. Unfortunately, the optimal motor choice for the hybrid under analysis is a P4 configuration, meaning that certain capabilities such as fine-tuned engine torque control present in pre-transmission motor mount configurations is lost.

Production option engine: Typically, a full hybrid vehicle will take advantage of the two powertrains, conventional and high-voltage, to reduce the required engine power while still meeting consumer acceptability metrics [2], either by reducing displacement or using an Atkinson Cycle engine to increase fuel economy. The 2.5 L engine chosen is a stock option for the base trim level 2019 Blazer and is capable of 200 hp, 191 lb-ft of torque, or approximately 150 kW, 250 Nm. As a result, the engine is not necessarily downsized and alone has the same power as the total powertrain of comparable crossover full hybrids as shown in Table 2.4, with specifications closer to the performance-focused Acura MDX Sport Hybrid or Lexus RX450h AWD.

Large traction motor: The high-voltage motor has an unusually high torque and power threshold for a non-plug-in hybrid vehicle at 80 kW, with the typical range being 30 to 50 kW as shown in Table 2.1. Additionally, because the motor is in a P4 position, as opposed to a more common Power-Split architecture, the total torque output of the motor reaches the road. The motor has ample torque to drive the hybrid Blazer through most EPA drive cycles in an EV-Only mode, as shown in Figure 2.4. However, because the hybrid Blazer does not have a plug-in battery charge port, a full-speed range EV-only mode is not preferred, with the motor typically used in an E-Launch and torque assist capability.

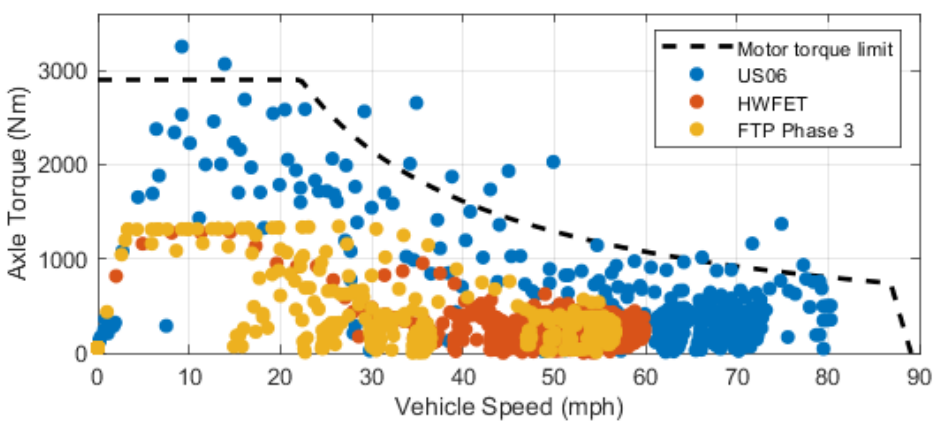

Figure 2.4: EPA drive cycle torque demand for hybrid Blazer with motor torque limit outline

High accessory load: The addition of hybrid capability features also adds a higher load on the 12 V system to power the component controller. The unusually high accessory load is considered and modeled, with further detail included in Chapter 4.2.2. Engine accessory load is commonly neglected from modeling in academic studies [5], but must be included to accurately measure the impact of hybridization.

Chapter 3

Methods of energy management

3.1 Offline optimization

Dynamic programming (DP) is a Markovian solving method for finding the global optimal solution for any given system [26]. Although DP is a powerful tool with many applications, the solution complexity increases exponentially with the size of the state vector, and as a result, cannot be efficiently applied to complex systems without simplifying assumptions.

Especially in academic circles, DP is commonly applied to hybrid vehicles with energy consumption as the chosen objective function. The application of DP methods is used to predict the optimal route of each state variable to minimize fuel consumption over a given speed trace. Although DP cannot be used in an online controller, the result from a DP simulation is an invaluable tool for development of online strategies, as the DP results offer the globally optimal path through a given scenario [27, 28].

The Hamiltonian system optimized under DP is defined as the following, where λ is the gradient of the cost-to-go function (otherwise known as the costate), x is the state vector, and u is the control vector [29].

$$H(x, u, t) = f(x, u, t) + \lambda^T g(x, y, t) \tag{3.1}$$

For a hybrid vehicle, the primary control inputs are the torque requests to the powerplants on the vehicle and the friction braking force. For a vehicle with two sources of tractive power, such as the parallel hybrid architecture under analysis, the torque production of the two powertrains, gasoline-powered and electric, must sum to be equal to the torque demand of the driver. With the driver torque demand being an input to the system, the control input can be simplified to the torque demand of one powertrain (which implies the torque demand of the other by subtraction). To keep the complexity of the DP model down, the control vector, which could include variables such as clutch control or transmission gear, are typically neglected for computational efficiency. [29].

One particularly interesting control problem for DP simulation of hybrid vehicles is the battery state of charge (SOC), which is a function of motor torque but cannot be directly controlled. To neglect the effect of charging or discharging the battery pack on the final energy consumption of the simulated vehicle, charge balanced behavior is desired, where the charge sustaining metric, CS, is defined as the fraction of the net change in energy of the battery pack, ΔE_{bat}, and the energy of fuel consumed by the engine, E_{fuel}, over a speed trace:

$$CS = \frac{\Delta E_{bat}}{E_{fuel}} \tag{3.2}$$

To force the simulation to charge balance over a given horizon, an additional constraint on the admissible SOC is enforced, typically forming an allowable SOC envelope, with the final SOC being equal to the initial SOC for charge balance model behavior [30].

3.2 Rule-based strategies

The most traditional method for hybrid vehicle control involves defining a set of rules which control engine and motor behavior depending on the current region of operation. A rule-based control strategy is typically computationally simple and is well-suited for online implementation in hybrid vehicles. The rules in the control strategy are typically derived from experience, and tuned through simulation to optimize fuel economy and emissions performance for a given vehicle [9]. As a result, rule-based control strategies are typically highly dependent on the specific vehicle architecture for which they were designed.

Rather than solving for the optimal control sequence, rule-based strategies use analysis of component efficiency at various operating points to inform a control strategy. Typically, such control strategies include E-Launch, where the vehicle uses only the electric motor at low speeds, as well as an Engine-Only region, where the vehicle uses the engine in regions of higher efficiency.

Research has been performed on how to optimize the rule-based control strategy development process by reducing the dependence of rule formulation on human intuition, typically by using the unstructured DP model results to inform operating behavior of the hybrid vehicle; examples of such research include methods for utilizing results of DP models to calculate optimal operating parameters within the defined rules [5, 27, 28, 31], using offline simulation adapted to operating maps for optimal engine performance [22], developing rules based on total powertrain efficiency [6], and specific optimization such as rule modification for cabin air temperature [31]. The hybrid energy management strategy developed in this paper falls into this category of control strategy, with a focus on rule development for battery SOC management and drive quality considerations.

3.3 Online optimization

The hottest area of energy management research in the past decade has been the development of methods of adapting optimization techniques from Markovian methods like dynamic programming to real-time online methods. The most commonly used method is the optimal control energy consumption minimization strategy (ECMS), which involves discretizing the Pontryagin's Minimum Principle (PMP) control formulation to run in an online controller [32].

Research has been performed in multiple applications of the ECMS algorithm, including as a control strategy for the HEVT hybridized Blazer [11, 33]. Studies have included adapting ECMS to a series hybrid city bus [34], accounting for transient thermal properties of powertrain components [31], maximizing the torque output from a power-split hybrid [4], and additional cost functions to influence the behavior of optimal algorithms, such as gear shift and engine start penalty functions [35].

One of the major design difficulties for the ECMS controller is the optimization horizon, which can be as short as a few controller cycles. Additionally, because the source of control inputs is a human driver, the unpredictability makes it challenging to maintain optimal operation. As a result, the ECMS algorithm alone is generally not adequately equipped to run on a vehicle, as the torque requests are instantaneous solutions of the system, which can result in large power variations between time steps, causing the system to rapidly switch between high and low torque requests. The result can be high jerk on the vehicle due to the lack of accounting for component response time, resulting in worse than expected fuel efficiency due to higher engine transient fuel consumption.

Solutions to these issues can be implemented, typically in the form of augmenting cost functions or correction factors, such as penalizing large engine power differentials between

time steps or frequent engine starts/stops [32]. However, adding additional cost functions is analogous to adding rules, and thus is susceptible to the same pitfalls as rule-based control strategies.

Additionally, the DP costate factor, reformulated to the equivalency factor in ECMS, is extremely dependent on the specific drive cycle for charge sustaining behavior. As a result, the equivalency factor is often formulated to a dynamic function of SOC, often requiring tuning depending on the specific vehicle configuration and drive cycle test.

Researchers have attempted to address the problem of ECMS on vehicle-specific tuning and rules. Recent studies [24] have focused on reducing the dependence of online real-time optimization-based methods on specific drive cycle, with the goal of maintaining a relatively balanced battery state of charge while reducing fuel consumption . Other studies [23] have embraced rules by attempting to merge rule-based and optimal control strategies by utilizing a rule-based strategy to control the engine operating points, then balancing efficiency against battery SOC using an ECMS strategy.

A summary of each of the discussed methods is provided in Table 3.1.

Table 3.1: Overview of methods (−/+: dis-/advantage) [5]

	DP		RB		ECMS
+	globally optimal	−	sub-optimal	−	sub-optimal
−	apparently unstructured result	−	tuning of many parameters	+	few calibration parameters
−	long computation time	+	relatively simple	+	short computation time
−	offline only	+	on/offline	+	on/offline
+	handling nonlinear constraints	−	dependent on topology	−	sensitive to deviations

Chapter 4

System Modeling

To develop the rule-based hybrid control strategy for use in the HEVT hybrid Blazer, a sufficient fidelity simulation model is required. The development and validation of the vehicle model is discussed in this chapter, including the glider model and conventional and high-voltage powertrains.

4.1 Glider physics

For a simulation model developed for energy consumption analysis, a 1-DOF (degree of freedom) longitudinal lumped-mass vehicle glider model is sufficient. The physics of the vehicle can be broken down into a few constituent equations for resistive forces, and a simple force balance provides a method to model dynamic behavior. Specifically, the resistive forces are broken down into F_{aero}, F_{rr}, and F_{grade}, the aerodynamic drag, rolling resistance, and grade forces, respectively, with the positive tractive effort labeled $F_{tractive}$, inertial force labeled F_{inert}, and the road angle labeled α, as shown in Figure 4.1. The force summation can be written as shown in Equation 4.1.

$$F_{inert} = F_{tractive} - F_{aero} - F_{rr} - F_{grade} \tag{4.1}$$

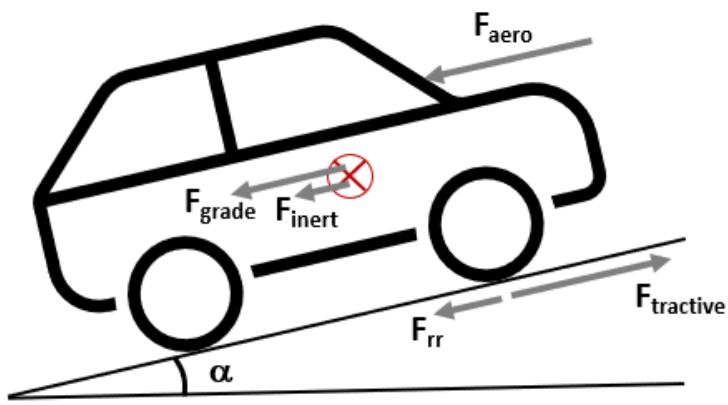

Figure 4.1: Free-body diagram of a vehicle

When the U.S. Environmental Protection Agency (EPA) measures the emissions performance and fuel economy of vehicles sold in the United States, testing is carried out on dynamometers, where the vehicle forces are mathematically modeled. In this EPA fuel economy testing, the road is assumed to be flat, with no headwind forces, no precipitation, and a reference ambient temperature of 20 °C. The EPA dynamometer parameters are experimentally determined by coast-down testing and quadratic fitting to road load data from 70 to 10 MPH based on the SAE J2263 standard [36, 37]. The reported road load forces for any tested vehicle can be used to model the glider forces, as shown in Equation 4.2.

$$\begin{aligned} F_{inert} &= F_{tractive} - \left(A + Bv + Cv^2\right) \\ F_{rr} &= A + Bv \\ F_{aero} &= Cv^2 \end{aligned} \tag{4.2}$$

The A, B, and C parameters along with the vehicle equivilant test weight (ETW), which are freely available online, are listed in Table 4.1 for the stock 3.6 L Blazer. The glider

parameters accurately represent the total vehicle drag, including aerodynamics, tire rolling resistance, and driveline mechanical drag.

Table 4.1: EPA dynamometer parameters for the 2019 Chevrolet Blazer RS AWD [38]

Parameter	Value	Units
ETW	4500	lb_m
A	30.65	lb_f
B	0.4421	$\frac{lb_f}{mi/hr}$
C	0.02399	$\frac{lb_f}{mi/hr^2}$

In addition, the inertial force is defined as the following, where the 1.03 scaling factor is an adjustment for the effect of the inertia of rotating components on vehicle acceleration, as defined by the SAE J2263 standard [37]:

$$F_{inert} = 1.03 \cdot \text{ETW} \cdot a \tag{4.3}$$

The EPA glider parameters for the stock vehicle configuration are then scaled to be accurate for the modified hybrid Blazer as a function of test mass, using the method listed in Equation 4.4. Note that the C parameter does not require scaling; this is due to the fact that the C parameter represents aerodynamic drag force which is not a function of vehicle mass.

$$\begin{aligned} A_{target} &= A_{ref} \cdot \left(\frac{\text{ETW}_{target}}{\text{ETW}_{ref}}\right) \\ B_{target} &= B_{ref} \cdot \left(\frac{\text{ETW}_{target}}{\text{ETW}_{ref}}\right) \\ C_{target} &= C_{ref} \end{aligned} \tag{4.4}$$

By applying mass scaling and unit conversion, the glider parameters shown in Table 4.2 are obtained. These values are used for simulating the hybridized Blazer, with the mass value calculated by adding 200 kg (440 lb) to the measured mass, a more modern estimate than the EPA-standard 300 lb [36], for two passengers to calculate the ETW for the hybrid vehicle.

Table 4.2: Mass-scaled hybrid Blazer glider model parameters

Parameter	Value	Units
ETW_{target}	2270	kg
A_{target}	156	N
B_{target}	1.82	$\frac{N}{m/s}$
C_{target}	0.589	$\frac{N}{m/s^2}$

The mass-scaled parameters provide a good estimate for the hybridized vehicle, as many of the contributing factors for the ABC parameters is unchanged. This includes aerodynamics, wheels and tires, and some driveline components. Specifically, the stock Blazer RS is an all-wheel-drive (AWD) vehicle, meaning a driveshaft connects the front and rear axles allowing for some torque to be applied to the rear wheels. The driveline resistance from this configuration is assumed to affect the road load equivalently to the hybridized vehicle, which features a FWD engine configuration with an e-axle unit on the rear axle.

4.2 Engine and transmission model

In order to model the fuel economy of the vehicle, a sufficiently accurate engine model is required to estimate fuel consumption. There are multiple methods available to model the fuel consumption of a conventional vehicle, each of which provide relatively accurate estimates. Two of these modeling methods are explored including operating point maps and the Willans Line [39], with the former utilized for the vehicle simulation model, and the latter utilized in the development of the hybrid control strategy.

4.2.1 Modeling methods

The first, and most common, modeling method is the use of mapped data for engine operating points. By testing an engine on a dynamometer, the fuel consumption over a wide range of torques and speeds is measured, and a smooth map is developed to predict fuel consumption at any given point, allowing simulation of engine fuel consumption for any given torque and speed operating point.

In addition to being relatively computationally taxing, especially for maps with a large number of data points, the primary criticism of this method is that the data is representative of averaged steady-state behavior of a warm system. Each operating point on the dynamometer is held until steady behavior is obtained for measurement, and as a result, the mapped data lacks the ability to accurately model the effect of engine transient behavior and cold starts on fuel consumption. An example of mapped engine data is shown in Figure 4.2 using publicly-available EPA test data for a 2.5L NA Chevrolet engine similar to the one used in the HEVT hybrid Blazer.

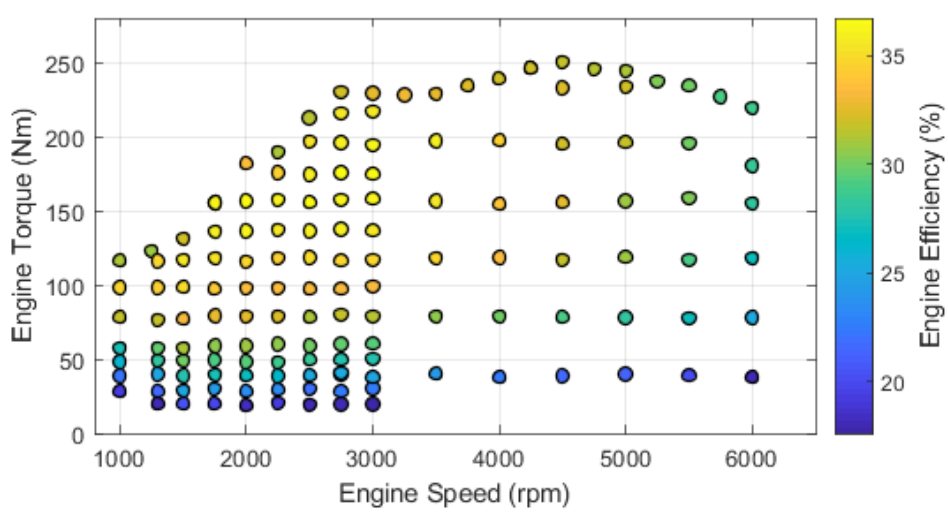

Figure 4.2: 2.5L Chevrolet engine efficiency map derived from EPA dynamometer data [40]

For the simulation model, smooth fuel maps were created using the calibration generation (CAGE) tool within the MATLAB Model-Based Calibration Toolbox. Using methods based on radial basis functions, the rough dynamometer data is smoothed to reduce possible error from noise during data collection, with the relative error between raw data and the smoothed engine map shown in Figure 4.3, with an average percent RMSE of 1.8 %.

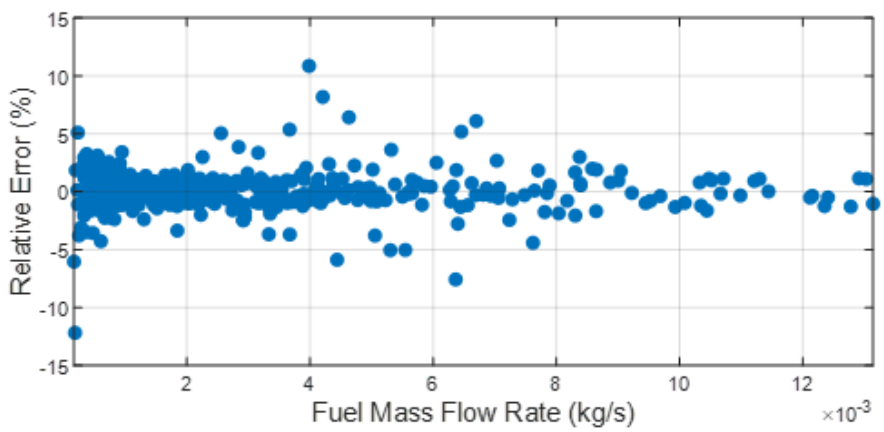

Figure 4.3: Operating point relative error for the smoothed 2.5 L engine fuel map

The second method, commonly used in embedded applications due to its computational efficiency, is the Willans Line. Within the typical operating region of an engine, the relationship of mechanical power produced linearly scales with fuel power required [41]. This relationship takes the following form, where a_w and b_w are the linear fit parameters:

$$P_{in} = a_w P_{out} + b_w \tag{4.5}$$

The Willans Line model is also equivalently expressed in terms of efficiency:

$$P_{in} = \frac{1}{\eta} P_{out} + b_w \tag{4.6}$$

Conceptually, the b_w term is the constant idle loss, the power required to overcome the mechanical drag of the engine, while η represents the efficiency at which additional torque can be produced, otherwise known as the marginal efficiency. The Willans Line is discussed further in Chapter 5 in reference to the development of the hybrid control strategy.

The same two modeling methods apply to the torque converter and transmission models. Mapped loss data can be utilized in the simulation model, but smoothing must be applied to remove unrealistic noise and peaks in the data.

4.2.2 Engine auxiliary load

The engine fuel map does not include the auxiliary loads on the engine (except the water pump), so to accurately predict the fuel consumption of the vehicle, the constant alternator load must be modeled. The primary focus of this modeling is the 12 V system electrical load, which is seen as a torque load from the alternator. The air conditioning compressor is neglected from analysis due to transient loads and infrequent usage on the actual vehicle.

Vehicle testing on the stock Blazer RS revealed that the stock vehicle has an electric power draw at idle of approximately 580 W. This number represents the net electric load of 380 W as well as a measured steady 200 W load charging the 12 V battery, with data available in Appendix A. Assuming the charging power on the 12 V battery is needed frequently, as the vehicle accessory loads are powered by battery alone during engine start-stop instances, the load of 580 W is considered nominal for modeling.

Using specification sheets for each component being added to the hybridized vehicle, the expected electric load can be adjusted. Added controllers and sensors for hybrid functionality and CAVs features add an nominal 150 W electric load based on component datasheets. Additionally, the high-voltage motor and coolant pump require an estimated 200 W from the 12 V bus, bringing the total added electrical load to 350 W.

The alternator included with the 2.5 L powercube package is rated for 170 A and 2040 W. Using averaged efficiency figures from similar alternators, the alternator is assumed to be 69.5% efficiency at converting mechanical power to electrical power [42], with final calculated loads are summarized in Table 4.3.

Table 4.3: Auxiliary 12V load on engine

Vehicle architecture	Mechanical load (kW)	Electrical load (kW)
Stock	0.83	0.58
Hybrid	1.3	0.93

Optimization of the efficiency of accessory load systems has been explored [43], but modification of the alternator control systems for 12 V power is considered out of scope for the design project.

4.3 Model evaluation criteria

In order to evaluate the performance of the control strategy developed for the hybrid architecture under analysis, the criteria for valid input and output data to the simulation model must be established. For a vehicle simulation model, input data includes information such as the A, B, C, and ETW parameters, engine and transmission dynamometer data, and the drive cycle speed trace input, while output data primarily includes the simulated vehicle velocity, fuel consumption, and powertrain transient operating behavior. The glider, engine,

and transmission models have previously been discussed, so the last primary piece of input data for the simulation model is the drive cycle.

Drive cycles are a set of standardized velocity profiles which are the primary method used by the EPA to analyze vehicle emissions and fuel economy. Beginning with the Clean Air Act, the EPA developed two drive cycles to simulate city and highway driving as a means of accurately evaluating vehicles sold in the United States. The city drive cycle is the FTP (Federal Test Procedure), otherwise known an LA4 or UDDS (Urban Dynamometer Drive Schedule), while the highway drive cycle is the HWFET (Highway Fuel Economy Test), also abbreviated HFET or HWFE [44].

In addition to the FTP and HWFET, the need arose for a more aggressive drive cycle for high speed limits and higher-powered engines in the late 20th century. The US06 drive cycle was developed in the mid-1990s as the combination of specific portions of the previous CARB ARB02 and EPA REP05 drive cycles which were chosen for "aggressive driving and transient operation" [45]. The result is a shortened drive cycle which tests emissions behavior during high-load scenarios, providing a test procedure which allowed the EPA to enforce tighter emissions control.

The HWFET and US06 are "hot start" drive cycles, meaning that the vehicle has been warmed up before starting the test, typically by completing a warm up drive cycle to bring the powertrain and tires to steady-state operating conditions. Notably, for modeling considerations, the lack of significant thermal transients over these drive cycles makes it easier to accurately simulate, as most data used to derive powertrain models are from hot systems [45].

The FTP, however, consists of both a "cold start" and "hot start" portion, with the entire UDDS cycle completed after cold soaking the engine, immediately followed by repeating the

first 505 seconds of the UDDS in a hot cycle. As a result, FTP Phase 3, or the ”Hot 505,” is utilized for comparison, with the cold start portions neglected.

4.3.1 Drive cycle speed error criteria

Every mass-market vehicle sold in the United States undergoes the same set of drive cycle tests to produce fuel economy figures which are directly comparable between vehicle models. To reduce testing variability and minimize sources of error, extensive calibration and qualification criteria are defined [36].

One specific criteria is the maximum allowable vehicle speed deviation from the prescribed speed trace. As shown in Figure 4.4, the buffer is defined as the speed window of ±1 second of the speed trace, with an additional buffer of 2 mph applied. The EPA additionally states that ”the driver should attempt to follow the target schedule as closely as possible” but that ”minimum throttle action should be used to maintain the proper speed-time relationship” [45], essentially creating a balancing act for the test drivers between mild driving and meeting the required drive cycle speed trace.

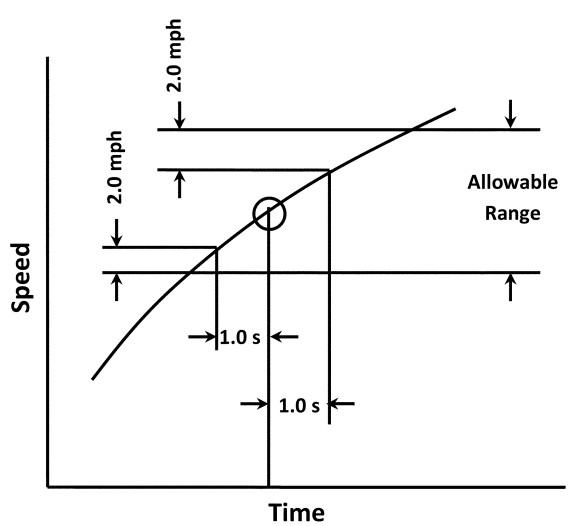

Figure 4.4: Example of rising edge drive cycle allowable range [46]

Additionally, the EPA drive cycles are provided as 1 Hz data files, so for a simulation model running at a higher rate, results are affected by the interpolation method used on the input data. Typically, linear interpolation would be considered standard, but smoother methods are desired. For the simulated vehicle behavior, the drive cycle data was pre-processed in MATLAB using the "pchip" method, a shape-preserving piecewise cubic interpolation method, due to its smoothed results with minimal error from the original linearized drive cycle data, with more information provided in Appendix B for the drive cycles upscaled to 100 Hz.

To ensure the simulated test results are comparable to real-world data, the speed trace error testing criteria must be enforced for simulated hybrid Blazer results. For any EPA drive cycle, the test vehicle must follow the speed trace within the specific buffer. The actual speed trace error between the simulated vehicle following 100 Hz smoothed input cycle and the source 1 Hz EPA data was evaluated, with the error bounds shown in Figure 4.4 calculated. Although the US06 is considered a "best effort" drive cycle, for the purposes of the vehicle simulation, any error outside the EPA boundary was considered disqualifying. The results of the US06, Hot 505, and HWFET are provided in Figures 4.5, 4.6, and 4.7, respectively.

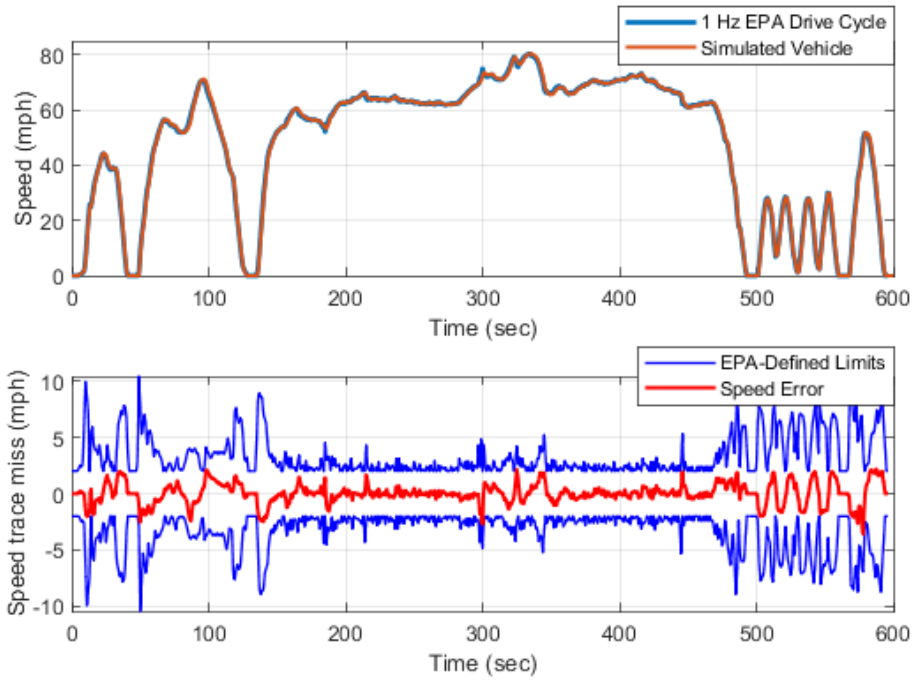

Figure 4.5: US06 model validation simulation results

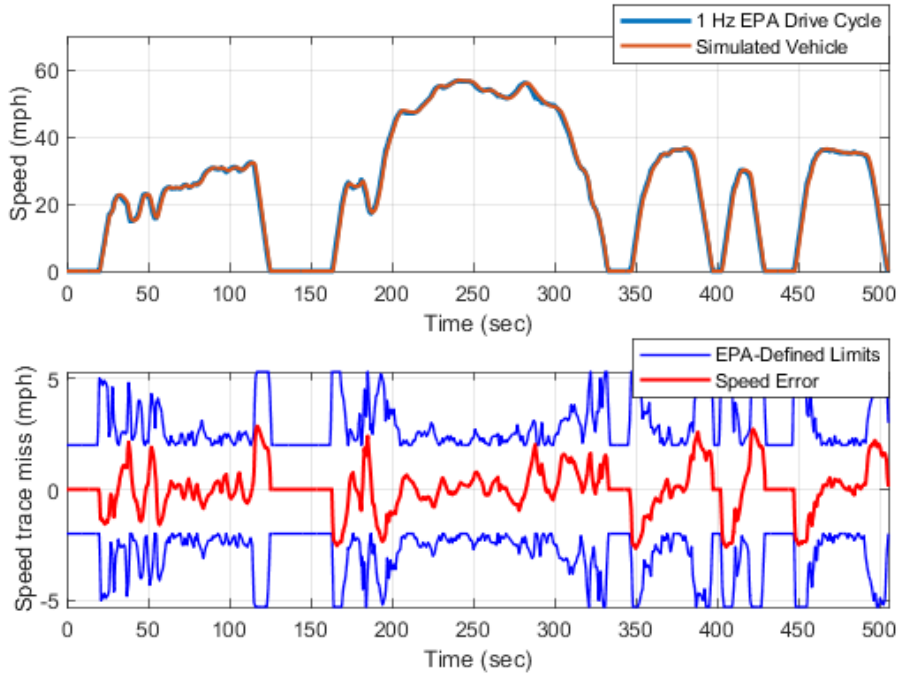

Figure 4.6: Hot 505 model validation simulation results

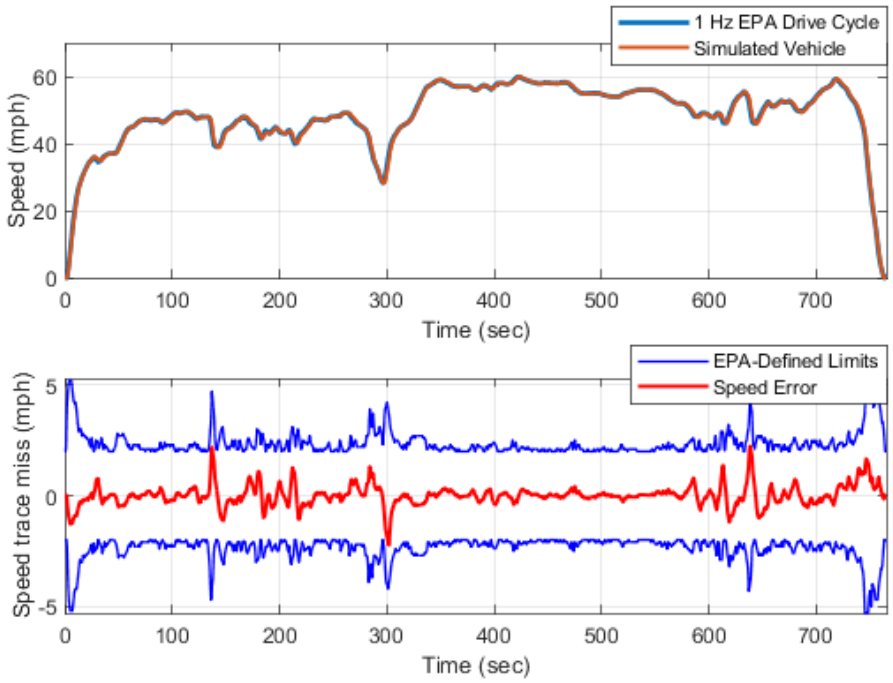

Figure 4.7: HWFET model validation simulation results

Tuning of the PI controller driver model was required for each drive cycle, as the "laziest" controller possible was preferable to better approximate efficient human driver behavior, with the goals of reducing error between the simulated vehicle and drive cycle target speeds, minimizing overshoot, and maintaining reasonable SAE J2951 criteria, as further discussed in Section 4.3.2. Gain values for each drive cycle available in Table 4.4. The output of the driver model is a control signal with the range $[-1, 1]$, with positive values representing accelerator pedal percentage and negative values brake pedal percentage. The same driver models developed in this chapter are applied for the remainder of this paper.

Table 4.4: Simulation PI controller driver model gain values

Drive cycle	K_P	K_I
US06	0.3	0.03
Hot 505	0.15	0.015
HWFET	0.2	0.02

4.3.2 SAE J2951 evaluation criteria

Beginning in 2014, the EPA began reporting a new set of metrics with which to evaluate vehicles undergoing fuel economy testing. Based on the SAE J2951 standard [47], these metrics aim to accurately evaluate the difference between the mandated EPA drive schedules and the actual velocity and propulsive effort of the test vehicle. Each parameter is a measure of the percent difference between of the test vehicle speed trace and original drive cycle after applying a double moving average filter.

The first metric used by the EPA, Energy Economy Rating (EER), is the percent difference of ”distance per unit cycle energy,” where unit cycle energy is the sum of the positive tractive work. A negative rating means that the test vehicle either created more positive tractive work in the same distance, or the same tractive work in less distance, as the base 1 Hz drive cycle.

The second metric is the Absolute Speed Change Rating (ASCR), the percent difference of the ”discrete approximation for the integral of the absolute magnitude of acceleration.” A negative rating means that the absolute acceleration of the test vehicle is, on average, lower than the base 1 Hz drive cycle, indicating that the test driver is less aggressive than the base cycle.

The final EPA-reported test metric is the Inertial Work Rating (IWR), the percent difference of the positive work due to the inertial load of the vehicle mass. A negative rating means that the test vehicle either accelerated less in the same distance, or accelerated at the same rate for less distance, as the base 1 Hz drive cycle.

The SAE J2951 standard provides recommended limits for the EER and ASCR based on one standard deviation from historical data, with the SAE Average as the recommended standard limit based on a grouping of similar data, and the SAE Maximum as the recommended

absolute limit based on all data including outlier data, as shown in Table 4.5. The SAE J2951 standard additionally recommends the Root Mean Squared Speed Error (RMSSE) as a measure of the driver's performance in following the speed trace over the drive cycle, but the EPA has opted to not report the RMSSE. Likewise, the SAE J2951 standard does not have a recommended limit for IWR as reported by the EPA, only listing limits for EER, ASCR, and RMSSE.

Table 4.5: SAE drive cycle metrics [47]

Drive cycle	SAE Average		SAE Maximum	
	EER	ASCR	EER	ASCR
US06	± 1.02	± 1.94	± 1.84	± 2.66
Hot 505	± 1.26	± 1.83	± 2.32	± 2.77
HWFET	± 0.75	± 4.08	± 1.46	± 6.76

To further validate the results of the vehicle simulations, the SAE J2951 criteria characteristics can be compared. While the EPA reports the IWR, EER, and ASCR of each drive cycle test, the metrics are for each drive cycle as a whole, meaning that it is not possible to derive the data for the Hot 505 independent of the rest of the FTP drive schedule.

The calculated SAE metrics for the validation simulations are provided in Table 4.6. For the Hot 505 and HWFET simulations, the SAE limits defined in Table 4.5 were used as a primary guiding factor for driver model tuning, with the EPA reported results serving a ballpark estimate for allowable limits.

Table 4.6: EPA and simulated drive cycle metrics

Drive cycle	EPA Reported [38]			Simulated		
	IWR	EER	ASCR	IWR	EER	ASCR
US06	−6.801	−1.604	−3.697	0.047	0.025	−4.271
Hot 505	-	-	-	0.140	0.054	−2.114
HWFET	−0.549	−0.455	−0.380	0.033	0.011	−0.691

For the US06 drive cycle EPA results, the large negative IWR indicates less positive tractive work, while the moderate ASCR indicates relatively close adherence to the drive cycle on the average. As the EPA does not report RMSSE, it is impossible to guess the overall adherence to the speed trace, but the reported numbers indicate that the US06 drive cycle featured short bursts of high accelerator pedal input, followed by longer periods gliding behavior with no accelerator pedal input, in a ”pulse and glide” technique.

Continuing the analysis of the EPA results for the 2019 2.5 L Blazer, the SAE J2951 metrics reported by the EPA for the HWFET drive cycle were compiled for the 2019 test car list data, and standard statistical analysis was performed, as shown in Figure 4.8. Data was filtered to only include results for the specific drive cycle, and data points with missing or out of range IWR, ASCR, or EER values are excluded. Notably, the mean for the ASCR and EER are relatively close to zero, most of the results fall within the SAE average range, and the 2.5 L Blazer test results fall within both one standard deviation as well as the SAE average range. The relatively Gaussian distribution of HWFET data serves as a good comparison for US06 data.

The same analysis was performed on US06 data for the same 2019 model year, as shown in Figure 4.9. The much wider distribution as well as the off-center mean is the result of the US06 being a ”best effort” drive cycle, with the mean for each metric being around one standard deviation from zero. The high variance and off-center mean warrant further inspection, specifically concerning the effect of large magnitude, negative signed SAE J2951 metrics on reported fuel economy for test vehicles, and is considered future work for the purpose of this report.

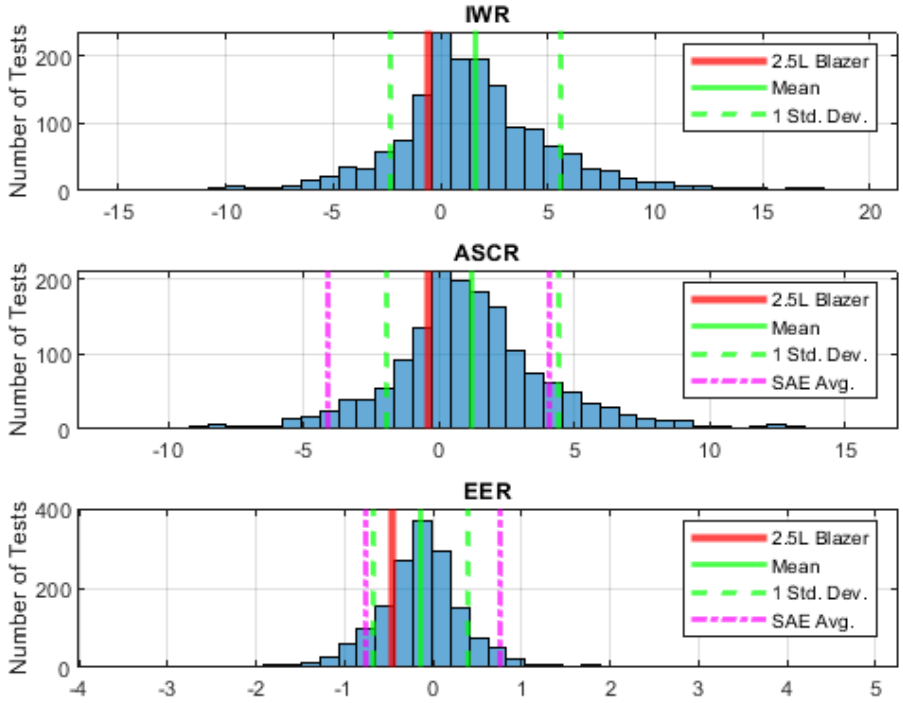

Figure 4.8: HWFET 2019 EPA test car list data reported SAE criteria

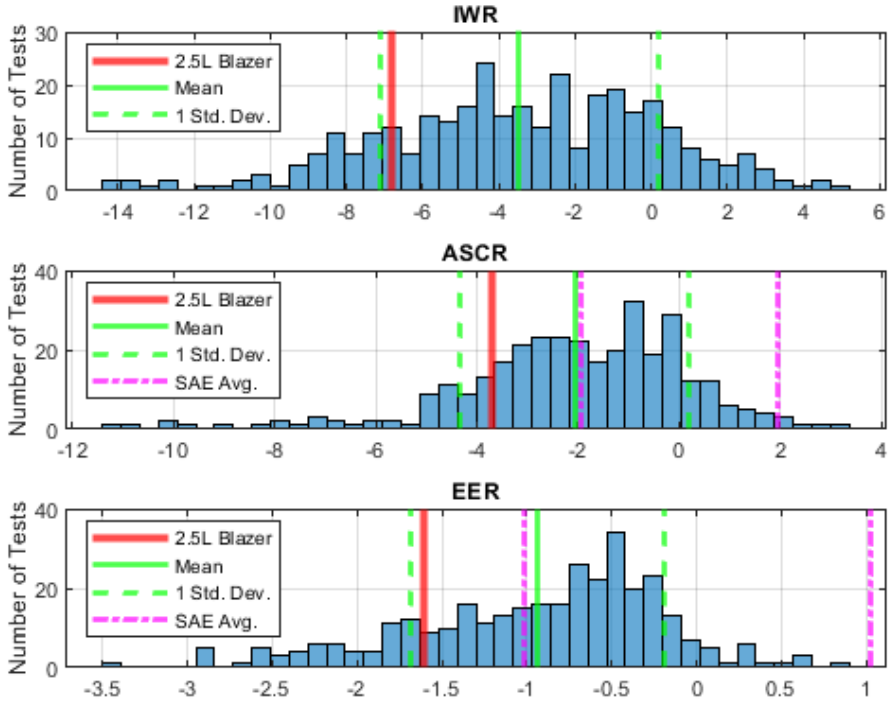

Figure 4.9: US06 2019 EPA test car list data reported SAE criteria

4.3.3 Energy consumption validation

To ensure the modeled energy consumption is based in reality, any available real-world test data for comparable vehicle configurations can be used to validate the vehicle model. Ideally, model validation would occur by using test correlation to compare time-varying real-world test data to simulation results [48]; however, in the absence of a functional test prototype, comparable EPA fuel economy results serve as the best reference. Specifically, the engine and transmission are validated against an existing vehicle by using the specified ABC parameters and reported fuel economy. For the simulation model developed in this paper, the 2019 Blazer 2.5 L parameters are used for validation, with the glider parameters shown in Table 4.7. The simulation results can then be directly compared drive cycle energy consumption results from EPA test data.

Table 4.7: Blazer 2.5 L validation glider parameters [38]

Parameter	Value	Units
ETW	1930	kg
A	119	N
B	3.53	$\frac{N}{m/s}$
C	0.550	$\frac{N}{m/s^2}$

The EPA testing results are listed in miles per gallon (MPG), so the correct conversion factors from simulated fuel power from the modeled engine to fuel volume must be identified. For each vehicle test, the type of fuel used is listed, and fuel batch test data is provided regularly for each fuel type, as summarized in Table 4.8.

Table 4.8: EPA Tier 2 Cert Gasoline properties [49]

Parameter	Value	Units
Fuel Net Heating Value	11.86	$\frac{kWh}{kg}$
Volumetric Energy Density	33.32	$\frac{kWh}{gal}$

Utilizing the mapped efficiency data for the engine and transmission along with the driver

model previously developed for each drive cycle, the vehicle model was simulated over the US06, HWFET, and Hot 505. The corresponding EPA data and simulated fuel economy are provided in Table 4.9.

Table 4.9: Validation simulation results for the Blazer 2.5 L

Drive cycle	EPA (mpg) [38]	Simulated (mpg)	Error (%)
US06	24.2	25.4	5.0
Hot 505	31.4	30.6	2.5
HWFET	39.8	38.6	3.0

Generally, error under 5% is valid due to variability in real-world testing procedures and results. The Hot 505 and HWFET results fall within this boundary, with the US06 simulated results being a bit more efficient than the actual vehicle. The increased efficiency can be attributed to the model's inability to capture the high-load transient behavior of the US06 drive cycle as seen in Figure 4.10, especially using models derived from steady-state engine and transmission data.

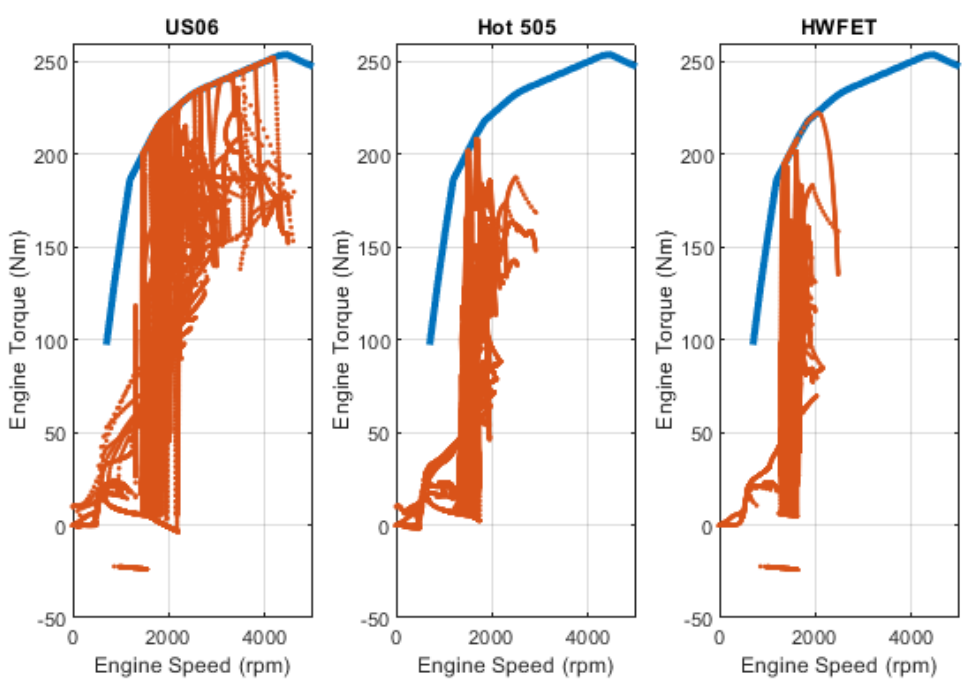

Figure 4.10: Simulated drive cycle engine operating points

4.4 Motor and battery models

To simulate the effect of the added high voltage powertrain in the hybridized Blazer, accurate models for the high voltage e-axle system and battery pack are required. Data supplied by the manufacturers is used to develop map models for powertrain efficiency.

4.4.1 Motor model

To begin modeling the high-voltage motor, manufacturer data was obtained for a wide range of operating points for the e-axle, shown in Figure 4.11.

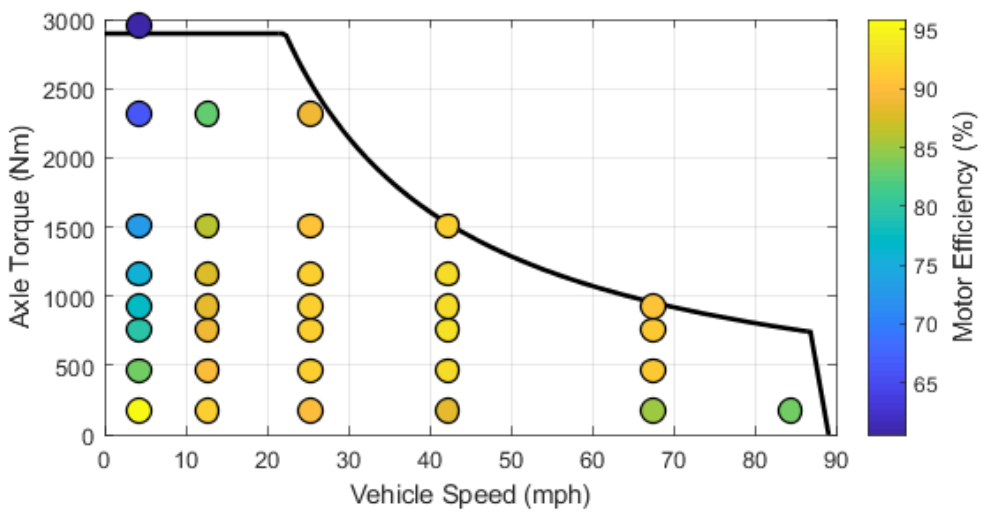

Figure 4.11: High-voltage motor manufacturer-supplied efficiency map coverage

The data points must be converted into a smooth efficiency map to be useful for simulations. An equation describing the losses of a motor can be applied and fit to the data [50]:

$$P_{loss} = k_c T^2 + k_i \omega + k_w \omega^3 + C \tag{4.7}$$

Where k_c is the copper loss coefficient, k_i is the iron loss coefficient, k_w is the windage loss coefficent, C is the constant power loss term, T is the the torque produced by the motor,and ω is the angular frequency of the motor as a function of vehicle speed, loaded wheel radius, and motor gearing. The manufacturer data was used to tune the loss coefficients to formulate a smooth loss map, as shown in Figure 4.12. The same manufacturer data points are shown for comparison, with a different color key due the efficiency map approaching zero at the axes.

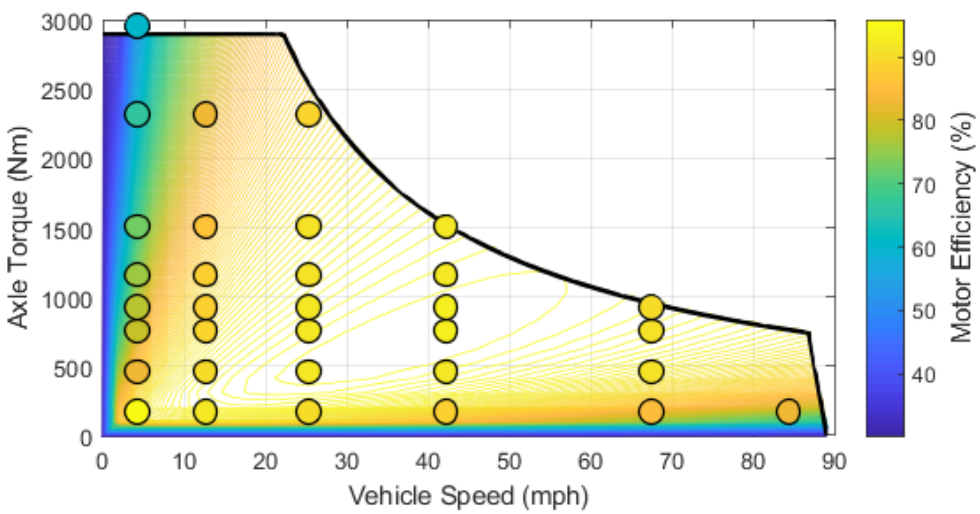

Figure 4.12: High-voltage motor smooth efficiency map contour plot

After tuning the efficiency map for the motor data, additional losses for the high-voltage inverter and e-axle gearbox must be considered, including electrical power loss, mechanical efficiency, and rear driveline spin loss.

4.4.2 Battery model

For any battery system, the power at the terminals of the battery pack can be modeled using simple set of power balance equations:

$$P_{in} = P_{out} + P_{loss} \tag{4.8}$$
$$P_{out} = I \cdot (V_{OC} - I \cdot R_{int})$$
$$P_{loss} = I^2 \cdot R_{int}$$

Where the open circuit voltage, V_{OC}, is defined by the state of charge (SOC) of the battery pack. To accurately model the effect of the SOC on the pack, manufacturer data is utilized to develop a model. With the test data shown in Figure 4.13 for a single cell within the battery pack, a model can be developed. Neglecting pack temperature, the change in state of charge has the most significant effect on the operating range of the battery pack, and the relationship can be linearized within the expected region of operation (approximately 30% to 80% SOC).

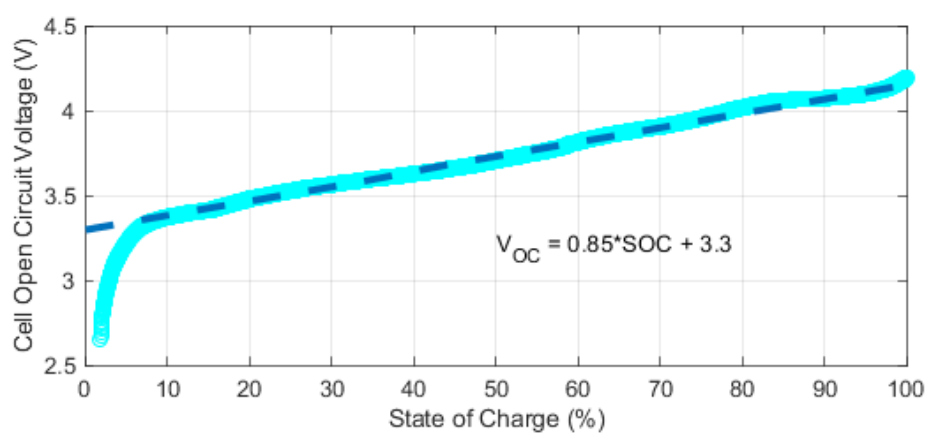

Figure 4.13: High-voltage energy storage system battery cell voltage curve

4.5 Total powertrain capability

To develop a total powertrain hybrid control strategy, it is useful to have a model which enables the direct comparison of engine and motor torque capabilities by converting both to axle torque. Framing the engine torque as axle torque allows the control strategy to neglect the transmission gears and shift control, as the engine power is constant through gearing. Additionally, framing the driver acceleration request as an axle torque means that the summation of the torque production of each powertrain being equal to the driver axle torque request.

Starting with the engine in Figure 4.14, the maximum torque capability at a given engine speed is plotted, with engine torque and speed converted to axle torque and vehicle speed through each transmission gear. The maximum available torque at any given vehicle speed is found through by comparing maximum axle torque capability in each gear, forming the engine axle torque envelope.

The motor model is simpler due to the single-gear transmission in the e-axle package. The positive torque envelope, as previously shown in Section 4.4, is plotted in Figure 4.15, with the maximum torque capability of 250 Nm and 80 kW converted to axle torque. The negative torque envelope is also included, with the high-voltage motor having 75% of the torque and power capability in the negative region.

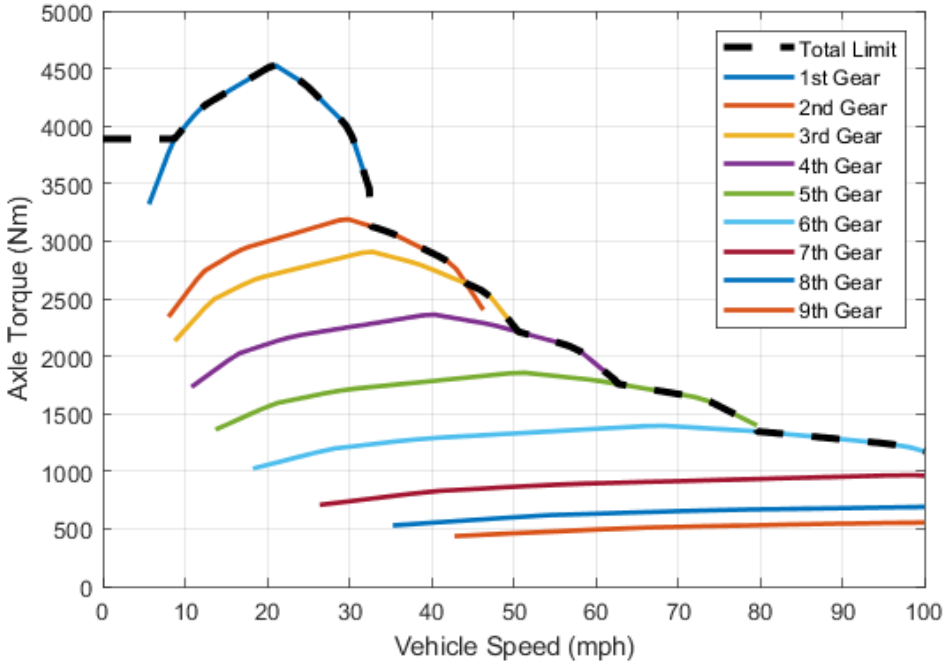

Figure 4.14: Engine axle torque envelope overlaid on the maximum torque in each gear

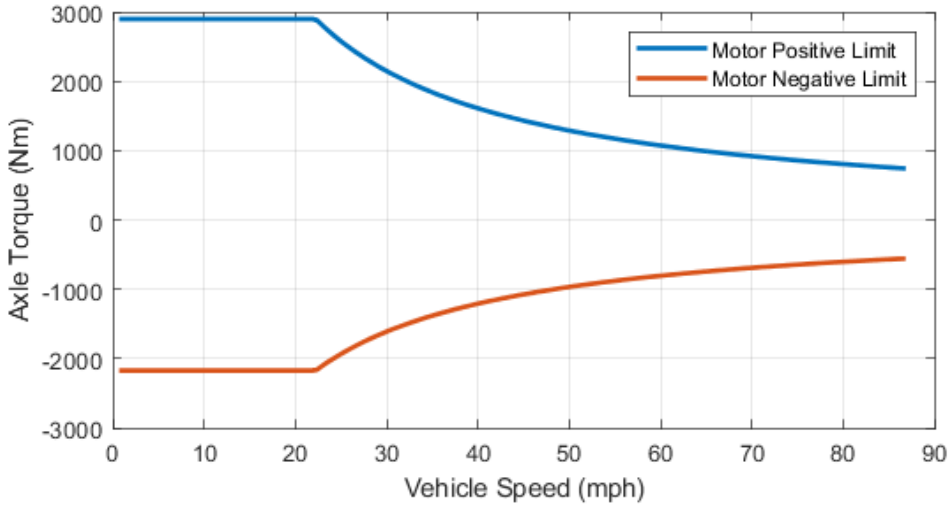

Figure 4.15: High-voltage motor positive and negative axle torque envelope

The engine and motor torque envelopes are overlaid, and the positive torque capabilities of the engine and motor are added together to find the total powertrain axle torque capability at any given vehicle speed, as shown in Figure 4.16.

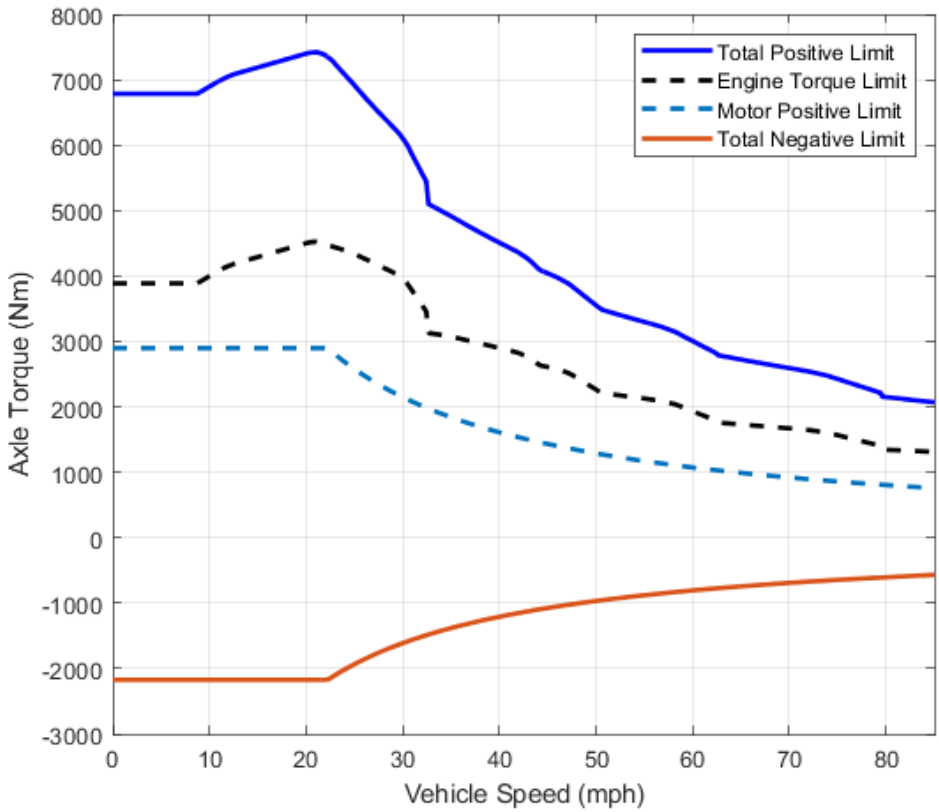

Figure 4.16: Total powertrain axle torque envelope

Chapter 5

Rule Formulations

A rule-based strategy is developed using the Willans Line of the engine and transmission dynamometer data. Generally, the rules and restrictions which comprise the control strategy are strictly deterministic and time-invariant, being only functions of driver demand, vehicle speed, and battery state of charge.

5.1 Willans Line estimation method

To more easily form conclusions about ideal engine operating regions, a simplified model is needed. The Willans line is a relatively accurate linear estimation methods for fuel power requirements to produce propulsive axle power, as previously introduced in Section 4.2.

5.1.1 Engine Willans Line

The engine efficiency data for the hybrid Blazer engine can be analyzed to form general conclusions about the efficiency of different regions of engine operation. In Figure 5.1, a linear fit is applied for a mechanical power output range from 0 to 60 kW, providing a good prediction of the fuel power input required to produce a given mechanical power output.

The power range for the fit from 0 to 60 kW is sufficiently linear, with an R^2 value greater than 0.95 in this range, meaning that the linear model provides an accurate estimation of

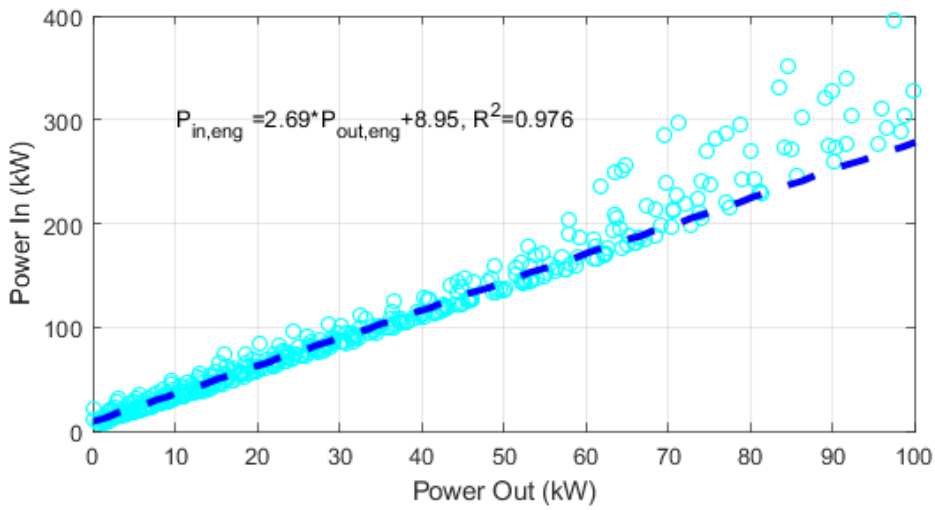

Figure 5.1: Willans line for the hybrid Blazer for data from 0 to 60kW

fuel power input to produce torque at the engine. However, the engine Willans Line alone does not capture the total efficiency of the powertrain to convert fuel power to propulsive power, as the transmission itself has losses.

5.1.2 Transmission Willans Line

Similar to the engine model, loss data for the 9-speed transmission utilized in the hybrid vehicle architecture can be used to define the efficiency of the system. Figure 5.2 plots the transmission data along with the linear Willans Line fit, with an R^2 value over 0.95 over the full range of data.

5.1.3 Combined Willans Line

The last step to create a useful model of the powertrain is to combine the Willans Lines for the engine and transmission along with the accessory load into a total powertrain model. The combined Willans Line for the conventional powertrain can be derived using the following

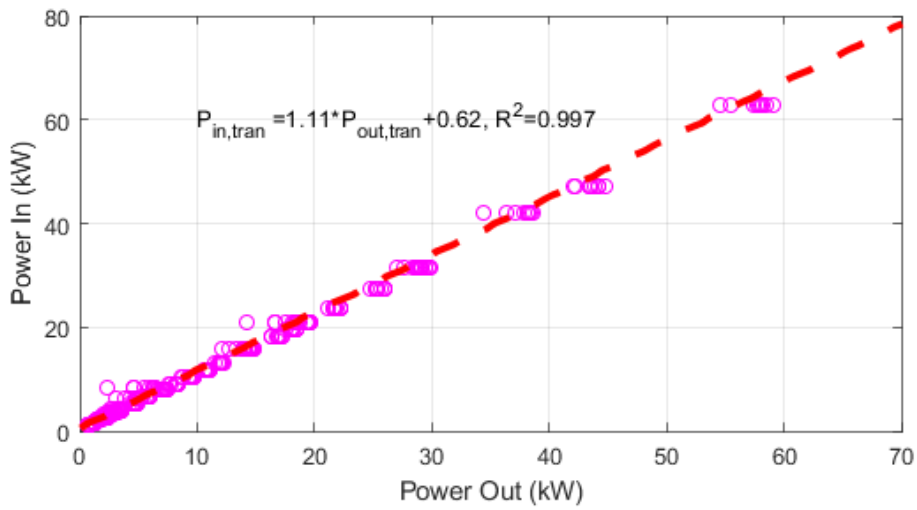

Figure 5.2: Willans line for the hybrid Blazer 9-speed transmission

set of equations, where the constant loss term for the transmission is propagated upwards as a function of engine efficiency, and the accessory load is applied at the engine.

$$P_{in,eng} = a_{w,eng} \cdot P_{out,eng} + b_{w,eng}$$

$$P_{in,eng} = a_{w,eng} \left(P_{acc} + P_{in,trans}\right) + b_{w,eng}$$

The equation can be equivalently expressed, assuming constant accessory power load:

$$P_{fuel} = a_{w,comb} \cdot P_{axle} + b_{w,comb} \tag{5.1}$$

$$\text{where } a_{w,comb} = a_{w,eng} \cdot a_{w,trans}$$

$$b_{w,comb} = a_{w,eng} \cdot P_{acc} + a_{w,eng} \cdot b_{w,trans} + b_{w,eng}$$

The derived linear equations for the engine and transmission are combined to determine the

total efficiency of the front powertrain, as shown in Figure 5.3

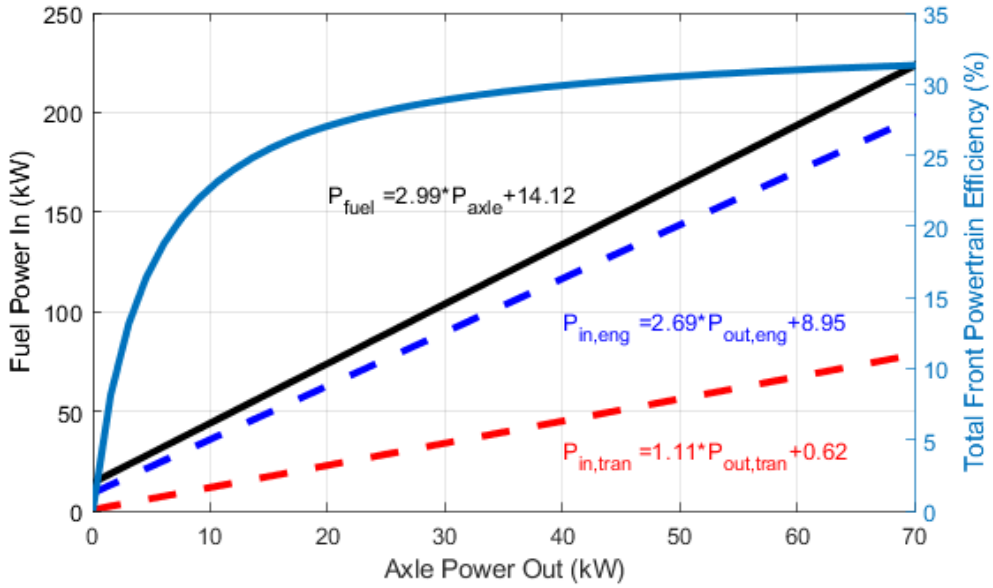

Figure 5.3: Combined Willans line for the vehicle front powertrain

5.1.4 Estimation boundaries

As previously noted, the Willans Line linearization of the engine power function is only accurate up to a certain threshold, approximately 60 kW. However, by combining the engine and transmission Willans lines, $P_{out,eng}$ is now P_{axle}, so as seen at the axle, the upper estimation limit for the engine is reduced due to losses from the accessory power load and transmission efficiency. This means 60 kW produced by the engine is seen as 52.3 kW of mechanical power at the axle, so the estimation limit for the combined Willans line must be similarly adjusted.

In addition to this upper boundary, a target minimum efficiency of 28% is defined as the lower boundary of engine operation. The lower boundary was chosen to maximize the powerband of engine operation without encroaching on the region of diminishing returns on increased torque range. Figure 5.4 shows the region of predictable engine efficient operation, with up-

per and lower engine power thresholds applied to the engine-transmission combined Willans Line efficiency curve previously shown in Figure 5.3.

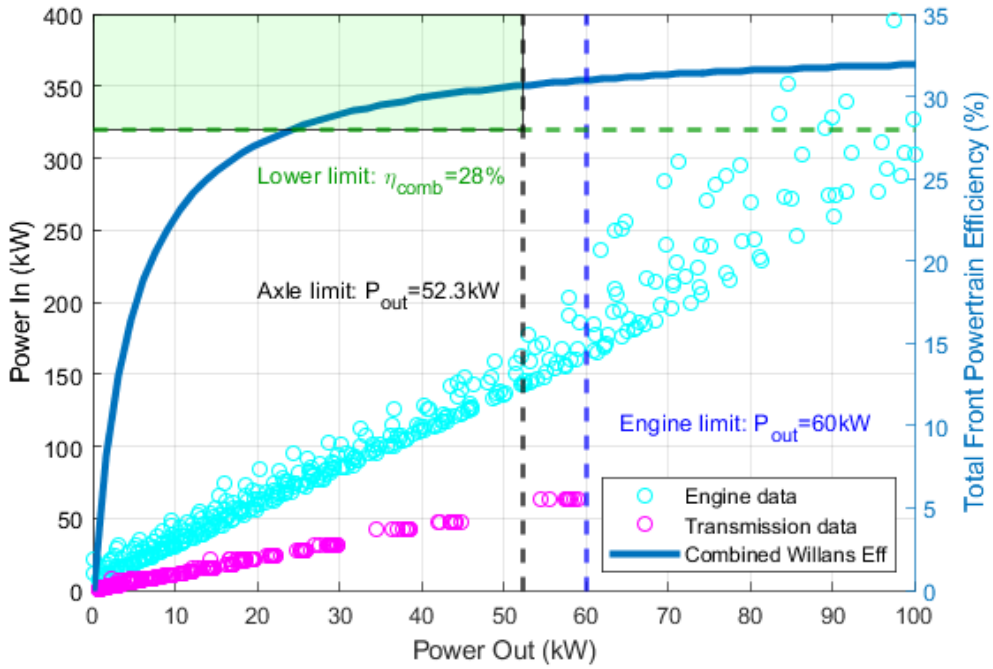

Figure 5.4: Region of predictable engine efficient operation

The power output associated with the efficiency threshold can be easily derived. The general equation for the efficiency of a system is defined by

$$\eta = \frac{P_{out}}{P_{in}} = \frac{P_{axle}}{P_{fuel}} \tag{5.2}$$

Using the equation for the Willans Line, the efficiency equation can be re-framed, and the power limits can be defined as an axle torque limit as a function of the efficiency limit and the current vehicle speed. By solving for the output power, we can find the associated efficiency-derived lower axle torque threshold, $T_{low}(v, \eta)$.

$$\begin{aligned} \eta &= \frac{P_{out}}{b_1 P_{out} + b_0} \\ P_{out} &= \frac{-b_0}{b_1 - \frac{1}{\eta}} \\ T_{low}(v, \eta) &= \frac{r_w}{v} \cdot \left(\frac{-b_0}{b_1 - \frac{1}{\eta}} \right) \end{aligned} \tag{5.3}$$

Where b_0 and b_1 are parameters from the Willans line model, η is the lower efficiency threshold, and r_w and v are the loaded wheel radius and vehicle speed used to calculate the axle rotational speed. Similarly, the engine axle torque limit due to the upper power threshold, $T_{up}(v)$, can be derived.

$$T_{up}(v) = \frac{r_w}{v} \cdot P_{thresh} \tag{5.4}$$

Where P_{thresh} is the upper power threshold for accurate range of the Willans Line estimation, chosen as 52.3 kW at the axle for the previously specified 60 kW limit at the engine. By reanalyzing the results shown in Figure 4.10, the 60 kW power limit at the engine can be overlaid, as shown in Figure 5.5.

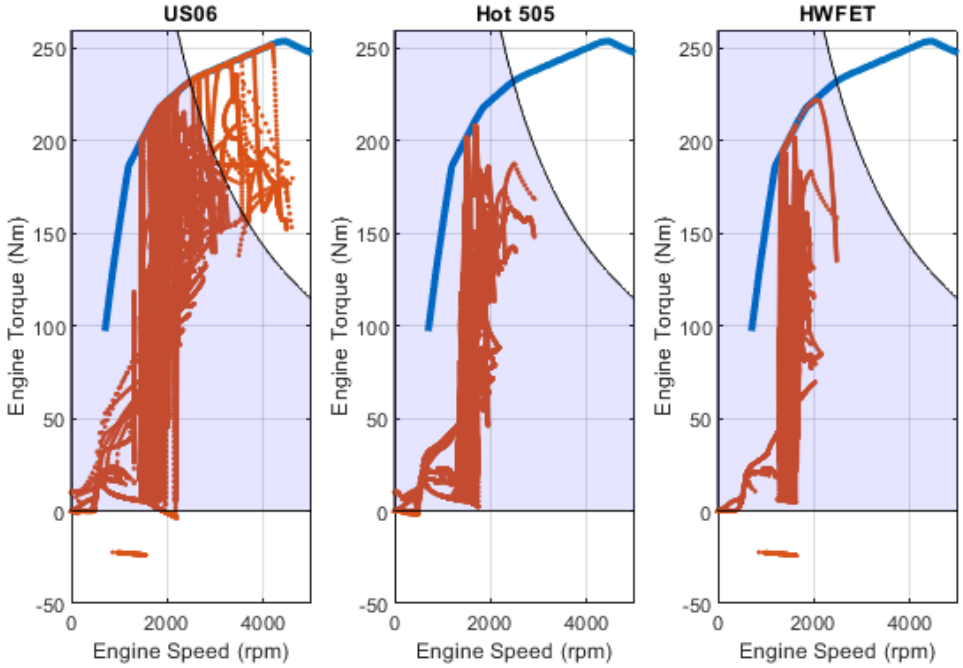

Figure 5.5: Engine operating points from Figure 4.10 with 60 kW engine estimation limit overlaid

The two drive cycles with minimal error from the EPA reported fuel economy, the Hot 505 and HWFET, have operating points which fall completely below the 60 kW limit, while the US06, which had slightly more error, has engine operating points above 60 kW. The primary conclusion that can be drawn from this information is that the simulated hybrid vehicle model, which limits engine torque to 60 kW under normal usage, will benefit from the high accuracy demonstrated in the low-power engine operating regions.

5.2 Hybrid rules definition

Given the ideal region of operation for the engine derived from the Willans Line for the front powertrain, a few different regions of operation can be defined. For each region, the following

region and variable definitions are used. The regions are mapped to the total vehicle torque envelope in Figure 5.6, with the dashed lines representing the engine and motor axle torque envelopes, and the bold outline representing the total vehicle torque envelope.

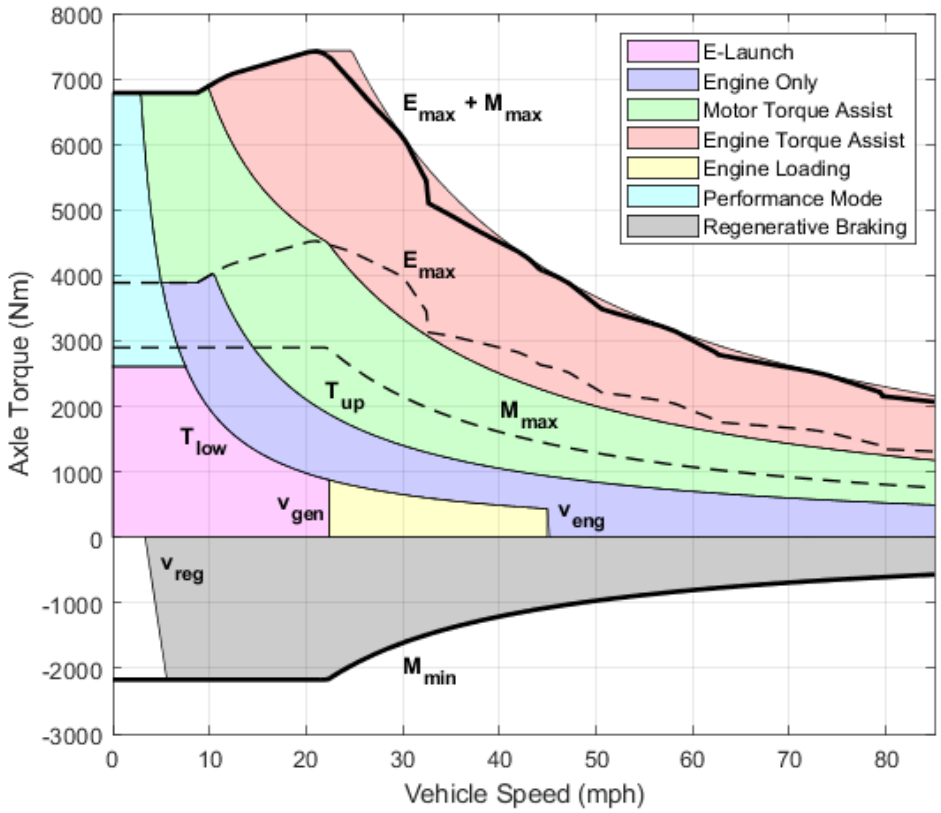

Figure 5.6: Regions of powertrain operation, with powertrain torque limits marked

E-Launch: Axle power is too low to justify using the engine, so the high voltage motor is used as the sole source of tractive power. Because the high voltage motor cannot be used for all positive tractive effort, mainly due to the fact that the vehicle is not a series or plug-in hybrid, the upper boundary of the E-Launch region is defined as the lower boundary of the Engine Only region, $T_{low}(v, \eta)$, with the maximum torque of approximately 90% of the total motor torque, $M_{max}(v)$, and the maximum speed defined as v_{gen}.

Engine Only: The operating region defined by the Willans Line boundaries, with the lower power threshold, $T_{low}(v, \eta)$, set as a function of the minimum engine efficiency and upper power threshold, $T_{up}(v)$, set as the maximum estimation boundary of 52.3 kW at the axle. Additionally, after experimentation showing especially high operating efficiency at highway speeds, past a certain vehicle speed threshold, all torque requests with power less than $T_{up}(v)$ will be supplied solely by the engine, defined as v_{eng}.

Motor Torque Assist: The powerband above 52.3 kW where it is more efficient to supplement engine torque with motor torque than to push the engine above $T_{up}(v)$. The region extends until approximately 90% of available motor torque, $M_{max}(v)$, has been used.

Engine Torque Assist: The highest power region where the engine torque request is allowed to exceed the 52.3 kW axle power limit to its maximum torque, $E_{max}(v)$, to meet the driver acceleration demand.

Engine Loading: The moderate-speed, low-power region, beginning at the speed v_{gen} and ending at v_{eng}, where the engine is held at the minimum efficiency threshold, $T_{low}(v, \eta)$, and the motor is used as a generator in the negative power region. The net sum of axle torque is equal to driver demand, but the battery pack is allowed to charge.

Performance Mode: The low-speed, high-torque region where launch control is considered more important than energy consumption management. Maintaining wheel traction with the road surface is the primary concern in this region. This region is controlled similarly to the Engine Torque Assist mode, where the motor is held at approximately 90% of $M_{max}(v)$ and the engine is used to provide the remaining torque request.

Regenerative Braking: The negative power region where the motor acts as a generator to recapture kinetic energy to charge the battery by slowing the vehicle, with the maximum negative torque limit set by the high-voltage motor torque limit, $M_{min}(v)$, and a low-speed regen torque cutoff of v_{reg} to minimize low-efficiency operation. Additionally, the accelerator pedal maps feature a "one pedal" strategy, where lifting off the pedal results in regenerative braking without needing to press the brake pedal, as further discussed in Section 5.3.

With the operating regions defined, the rules for the hybrid vehicle energy management strategy can be formulated:

E-Launch	for $T_{axle} \in [0, \min\{T_{low}(v,\eta), M_{max}(v)\})$ and $v < v_{gen}$
Engine Only	for $T_{axle} \in [T_{low}(v,\eta), \min\{T_{up}(v), E_{max}(v)\}]$ or $T_{axle} < T_{up}(v)$ and $v \geq v_{eng}$
Motor Torque Assist	for $T_{axle} \in (\min\{T_{low}(v,\eta), T_{up}(v), E_{max}(v)\}, \min\{E_{max}(v) + M_{max}(v), T_{up}(v) + M_{max}(v)\}]$
Engine Torque Assist	for $T_{axle} \in (T_{up}(v) + M_{max}(v), E_{max}(v) + M_{max}(v))$
Engine Loading	for $T_{axle} \in [0, \min\{T_{low}(v,\eta), M_{max}(v)\})$ and $v \in [v_{gen}, v_{eng}]$
Performance Mode	for $T_{axle} \in [M_{max}(v), \min\{E_{max}(v) + M_{max}(v), T_{low}(v,\eta)\}]$
Regenerative Braking	for $T_{axle} \in [M_{min}(v), 0)$ and $v > v_{reg}$

where $E_{max}(v)$ is the maximum torque the engine can produce at the given speed, $M_{max}(v)$ is maximum torque the motor can produce, v_{gen} is the speed for the motor to switch from low torque propulsion to Engine Loading, and v_{eng} is the speed for Engine Loading to be disabled in favor of Engine Only operation. Within each mode, the engine axle torque is defined as the following:

$$T_{eng} = \begin{cases} 0 & \text{for E-Launch} \\ T_{axle} & \text{for Engine Only} \\ T_{up}(\omega) & \text{for Motor Torque Assist} \\ T_{axle} - M_{max}(\omega) & \text{for Engine Torque Assist} \\ T_{low}(\omega, \eta) & \text{for Engine Loading} \\ T_{axle} - M_{max}(\omega) & \text{for Performance Mode} \\ 0 & \text{for Regenerative Braking} \end{cases} \tag{5.5}$$

Similarly, the motor axle torque is defined as the following:

$$T_{mot} = \begin{cases} T_{axle} & \text{for E-Launch} \\ 0 & \text{for Engine Only} \\ T_{axle} - T_{up}(\omega) & \text{for Motor Torque Assist} \\ M_{max}(\omega) & \text{for Engine Torque Assist} \\ T_{low}(\omega, \eta) - T_{axle} & \text{for Engine Loading} \\ M_{max}(\omega) & \text{for Performance Mode} \\ T_{axle} & \text{for Regenerative Braking} \end{cases} \tag{5.6}$$

The rules can be alternatively visualized in a power-speed plot, with an approximate plot shown in Figure 5.7. This version is particularly good at showing how small the performance region is relative to the other operating regions, and why little consideration toward energy efficiency is required for the performance mode.

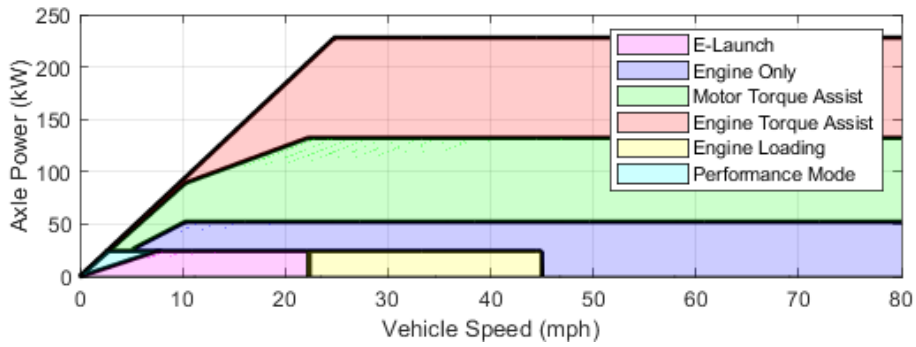

Figure 5.7: Regions of powertrain operation as a function of power

Additionally, further insight into the Engine Only cutoff speed, v_{eng}, may be gained by analyzing the axle torque requirement for road load on zero grade at constant speed, as shown in Figure 5.8. As speed increases, the torque required to hold the speed due to resistive forces discussed in Chapter 4.1 increases quadratically, while the engine lower power threshold, T_{low}, decreases inversely. Minor perturbations in the axle torque can push the request over the T_{low} threshold, with a 0.3 m/s^2 acceleration torque line shown for reference. The chosen 45 mph value for v_{eng} balances the diminishing returns of extending the Engine Loading region to higher speeds, preventing the control strategy from rapidly changing between rule modes and reducing energy consumption in some scenarios, as further discussed in Chapter 7.

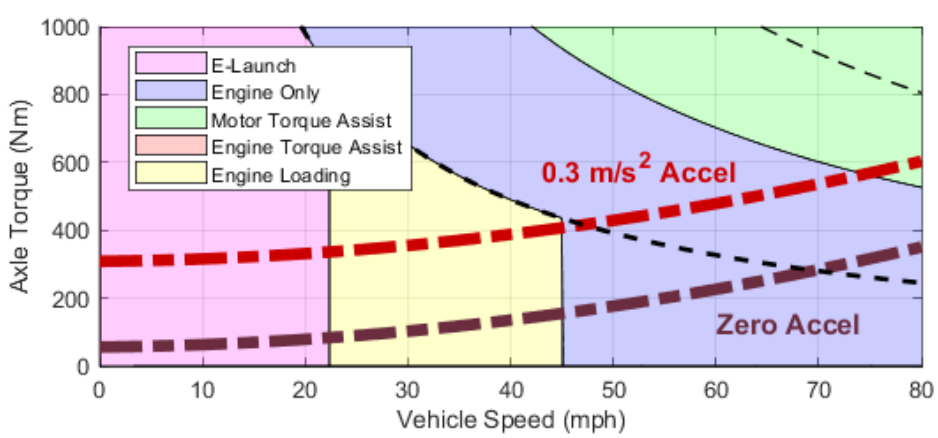

Figure 5.8: Road load axle torque overlaid on rule regions

5.3 Battery energy management

Thus far, the rules described have been made to optimize fuel economy, but the transient behavior of the vehicle, mainly the state of charge of the high voltage battery pack, must be considered. The control strategy has two methods to charge the battery pack: regenerative braking and loading the engine while using the motor as a generator. Because regenerative braking is situationally dependent upon the driver deceleration request, the control strategy must rely on engine loading as the primary means with which to maintain the battery state of charge.

State of charge management becomes especially important on a full hybrid without plug-in capability, as all energy discharged from the pack must be recaptured during driving. This ability to recharge during regular driving is critical for the hybrid architecture under analysis due to the lack of a P0 or P1 motor, which would allow the battery to charge while the car is stopped. Through analysis and manipulation of the Engine Loading behavior, rules can be added to the control strategy to ensure charge balanced behavior.

5.3.1 SOC function for speed

The first of two proposed rules is a function to govern the speed threshold for Engine Loading to engage. As the battery SOC increases, the function pushes the Engine Loading threshold toward faster speeds to decrease the likelihood or remove the possibility of entering Engine Loading to prevent over-charging the pack. Likewise, as the battery SOC decreases, the function pushes the Engine Loading threshold toward lower speeds to engage Engine Loading during city driving.

The desired behavior of the Engine Loading boundary, including an upper and lower fixed-size engagement hysteresis, is shown is shown in Figure 5.9. The arrows indicate the movement of the Engine Loading region threshold speed, v_{gen}, where the hatched regions indicate the engagement hysteresis. The hysteresis regions remain static, with the lower threshold set to 10 mph below v_{gen} and and the upper threshold to 5 mph below the Engine Only cutoff speed, v_{eng}.

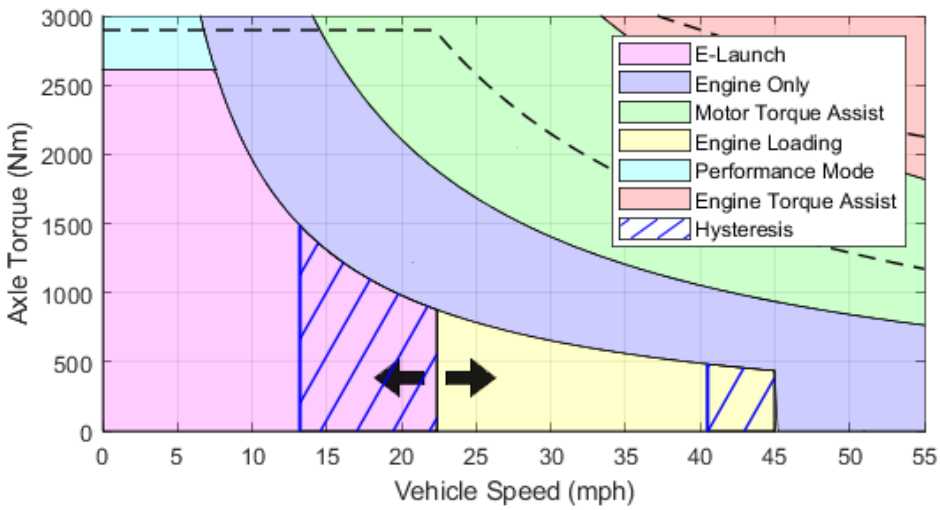

Figure 5.9: Engine Load threshold plot over rules, with hysteresis region marked

Taking into account the limits of the battery pack, the upper and lower boundaries for the movement of v_{gen} are chosen. A smooth function for v_{gen} is desired, with an exponential curve being favorable due to the flat behavior at the lower boundary and the increasing behavior at the higher limit. A middle point of 50% SOC near the motor base speed is defined, with an upper limit of 70% SOC at the Engine Only boundary v_{eng} and a lower limit of 10 mph to maintain a small buffer to the regenerative braking cutoff v_{reg}. Using the MATLAB Curve Fit tool, a smooth function with favorable characteristics for use as the Engine Loading boundary condition was found, as shown in Figure 5.10.

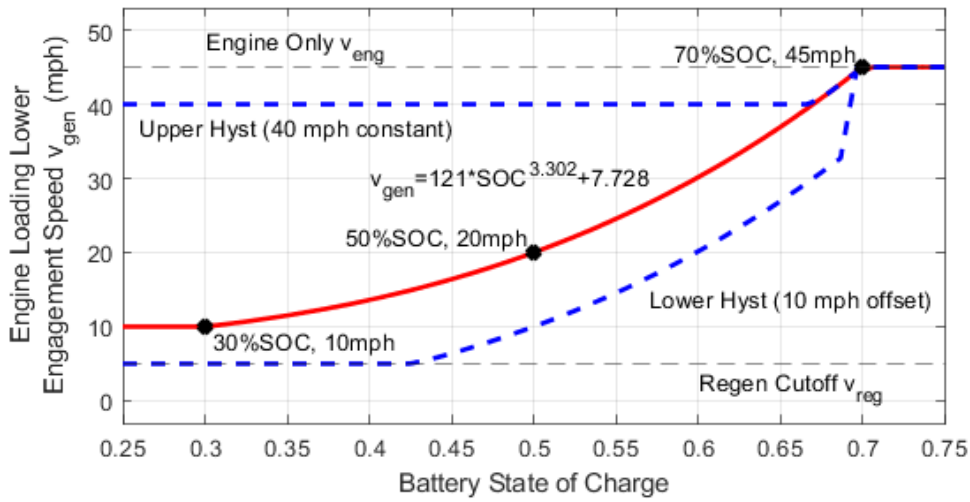

Figure 5.10: Engine Load threshold as a function of speed

The lower hysteresis for v_{gen} maintains a constant 10 mph offset from v_{gen} through the normal operating region and saturates at a lower limit of v_{reg} to prevent the motor from being used in an inefficient region. The upper limit holds a constant 5 mph offset from the Engine Only cutoff speed v_{eng}, and is saturated to v_{gen} at high SOC. When the SOC approaches the upper limit of 70%, both hysteresis boundaries are set to zero as the Engine Loading region disappears.

5.3.2 SOC function for power

The second proposed rule is a power-based Engine Loading mode hysteresis. When the vehicle transitions from E-Launch to Engine Only during normal acceleration, the engine remains on and loaded as the driver backs off the accelerator pedal, forming a hysteresis region from the lower efficiency boundary T_{low}, as shown in Figure 5.11.

One problem not yet addressed is powertrain behavior within the Engine Loading region near zero torque demand, where a driver may alternate between light braking and light

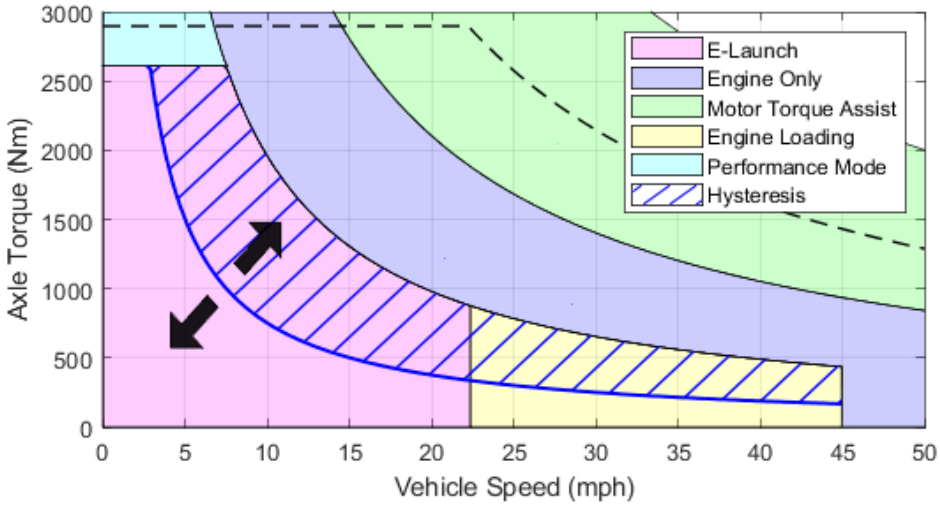

Figure 5.11: Engine Load hysteresis plot over rules

acceleration requests. As the rules currently stand, this behavior of bouncing into and out of Regenerative Braking and Engine Loading will cause the engine to pulse, from zero torque during braking to the minimum threshold during acceleration.

To combat this undesired behavior, a special condition can be added utilizing the power hysteresis function developed in this chapter. Specifically, when the vehicle is in the Engine

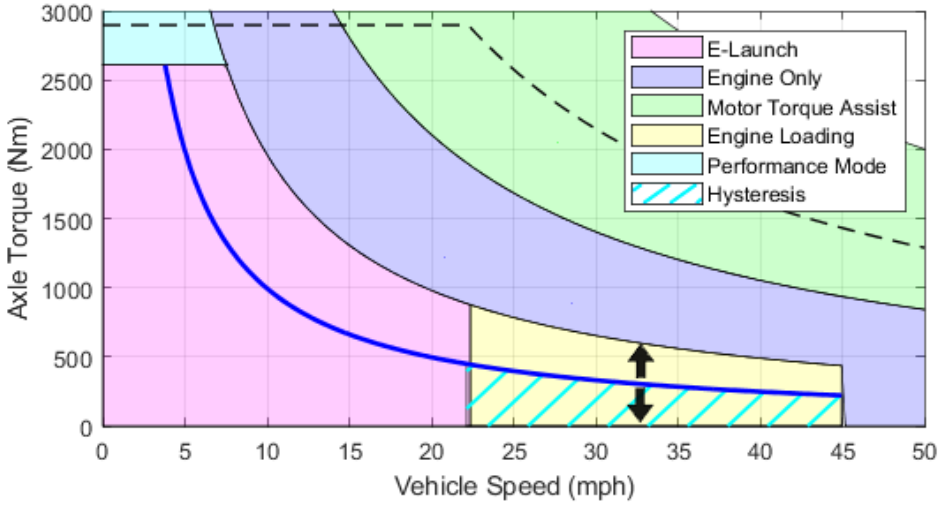

Figure 5.12: Engine Load re-engagement hysteresis from Regenerative Braking

Loading region, briefly transitions to Regenerative Braking, then back to positive torque, the engine will not re-engage until the torque request exceeds the power hysteresis threshold, as shown in Figure 5.12.

As with the previous function, an exponential curve provides favorable characteristics, as shown in Figure 5.13. As the SOC drops, the hysteresis function expands to 20 kW, keeping the powertrain in Engine Loading, while at the upper SOC limit of 70%, the hysteresis zone decays to zero. The Engine Load engagement threshold is also shown as the difference between the hysteresis equation and the engine efficiency boundary of about 22 kW.

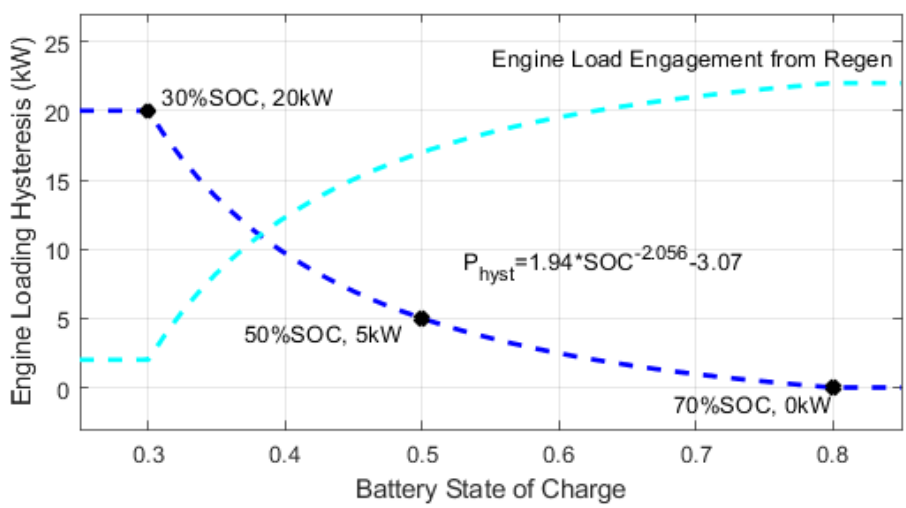

Figure 5.13: Engine Load hysteresis function

5.3.3 One pedal regenerative braking

To maximize the effect of hybridization on the vehicle, a ”one pedal” control strategy is used, where reducing the accelerator pedal input causes the vehicle to begin slowing down without the driver needing to press the brake pedal [51]. As a result, all of the energy from deceleration can be recaptured with regenerative braking to charge the battery without the need for the driver to engage the friction brakes.

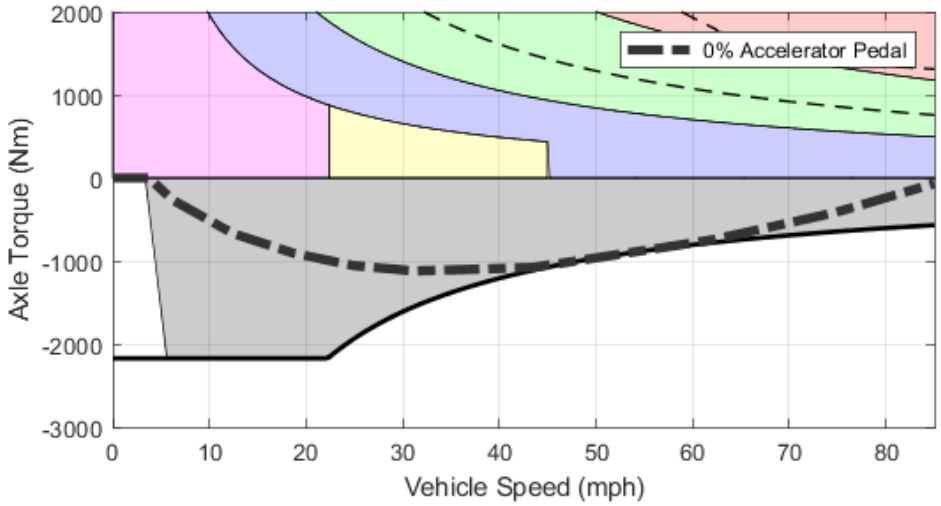

Figure 5.14: Zero accelerator pedal input axle torque request

The torque request for zero accelerator pedal input as a function of speed is shown in Figure 5.14 overlaid on the Regenerative Braking region of the rules. The torque request line was chosen to maximize the amount of recaptured energy during vehicle deceleration, while tapering off smoothly at high speeds due to physical limitations of the motor as well as low speeds due to low generator efficiency.

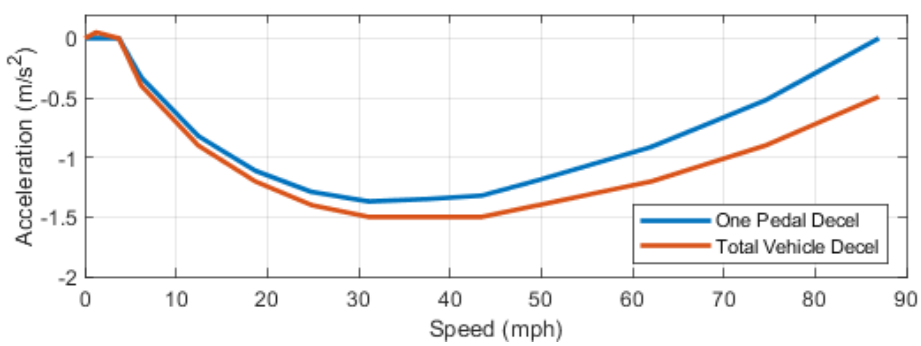

Figure 5.15: Zero accelerator pedal input deceleration

The acceleration rate associated with the axle torque for one pedal is provided in Figure 5.15, with the specific deceleration contribution of the one pedal negative motor torque shown next to the total actual vehicle deceleration including drag losses. Notably, one pedal will not

bring the vehicle to a stop; the driver must press the brake pedal to engage the friction brakes to complete the braking maneuver. The one pedal response tapers off at low speeds to encourage the driver to press the brakes before regen torque is completely removed. The transition from the positive to negative torque regions is addressed in Chapter 6.

5.3.4 Charge and discharge safety limits

To ensure the battery is not charged or discharged past the safe range, safety limits are imposed on the hybrid energy management strategy so SOC does not exceed a range of 20% to 80%, as shown in Figure 5.16. The limits built-in to the SOC functions for speed and power are both 30% and 70% to attempt to maintain SOC without limiting the motor response, so the additional restrictions imposed on this section are primarily imposed to prevent one pedal charging or Motor Assist discharging from forcing the battery out of the safe SOC range.

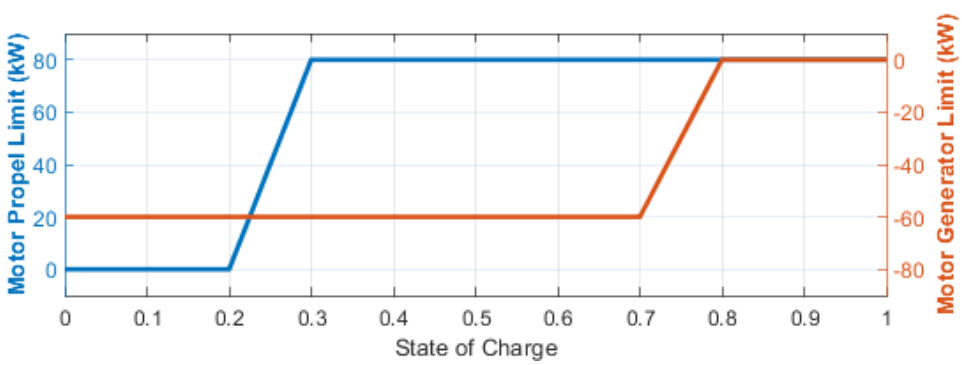

Figure 5.16: Zero accelerator pedal input deceleration

From a safety perspective, the total axle torque request of the driver must be honored, so the difference between the axle torque request at zero pedal and the allowable motor generator torque is filled in with a friction brake request, providing a consistent pedal response for the driver.

Chapter 6

Drive quality

Most academic hybrid energy management strategies focus on the fuel economy of the vehicle as the primary performance criteria. However, because the control strategy developed in this paper is being purpose-built for implementation on a competition vehicle being judged on a variety of performance criteria, including ride and drive quality, it is necessary to define and adhere to drive quality metrics.

In this work, drive quality is defined as the pleasure or appeal of a vehicle to be operated. The main application of drive quality management for the hybrid control strategy is the instantaneous torque switching due to alternating torque requests to the engine and motor, typically due to transitions between control mode regions. The need for mode transition drive quality control is made obvious through analysis of the competition-defined pedal maps, as shown in Figure 6.1. For each pedal position, if held constant, the operating points travel through multiple rule regions, meaning that almost any acceleration event will cause the vehicle to undergo multiple mode transitions.

At specific mode transitions for the rule-based control strategy, as shown in Figure 6.2, there is a sharp decrease in torque from one source and a corresponding increase from the other, as the motor and engine take turns propelling the vehicle. Without arbitration, the sharp drops and rises in torque lead torque holes and sharp changes in acceleration, especially due to differences in time constants between the engine and motor.

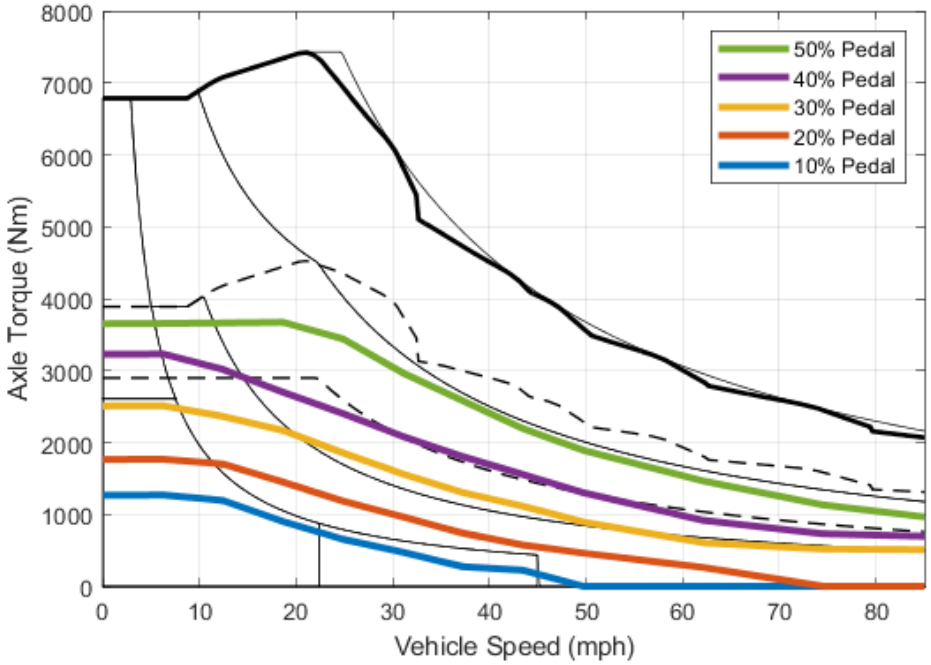

Figure 6.1: Competition-required pedal torque response

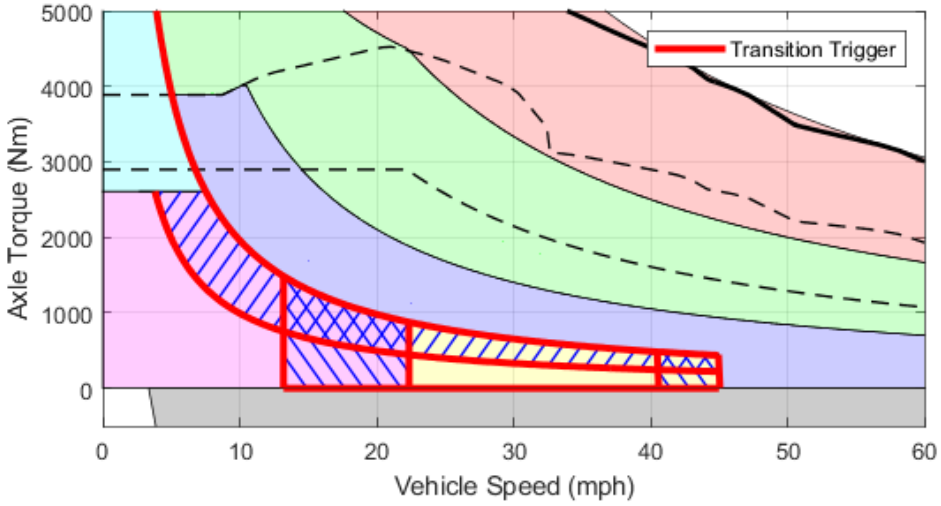

Figure 6.2: Highlighted mode transitions which require crossfading torque

Because the front powertrain has not been modified from a stock configuration, the manufacturer-tuned drive quality control systems are assumed to handle any considerations specifically relevant for the engine-transmission pair, including shift quality and torque response. The primary differentiation is the dual control of the high-voltage motor in combination with the engine, where mode transitions between the two powertrains could lead to noticeable torque holes.

6.1 Drive quality criteria

Drive quality is by definition a subjective metric; however, research has been performed into creating quantifiable metrics which serve as direct predictors of drive quality. Two primary measurements are used for quantifying drive quality, including acceleration, in units of m/s^2, and jerk, the first derivative of acceleration, in units of m/s^3.

A majority of research on drive quality is focused on the torque response of an engine-transmission system [52], commonly using the two-mass spring model to model the behavior of driveline components [53]. The research into engine response and gear shifts are directly transferable to the primary focus of engine-motor torque interaction in hybrid vehicles [25].

The metrics which are directly impacted by the hybridization process primarily include response delay to pedal tip-in, torque bump/overshoot due to pedal tip-in, peak and sustained jerk and vibration, and torque smoothness/surge and overshoot [54, 55]. These same metrics are used within commonly utilized drive quality software tools such as AVL-Drive, although the exact limits and correlation are proprietary [54, 56].

For pedal tip-in response, research has shown [57] that ratings for drive quality are dependent on a controlled rise rate and response for powertrain torque, with jerk less than 30 m/s^3 rated

favorably. The EcoCAR Mobility Challenge defines launch jerk, each of which must be met within 0.3 seconds of pedal tip-in, with the vehicle response aggressiveness directly related to the percent accelerator pedal, as listed in Table 6.1, with a tolerance threshold of ± 1 m/s^3.

Table 6.1: Competition-defined jerk from launch limits

Accel Pedal Percent (%)	Target Launch Jerk (m/s^3)	Response Time (s)
10	3	0.3
20	6.25	0.3
30	9.25	0.3
40	11.75	0.3
50	14	0.3

Next, jerk and vibration must be analyzed from two perspectives: peak and sustained. Research has shown that during regular driving, peak jerk between ± 1 m/s^3 and ± 4 m/s^3 is qualitatively indistinguishable, and jerk up to ± 10 m/s^3 is tolerable. However, peak jerk is not the only indicator of drive quality, as sustained lower magnitude jerk leads to driver discomfort, with an RMS jerk less than 1.67 m/s^3 considered acceptable and greater than 2.32 m/s^3 considered unacceptable [58]. The powertrain response peak and RMS jerk limits are summarized in Table 6.2.

Jerk frequency is also an important indicator of drive quality, with humans being especially sensitive to horizontal vibration in the 1 Hz to 2 Hz frequency range [55], with with jerk contributions of powertrain response mostly below 3 Hz [59]. High-magnitude sustained vibrations in the 2.5 Hz to 30 Hz range can be dangerous for humans; however, this range of vibrations on vehicle is typically due to suspension and tires [55] or engine idle vibrations [60], each of which are not the primary focus of the analysis in this paper.

To utilize the pool of research into adaptive cruise control (ACC) technology, the same drive quality evaluation criteria can be applied as constraints on the hybrid propulsion control strategy, specifically vehicle acceleration and jerk analysis, with limits in Table 6.3.

Table 6.2: Peak and sustained jerk limits

Metric	Allowable	Uncomfortable
Peak Jerk	< 10 m/s^3	> 10 m/s^3
RMS Jerk (Below 3 Hz)	< 1.67 m/s^3	> 2.32 m/s^3

Table 6.3: ISO 15622:2018 acceleration and jerk operational limits [61]

Application	Maximum Accel (m/s^2)	Maximum Decel (m/s^2)	Maximum Jerk (m/s^3)
Above 20 m/s	2.0	-3.5	2.5
Below 5 m/s	4.0	-5.0	5.0

Lastly, the torque smoothness/surge and overshoot are important metrics of drive quality. Torque surge is seen as unsteady or varying powertrain torque under constant pedal input, while overshoot is seen as powertrain torque overshoot during pedal tip-in. Torque smoothness as it relates to hybrids has been previously studied [62], with the primary focus being reduction of peak body acceleration difference (less than 3 m/s^2) on engine-motor torque transitions as well as damping low-frequency (10 Hz) oscillation. For percent overshoot, research has shown [57] that drive quality is rated favorably for lower acceleration percent overshoot, with target metric of less than 20% overshoot. These limits are summarized in Table 6.4.

Table 6.4: Torque surge and overshoot targets

Metric	Allowable	Uncomfortable
Torque Surge	< 3 m/s^2	> 3 m/s^2
Overshoot	$< 30\%$	$> 30\%$

6.2 Drive quality algorithms

By taking the set of drive quality criteria as a whole, a well-rounded and effective drive quality management strategy can be developed. Two separate algorithms are implemented

to work together to smooth out torque transitions and reduce jerk and lash on the vehicle: a rule mode transition algorithm and a pedal tip-in algorithm.

6.2.1 Mode transition algorithm

To alleviate torque holes and jerk during rule mode transitions, a torque crossfade algorithm is implemented. The crossfade triggers whenever one of the specified problematic mode transitions occurs, and it simultaneously fades the engine and motor in or out at a specified rate of 2000 Nm/s. The rate of 2000 Nm/s is chosen based on the expected limit of the smooth response time of the engine-transmission system to a torque command, and the limit may go up or down based on future in-vehicle testing results. The algorithm disengages once the engine and motor are producing torque within an error margin of the new mode torque requests. The behavior of the algorithm is shown in Figure 6.3.

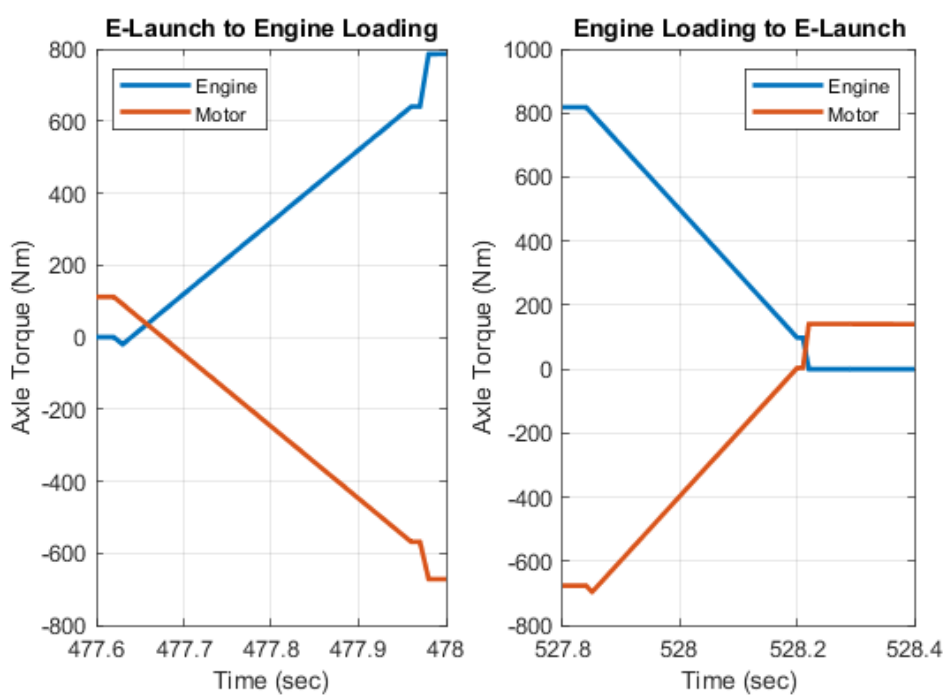

Figure 6.3: Constant speed mode transitions commanded axle torque crossfade

6.2.2 Pedal tip-in algorithm

Given the competition targets for transient acceleration during launch and the target response time of less than 0.3 seconds, a different algorithm is needed to handle torque smoothing outside of rule mode transitions. The second drive quality algorithm implements axle torque rate limits for the engine and motor torque requests, with a low-pass filter applied for smoothing, with limits shown in Table 6.5 and the Simulink implementation available in Appendix C. Rate limits are defined specifically for the motor, then for the total applied torque including both the engine and the motor. In case of total axle torque rate saturation, motor rate-limited torque takes priority, with the remaining difference in torque rate allocated to the engine.

Table 6.5: Pedal tip-in axle torque rate of change limits

Accel Pedal Percent (%)	Motor Torque Rate (Nm/s)	Total Torque Rate (Nm/s)
10	2500	2500
20	5500	5500
30	8000	8000
40	10500	11500
50	12500	14300

After the rate limit is applied, the engine and motor axle torque requests for the motor and engine are then passed through Laplace low-pass filter in the form $\frac{1}{t_c s+1}$ with the time constant $t_c = 0.05$ seconds to smooth the response.

At higher pedal positions, the allowable motor torque rate is more restrictive than the total axle torque rate. Because the electric motor has a shorter response time than a gasoline engine, the motor has a greater impact on initial acceleration and jerk. The total axle torque rate limit is chosen based on the launch performance in combination with the motor torque rates. Each rate limit was tuned with the simulation model and are anticipated to require tuning once in-vehicle test data becomes available.

6.3 Drive quality evaluation

To evaluate the performance of the drive quality algorithms, a number of ”worst case” scenarios are simulated. Primarily, the scenarios are step function changes in the accelerator pedal, forcing a step function axle torque request change, with the torque smoothing algorithms preventing spikes in vehicle jerk.

6.3.1 Launch control

The primary scenario under analysis is launch control, as this mode includes multiple rule mode transitions, high torque demand, and jerk and acceleration target metrics. The simulation is performed by holding the vehicle in idle for 2 seconds to achieve a steady engine speed, then smoothly letting off the brake pedal right before applying a step function input to the accelerator pedal, as shown in Figure 6.4. Using a shaped brake pedal curve both better simulates actual testing conditions as well as removes noise in the simulation acceleration data due to releasing the brake pedal.

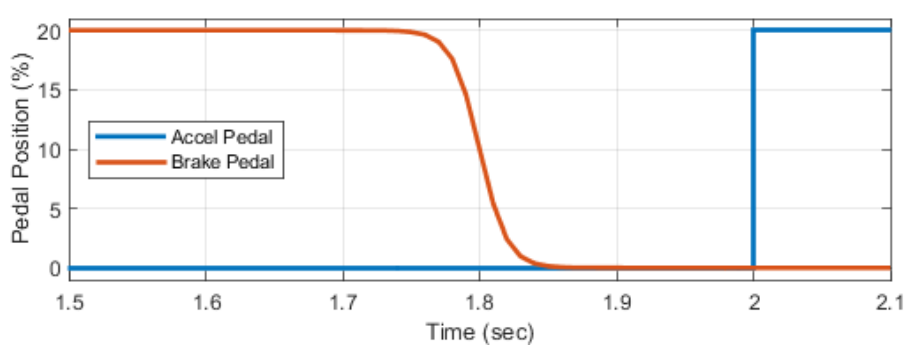

Figure 6.4: Accelerator and brake pedal inputs for launch simulations

The vehicle launch performance was evaluated at the accelerator pedal percentages defined in Table 6.1, with results for each scenario provided in Table 6.6 with and without the torque

smoothing algorithms activated. The simulated vehicle speed for each test is provided in Appendix D.

Table 6.6: Simulated peak jerk during launch simulations

Accel Pedal Percent (%)	Target Jerk (m/s^3)	With Smoothing (m/s^3)	Without Smoothing (m/s^3)
10	3.00	2.75	47.05
20	6.25	5.51	65.60
30	9.25	8.55	92.26
40	11.75	11.75	103.3
50	14.00	13.87	111.1

The effects of the added torque smoothing algorithms can easily be seen in the acceleration performance of the vehicle, with the crossfade algorithm maintaining acceleration during mode transitions and the torque rate limit algorithm maintaining reasonable and smooth launch jerk. With the torque smoothing algorithms, launch jerk is within the competition-specified ± 1 m/s^3 threshold of target, while without, the high-voltage motor produces significant jerk on the vehicle. Figure 6.5 shows the simulation results for each of the pedal inputs overlaid, with the simulation without torque smoothing shown in Figure 6.6.

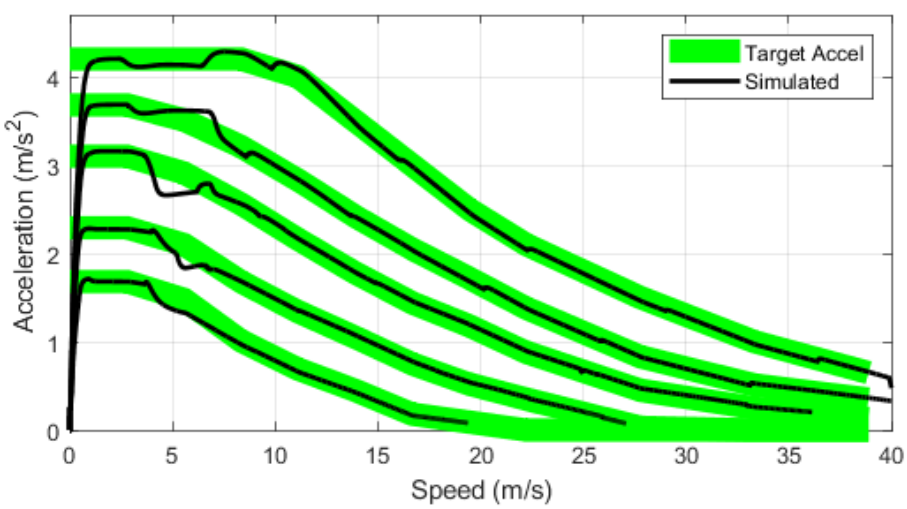

Figure 6.5: Target acceleration curve simulation with torque smoothing

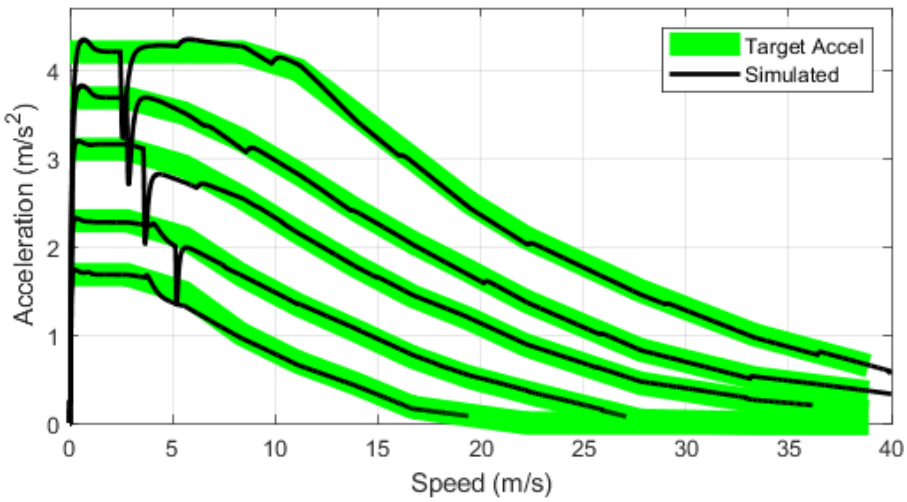

Figure 6.6: Target acceleration curve simulation without smoothing

Plots of target and actual acceleration, jerk as a function of speed, and jerk as a function of time are provided in Figure 6.7 for the simulations with the smoothing algorithms engaged and Figure 6.8 without smoothing. The top row of plots in each figure shows the vehicle acceleration compared to the target acceleration in green, the middle row shows the jerk as a function of speed with the limits from Table 6.1 in dashed lines, and the bottom row shows jerk as a function of time, with dashed lines showing the +/- 1 m/s^3 window from the target jerk.

While the smoothed case does not exactly follow the target acceleration trace, mostly due to the slower response time of the engine when switching torque requests from Performance Mode to Engine Only, it meets the jerk threshold requirements and follows the acceleration curve quite closely once the vehicle is above 10 m/s. In contrast, the unsmoothed vehicle response immediately jumps to the target acceleration, and when the modes switch from E-Launch or Performance Mode to Engine Only, the lack of torque smoothing causes a significant torque hole, where the high-voltage motor torque rapidly drops and the engine unsuccessfully attempts to fill in torque at the same rate.

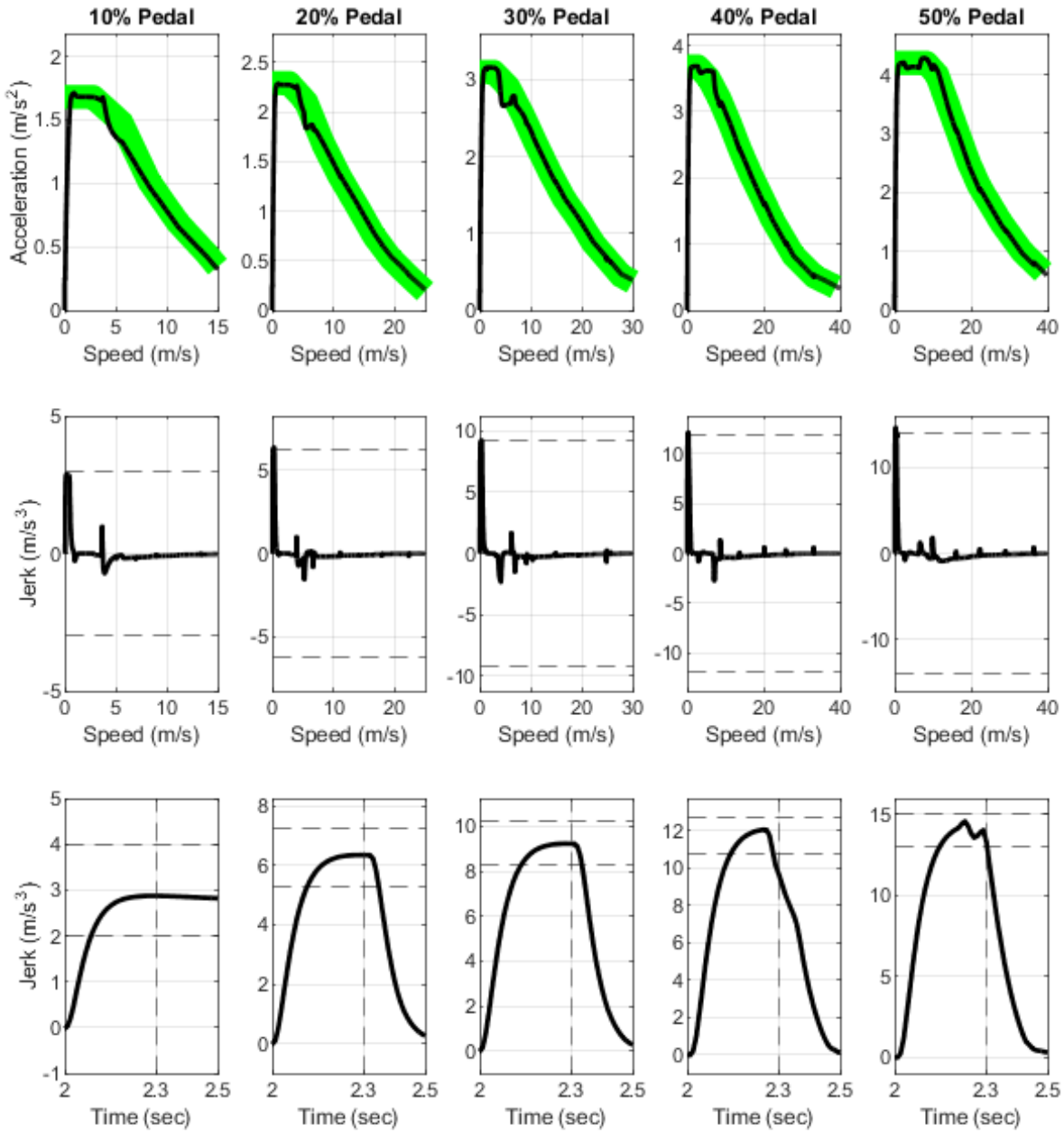

Figure 6.7: Simulated vehicle response for varying pedal inputs at launch with smoothing

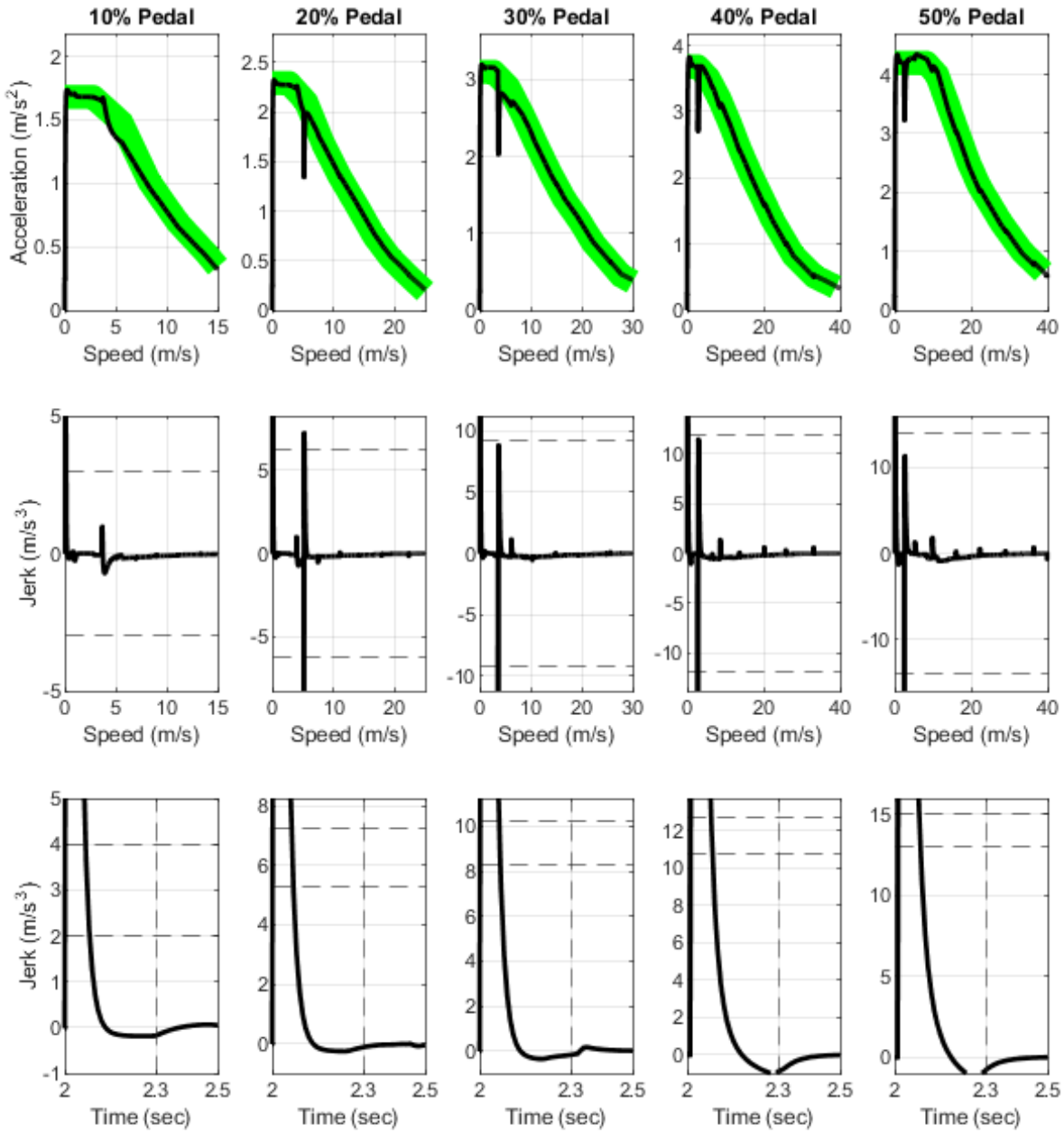

Figure 6.8: Simulated vehicle response for varying pedal inputs at launch without smoothing

6.3.2 Steady-state tip-in

The next scenario to be analyzed is maintaining an accelerator pedal input of 5% to steady-state conditions, then increasing the pedal with a step function. Pedal tip-in testing is important to ensure the torque rate limiting algorithm works outside the specific launch algorithm for which it was designed.

Lower pedal percentages have relatively smooth jerk profiles, while the higher pedals have a dual peak jerk profile. The primary reason for the difference in jerk profiles is the use of the engine in higher torque demands, causing the transmission to downshift mid-acceleration and introducing a lag, while the electric motor offers near-instantaneous response. This behavior could be mitigated by downshifting in response to the higher driver torque demand, but transmission shift control is considered future work for the purpose of this report.

While not ideal, the magnitude of jerk is well within acceptable limits, both for launch in Table 6.1 and for general jerk limits in Table 6.2.

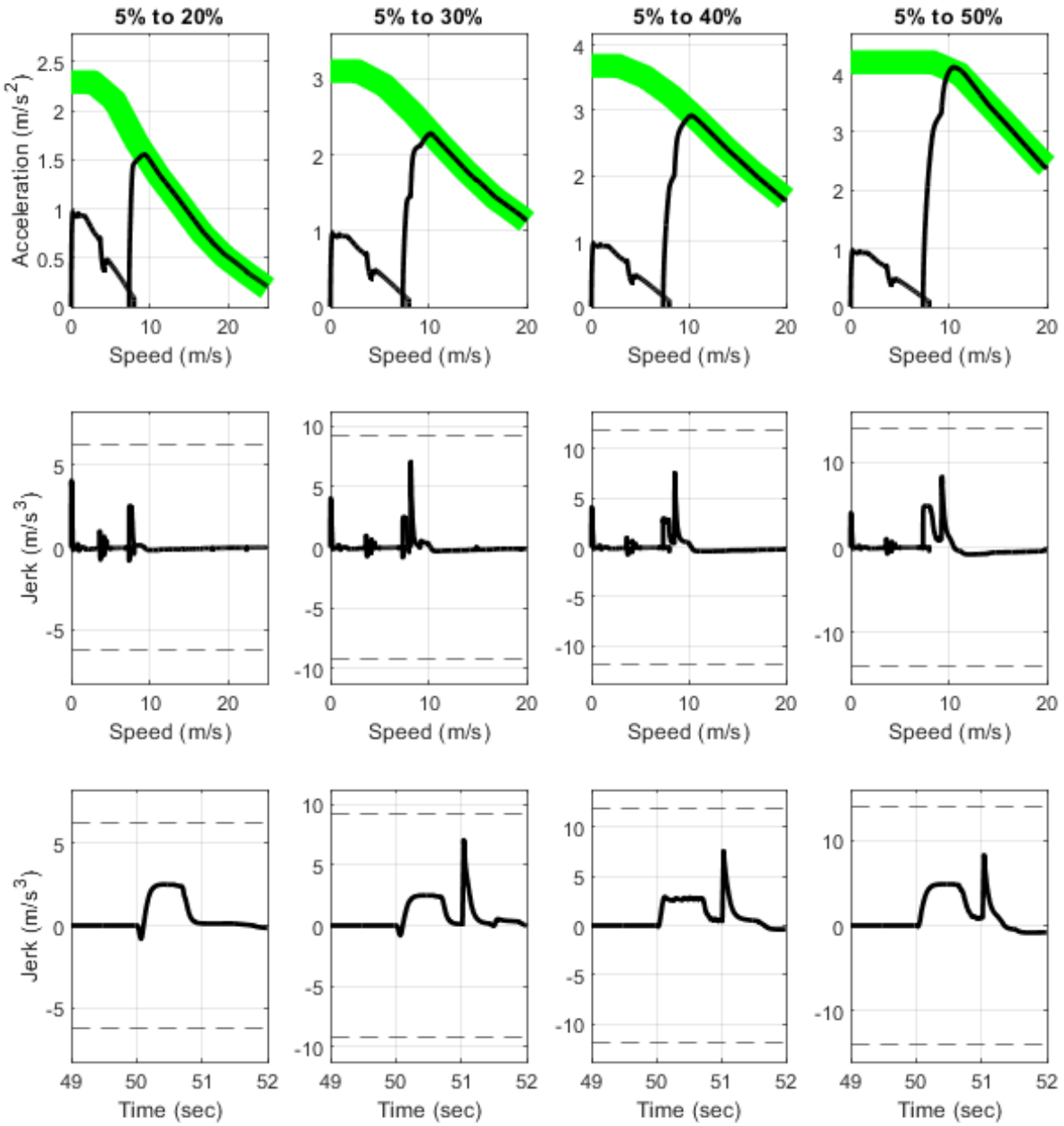

Figure 6.9: Accelerator pedal tip-in after achieving steady speed

6.3.3 Acceleration let-off

The next scenario to be analyzed is letting off the accelerator pedal during an acceleration event. The let-off test case, specifically the scenarios which cause net negative axle torque, are important for analyzing the drive quality of the one pedal algorithm previously introduced in Chapter 5.3.3.

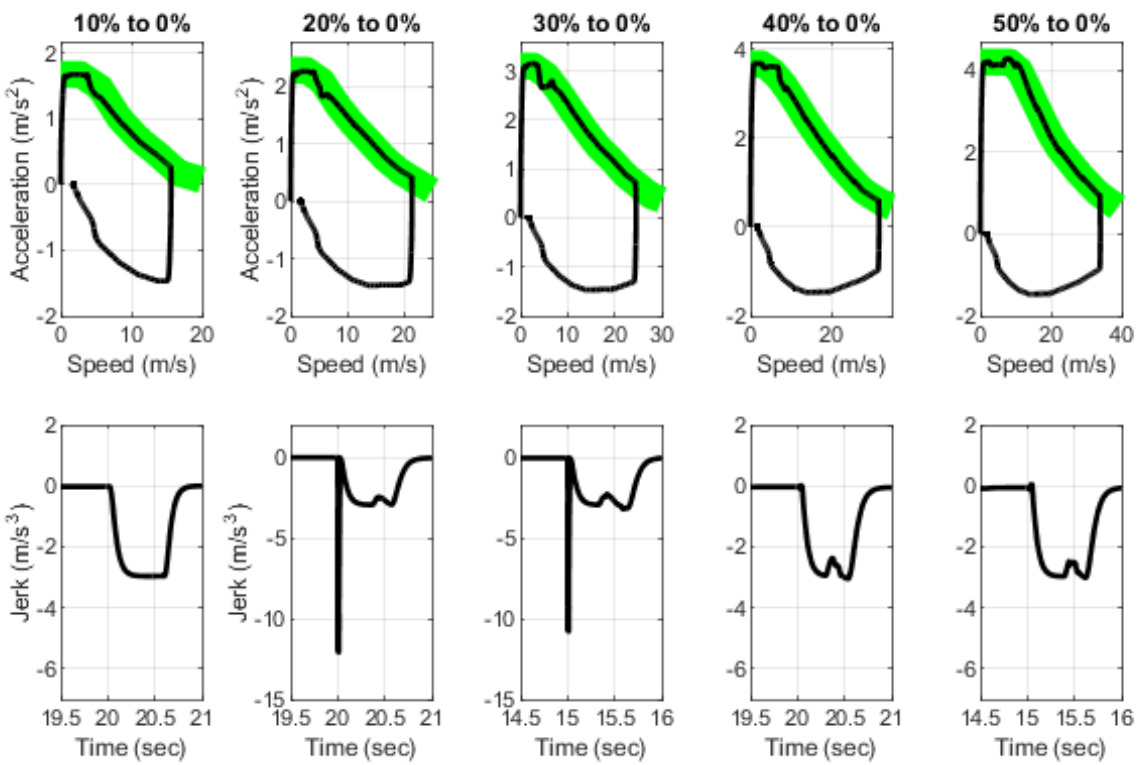

Figure 6.10: Accelerator pedal let-off to 0% from a constant pedal acceleration

Despite the step function pedal change, the drive quality torque limit algorithm is able to maintain a reasonable jerk through the transition from positive to negative net axle torque. Notably, the let-off from 20% and 30% have short duration spikes in jerk; this is due to the sudden motor engagement after operating in the Engine Only mode. The magnitude of the peak jerk for these cases is still within the reasonable neighborhood of 10 m/s^3, and because

these test cases are a "worst case" scenario, with the accelerator pedal changing as a step function, the peak jerk magnitude is acceptable.

The high jerk behavior is not present in other test cases, as summarized in Table 6.7 with plots in Appendix E, where the peak negative jerk is at or under -5 m/s^3, corresponding to the peak allowable jerk for ACC systems as shown in Table 6.3.

Table 6.7: Varying accelerator pedal let-off scenario simulation results

Start Pedal	Peak Jerk (m/s^3) Final Pedal				
	0%	5%	10%	15%	20%
10%	−2.96	-	-	-	-
20%	−12.1	−2.94	−2.74	-	-
30%	−10.8	−3.20	−2.58	−2.62	−2.28
40%	−3.04	−3.05	−2.99	−3.55	−3.55
50%	−3.01	−3.02	−3.02	−4.65	−5.04

6.3.4 Deceleration tip-in

The last scenario analyzed is pedal tip-in after decelerating with no accelerator or brake pedal inputs from 60 mph to 10 mph. The accelerator pedal input, as shown in Figure 6.11, is held at 20% until the vehicle reaches 60 mph, then released to 0% until the vehicle decelerates to 10 mph, at which point an input pedal position is tested. The brake pedal is never actuated, with the deceleration being a result of drag and one pedal regenerative braking.

The speed profile of the testing is provided in Figure 6.12, with acceleration and jerk profiles provided in Figure 6.13. Notably, the low pedal tip-in scenarios, specifically the 10% case, has a smooth velocity and jerk profile, while the more aggressive acceleration cases have lower jerk causing acceleration lag as well as the same dual-peaked jerk profiles as in the previous steady-speed cases. The effect is especially pronounced in this case due to the high

transmission gear during coast down, then the subsequent power downshift when the pedal request suddenly steps up.

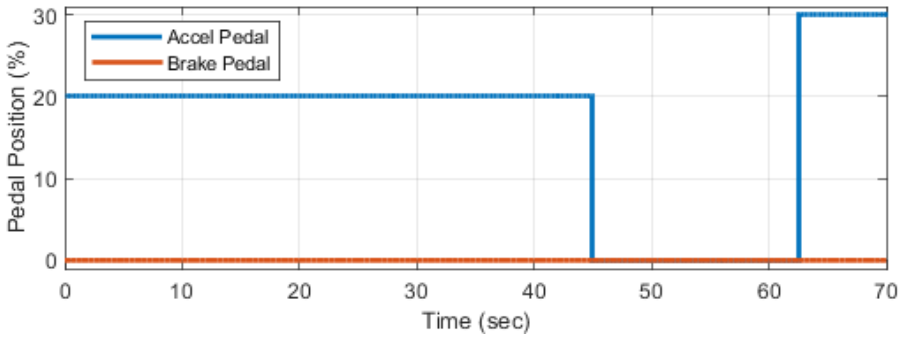

Figure 6.11: Accelerator and brake pedal inputs for deceleration to tip-in simulations

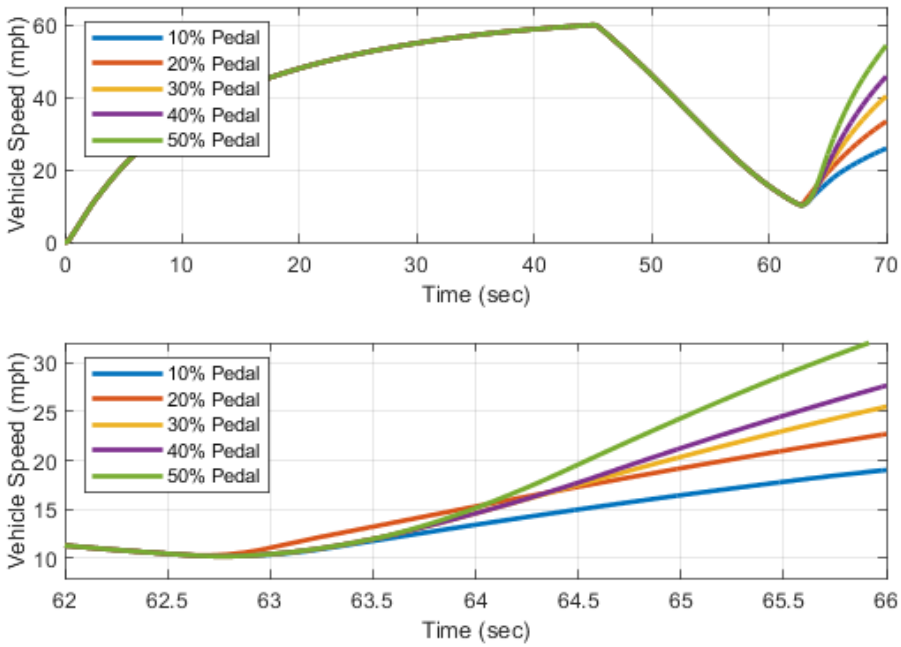

Figure 6.12: Vehicle velocity profiles for deceleration to tip-in simulations

The effect of power downshifts on the acceleration and jerk profiles could be mitigated by introducing a delay in the motor torque response to match the response time of the engine-transmission system; however, the magnitude of the jerk in the analyzed coast-down to

tip-in is still within reasonable limits. For a ”worst case” scenario with a step function input accelerator pedal change, the results are satisfactory.

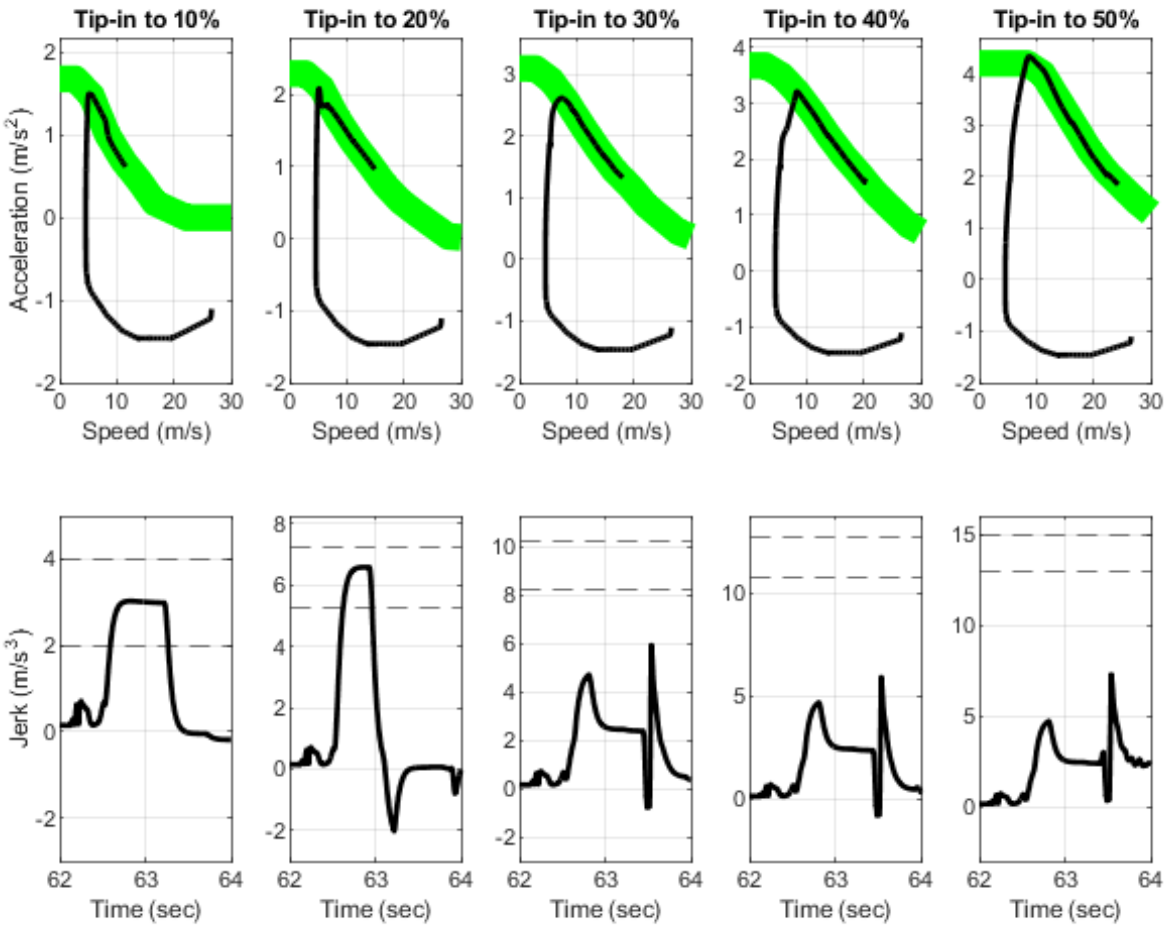

Figure 6.13: Varying deceleration to tip-in scenario simulation results

Chapter 7

Energy consumption simulation

One of the primary performance criteria for the hybrid control strategy is energy management, specifically the fuel efficiency over the EPA drive cycles. The PI driver model gains developed in Section 4.3.1 are used, along with the pchip interpolated drive cycle speed traces as further discussed in Appendix B.

The energy consumption of the vehicle is simulated, including the following model variants: the validation 2.5 L conventional model, the 2.5 L conventional model with increased hybrid mass and accessory load, and the full 2.5 L hybrid model. The parameters for each simulation model provided in Table 7.1. Results are presented, including simulated vehicle speed, battery SOC, engine and motor axle torque, control strategy mode, acceleration and jerk, and the driver accelerator and brake pedal commands for the EPA FTP Phase 3, US06, and HWFET drive cycles.

Table 7.1: Important parameters for the vehicle simulation model [38]

Parameter	Units	Stock 2.5 L	2.5 L Mass	Hybrid
Powertrain	-	ICE Only	ICE Only	Hybrid
ETW	kg	1930	2270	2270
A	N	119	156	156
B	$\frac{N}{m/s}$	3.53	1.82	1.82
C	$\frac{N}{m/s^2}$	0.55	0.589	0.589
Mechanical aux load	kW	0.83	1.3	1.3
Loaded wheel radius	m	0.36	0.36	0.36

7.1 Simulation results

Energy consumption is detailed in Table 7.2. Energy consumption as listed includes the original listed MPG for the stock vehicle and the proportional Watt-hours per mile based on Tier 2 Cert Gasoline test specification [49]. The simulated hybrid fuel economy is provided in MPG based on the competition-specified $32.3\frac{kWh}{gal}$ conversion factor, along with a more directly-comparable Watt-hours per mile figure. For the hybrid Blazer, the CS metric is listed as previously introduced in Chapter 3, with a positive value indicating a net charge of the battery, a negative value a net discharge, and a rating less than $\pm 1\%$ considered a negligable net battery energy change.

Table 7.2: Comparison of stock Blazer RS and simulated hybrid energy consumption

	Test Data		Simulated						
	Baseline 3.6 L		Stock 2.5 L		2.5 L Mass		Hybrid		
Drive cycle	mpg	$\frac{Wh}{mi}$	mpg	$\frac{Wh}{mi}$	mpg	$\frac{Wh}{mi}$	mpg	$\frac{Wh}{mi}$	CS Metric
Hot 505	26.0	1260	30.8	1090	28.6	1170	33.3	1010	-0.59%
HWFET	35.5	921	38.8	863	37.2	901	37.9	883	-0.49%
US06	21.7	1510	25.4	1320	23.5	1430	25.2	1330	$+0.38\%$

The hybrid Blazer features a nice boost in fuel economy over the Baseline 3.6 L test data. Additionally, except for a small drop in HWFET fuel economy due to increased mass, the hybrid Blazer matches or beats the Stock 2.5 L model. The hybrid Blazer has a 20% energy consumption reduction for the Hot 505, 3.6% for the HWFET, and 12% for the US06 over the baseline 3.6 L Blazer. The simulated hybrid Blazer drive cycle speed, engine and motor torque, battery SOC, and operating points and rule regions are provided below in Figures 7.1 through 7.6.

7.1.1 FTP Phase 3

The Hot 505 features a wide range of operating conditions, with the first hill completed entirely in the E-Launch region. The aggressive one pedal map allows the driver to complete a majority of the cycle with only the accelerator pedal, only needing to press the brake pedal to come to a stop. Additionally, jerk over the entire drive cycle is minimal, with a few spikes due to the vehicle coming to a stop, boding well for the expected drive quality of the control strategy on the physical prototype vehicle.

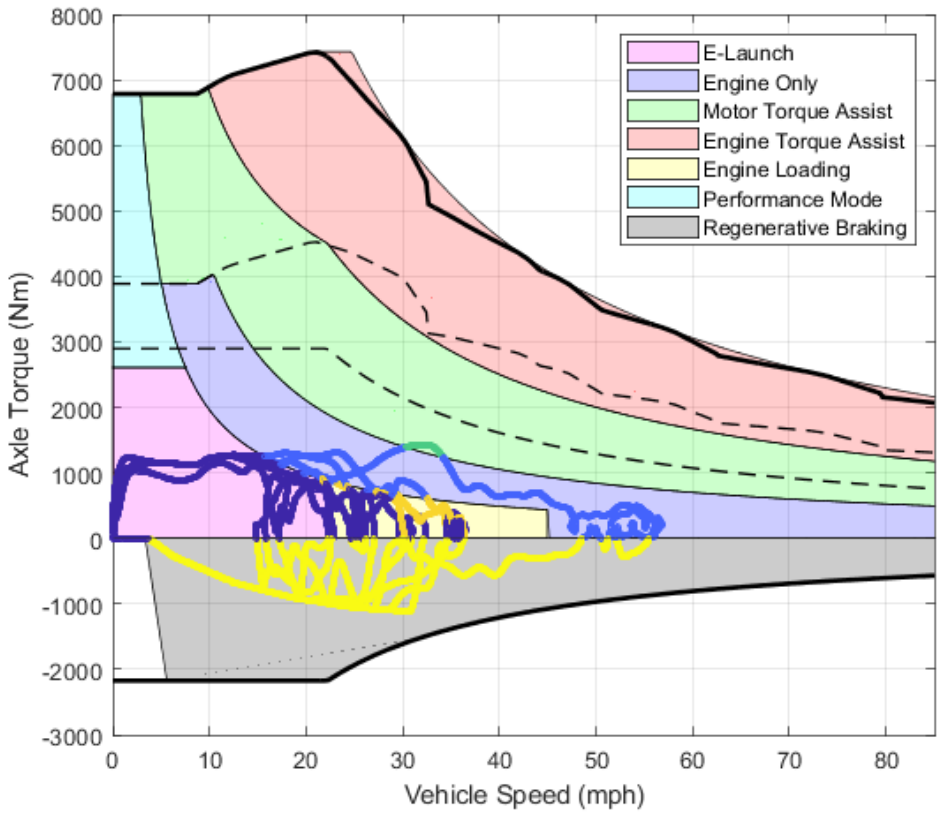

Figure 7.1: Hot 505 drive cycle operating points overlaid on Rule Regions

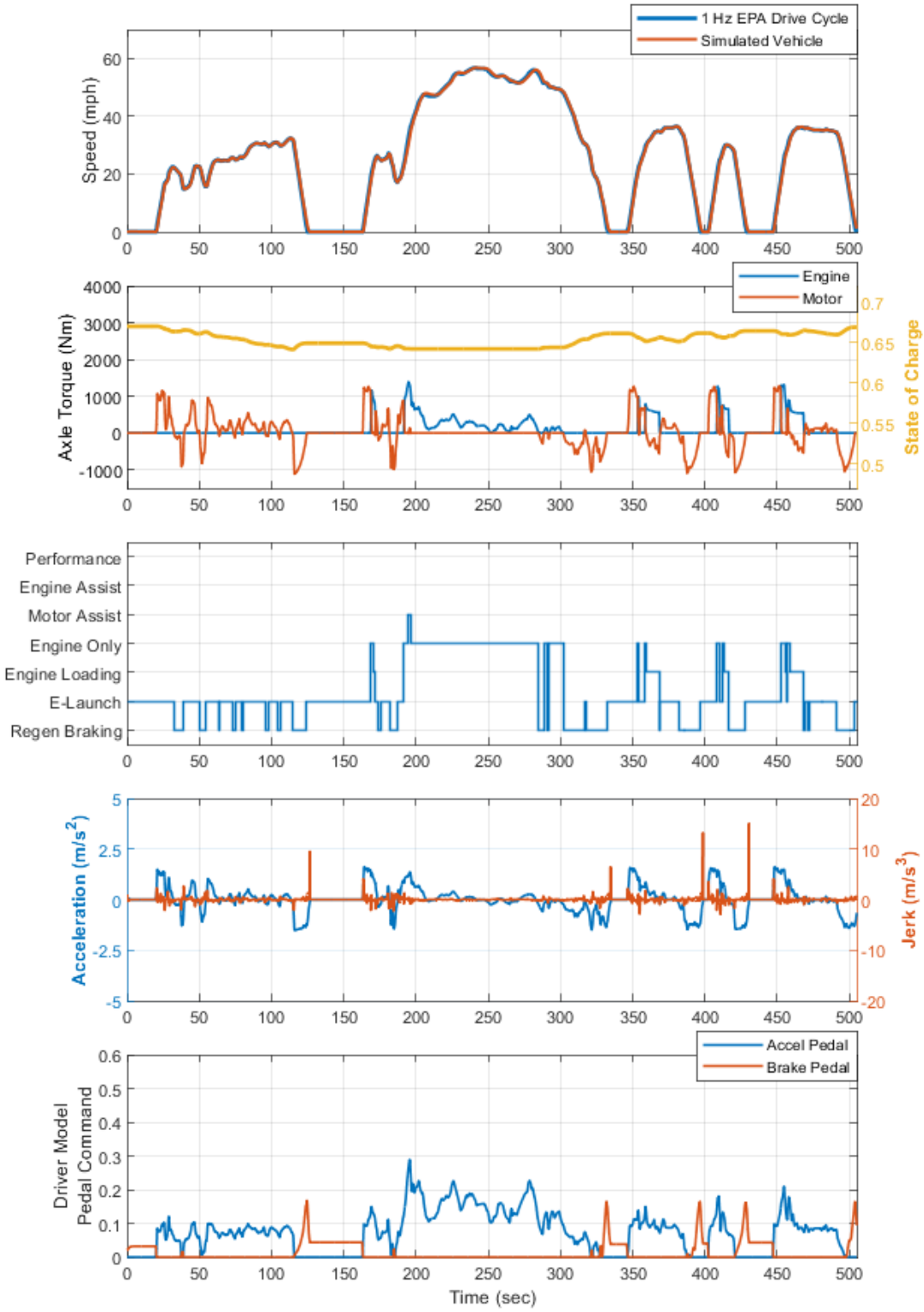

Figure 7.2: Hot 505 drive cycle simulation results

7.1.2 US06

The US06 is the most aggressive of the three drive cycles under analysis, and as such, features the highest axle torque demands, causing the vehicle to operate in the Performance Mode and Motor Torque Assist regions during acceleration events. Due to the engine cutoff speed v_{eng} being below the majority of the highway driving speeds, most of the drive cycle is spent in the Engine Only and Regenerative Braking regions, causing the charge balance SOC to be around 77%, with the safety limits from Section 5.3.4 kicking in. Additionally, despite the harsh acceleration and braking, jerk stays within reasonable limits, where most of the peaks can be attributed to vehicle stops.

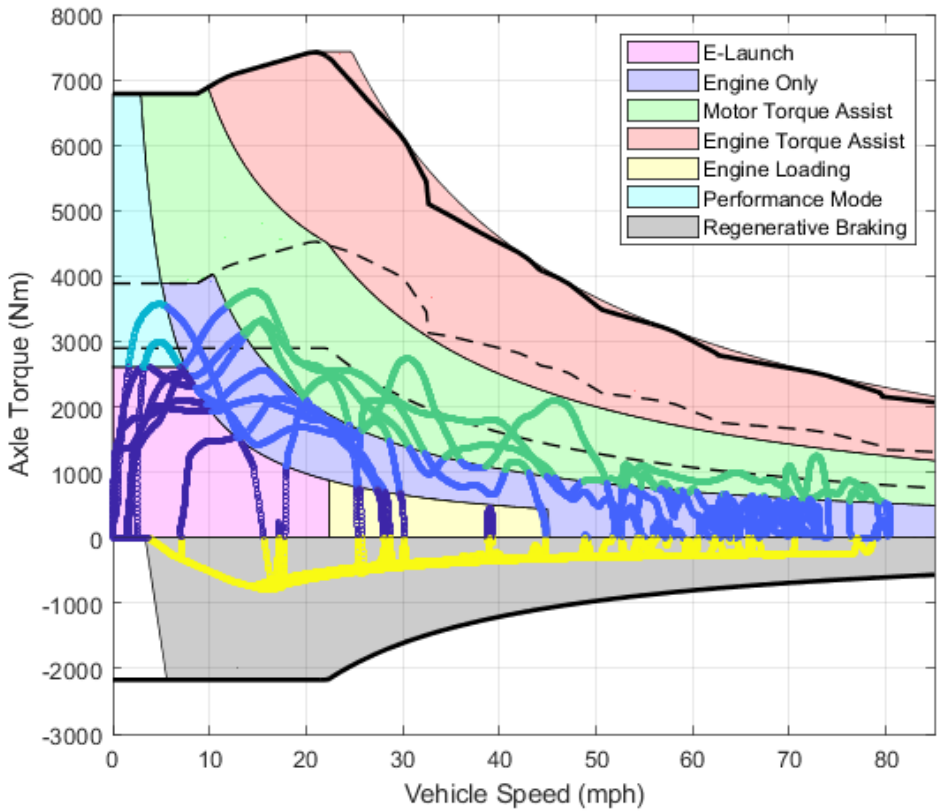

Figure 7.3: US06 drive cycle operating points overlaid on Rule Regions

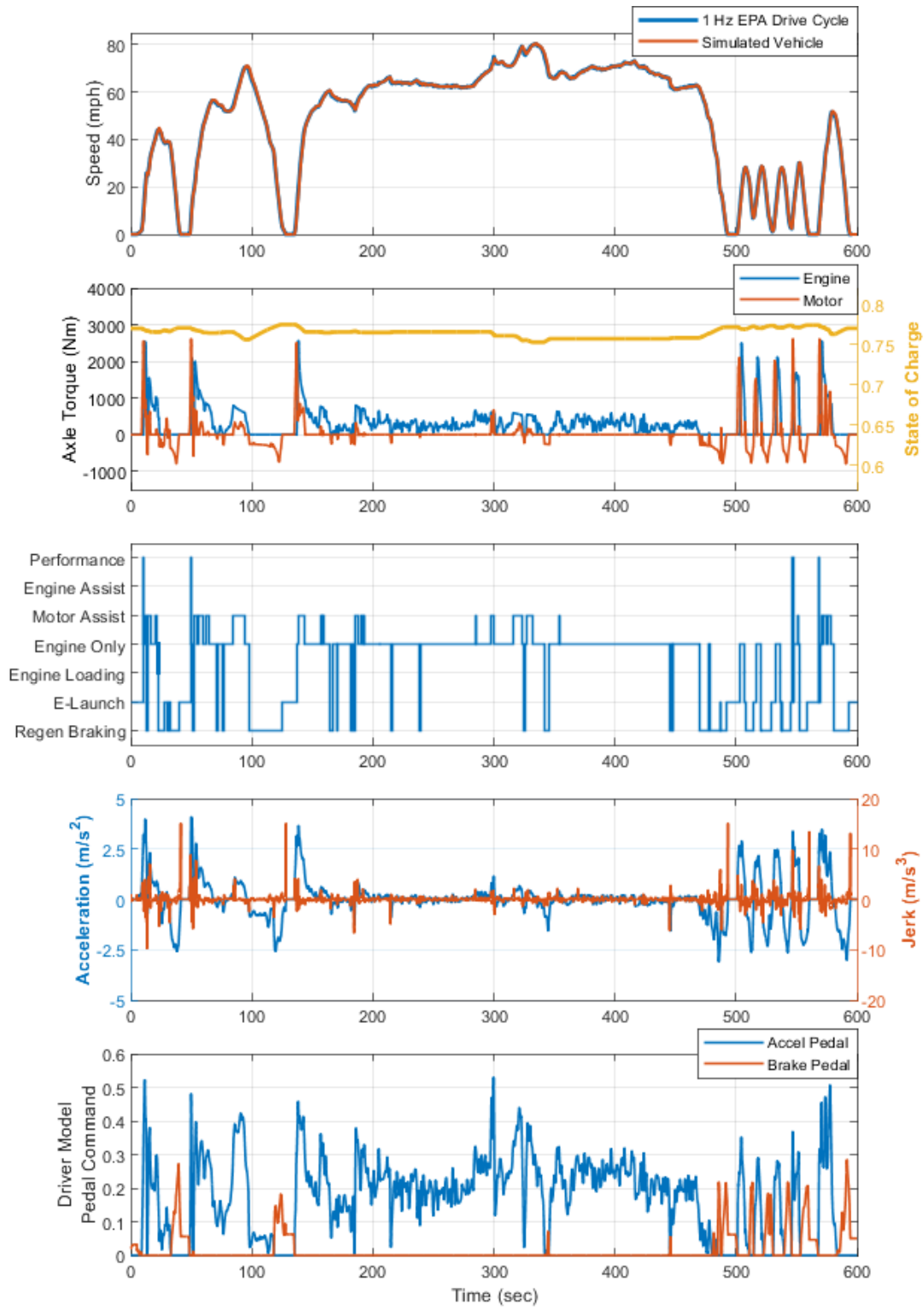

Figure 7.4: US06 drive cycle speed trace

7.1.3 HWFET

The HWFET drive cycle is interesting because it is only one hill, so the battery is discharged during the first acceleration event and charged with one pedal regenerative braking during the cycle. A majority of the time is spent in the Engine Only and Regenerative Braking regions, with the driver never having to press the brake pedal except to bring the car to a stop at the end of the cycle. The jerk is also extremely minimal throughout the cycle, with the one exception being the power downshift and Motor Torque Assist region at around 300 seconds.

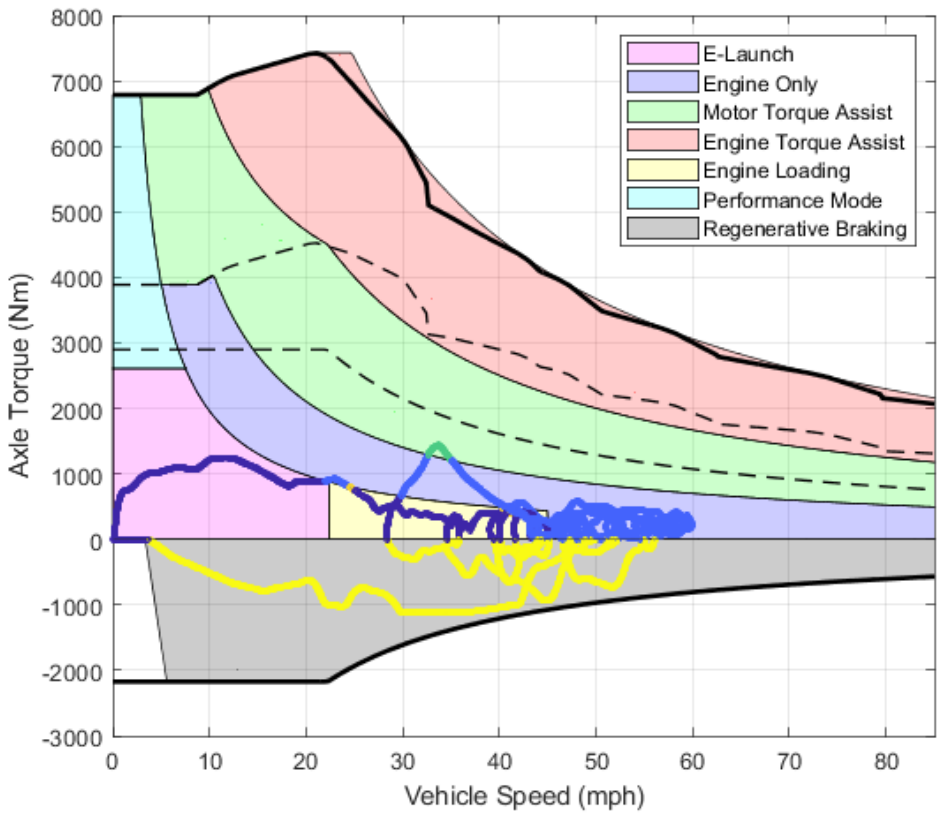

Figure 7.5: HWFET drive cycle operating points overlaid on Rule Regions

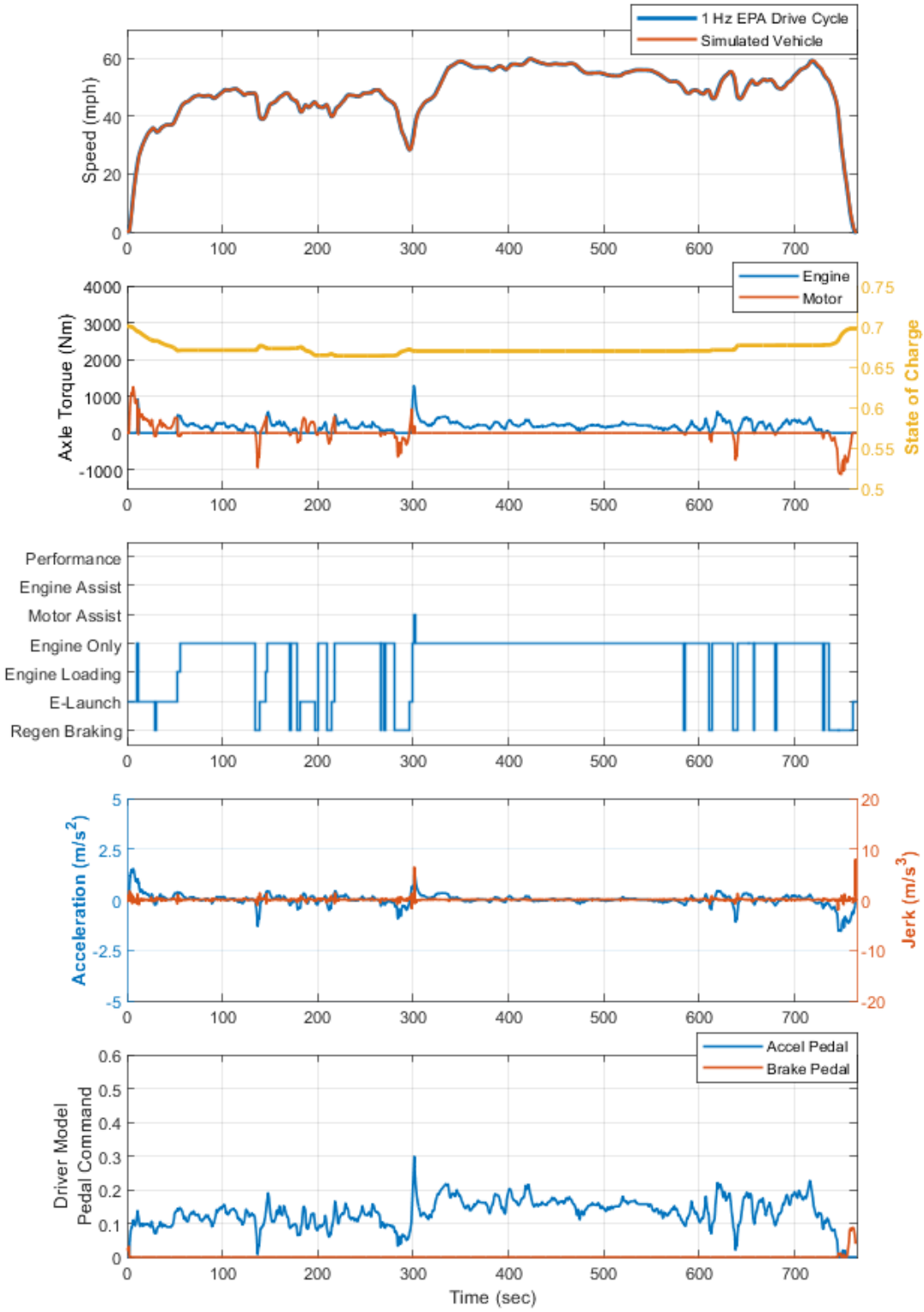

Figure 7.6: HWFET drive cycle speed trace

7.2 Sensitivity analysis

The proposed rule-based energy management strategy has a few parameters chosen to help optimize the algorithm fuel economy performance for the hybrid Blazer, specifically the lower engine efficiency threshold, η, and the Engine Loading to Engine Only cutoff speed, v_{eng}. A sensitivity analysis on the chosen parameters was performed, with results listed below.

7.2.1 Engine lower efficiency

For the Engine Only mode lower efficiency, variations of 2% from the originally selected 28% efficiency were analyzed. As shown in Figure 7.7, increases in the lower efficiency lead to large jumps in the output power, while decreasing the efficiency results in diminishing returns on increasing the size of the Engine Only powerband. The simulation results of the selected efficiency boundaries are presented in Table 7.3, with the fuel efficiency and charge sustaining metric presented for each test case.

Table 7.3: Sensitivity analysis for engine lower efficiency boundary

	$\eta = 22\%$		$\eta = 24\%$		$\eta = 26\%$		$\eta = 28\%$		$\eta = 30\%$	
Drive cycle	mpg	CS	mpg	CS	mpg	CS	mpg	CS	mpg	CS
US06	24.7	+0.15%	24.8	−0.62%	24.9	−0.21%	25.2	+0.38%	26.2	−0.64%
Hot 505	29.6	−0.55%	30.9	+0.50%	32.4	−0.07%	33.3	−0.59%	31.7	+0.52%
HWFET	35.9	−0.31%	36.1	+0.05%	36.7	−0.22%	37.9	−0.49%	36.7	+0.60%

The chosen 28% efficiency lower boundary provides a good balance between removing the low-efficiency operating points of the engine while still maintaining a reasonable engine power boundary. The primary effects of the varying lower engine power boundary is a higher loading torque in the Engine Loading region as well as a larger E-Launch region.

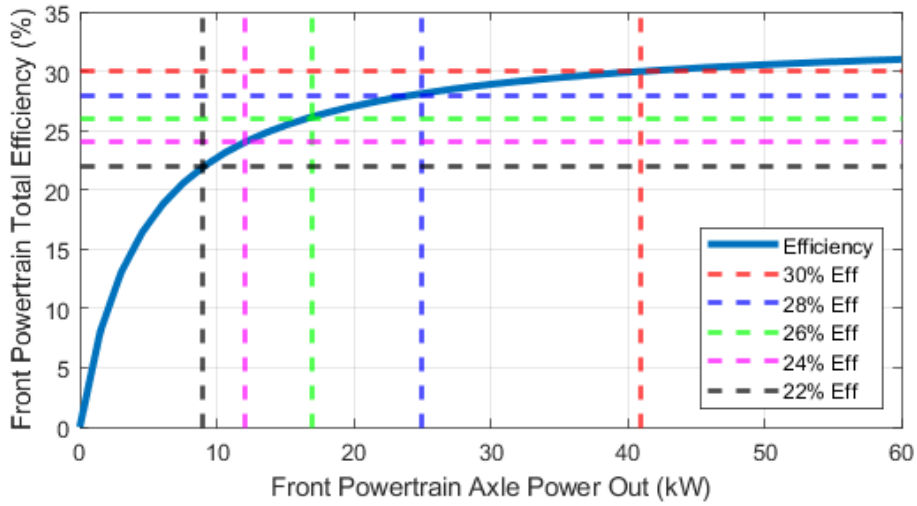

Figure 7.7: Engine lower efficiency sensitivity analysis power output

7.2.2 Engine Only speed

The second parameter is the Engine Loading to Engine Only cutoff speed, v_{eng}. Increments of 5 mph were chosen near the chosen 45 mph vehicle cutoff speed, with a focus on higher speed due to only minor changes at lower speed cutoffs. The case with no speed limit is also included, where the Engine Loading region extends outwards to the motor maximum speed of approximately 85 mph. Results are summarized in Table 7.4.

Table 7.4: Sensitivity analysis for Engine Only operation speed

	$v_{eng} = 40$ mph		$v_{eng} = 45$ mph		$v_{eng} = 50$ mph		$v_{eng} = 55$ mph		No limit	
Drive cycle	mpg	CS	mpg	CS	mpg	CS	mpg	CS	mpg	CS
US06	25.1	−0.18%	25.2	+0.38%	25.2	−0.22%	25.2	−0.24%	26.0	−0.11%
Hot 505	33.3	+0.18%	33.3	−0.59%	33.3	+0.18%	33.0	−0.4%	33.8	−0.89%
HWFET	37.7	+0.31%	37.9	−0.49%	37.2	−0.37%	36.1	+0.60%	34.7	−0.52%

Generally, the differences between the three drive cycles and how they are affected by the changing Engine Loading cutoff speed can be seen in the MIL simulation results plots in Figures 7.1, 7.3, and 7.5, specifically noting the operating points near the zero torque x-axis.

Comparing the ”45 mph” to ”No limit” cases, the Hot 505 has a negligible difference, the HWFET gains around 3 mpg, and the US06 loses around 1 mpg. The HWFET, being a relatively mild drive cycle, benefits from the 9-speed transmission and engine DFCO, maintaining top gear through the majority of the cycle. On the other hand, US06 has a higher fuel economy when there is no limit on electric motor operation, as the aggressive drive cycle benefits from the available motor torque assist near zero torque.

Chapter 8

Conclusion

As a part of the EcoCAR Mobility Challenge engineering design competition, HEVT was tasked with converting a stock 3.6 L Chevrolet Blazer RS into a hybrid electric vehicle. The engine was downsized to a 2.5 L engine, and a high-voltage powertrain was integrated using the best available combination from a limited selection of components.

A model for the conventional driveline including a 2.5 L engine and 9-speed transmission was developed. A model validation procedure for a control development process without access to a functional prototype vehicle was proposed using EPA test car list data including analysis of the driver model, engine model including accessory load, drive cycle speed trace miss criteria, and the SAE J2951 drive cycle parameters. The US06, HWFET, and FTP Phase 3 drive cycles were simulated, and the energy consumption data have 5% error or less for each analyzed validation case.

A Willans line model for the front powertrain was developed including the engine, transmission, and 12 V accessory load. A rule-based control strategy was proposed, with a region of optimal engine operation derived based on the combined Willans line model. Two algorithms for battery SOC management were proposed within the framework of the rule-based strategy, and a one pedal regenerative braking strategy was developed. Additionally, two algorithms for drive quality were proposed to meet the researched drive quality metrics, with vehicle response analyzed in a wide variety of worst-case scenarios to ensure viability and favorable response demonstrated in each case within the scope of the hybrid control system.

Despite including considerations for battery state of charge and drive quality management, the proposed hybrid energy management strategy has a 20% energy consumption reduction for the Hot 505, 3.6% for the HWFET, and 12% for the US06 over the baseline 3.6 L Blazer, with charge-sustaining hybrid behavior remaining within the allowable 30% to 80% SOC limits and with jerk and acceleration meeting competition targets and remaining within industry limits for each EPA drive cycle. The hybrid control strategy, including the energy management strategy, battery SOC management algorithms, and drive quality algorithms, is a well-rounded set of code ready for in-vehicle testing.

8.1 Future work

Because the proposed energy management strategy was developed completely in a simulation environment, the control system can be improved in multiple ways once the functional prototype hybrid Blazer is available in Year 4 of the EcoCAR competition. Multiple procedures must be completed, including model validation using test data correlation using defined methods [48], tuning the axle torque pedal maps for actual vehicle acceleration response, tuning the drive quality torque rate limit algorithms for actual vehicle powertrain response time, and modifying the pedal map to account for vehicle DFCO drag torque from the engine.

References

[1] W. Zhuang et al. "A survey of powertrain configuration studies on hybrid electric vehicles". In: *Applied Energy* 262.1 (2020), pp. 1–17.

[2] D. S. Cardoso, P. O. Fael, and A. Espírito-Santo. "A review of micro and mild hybrid systems". In: *6th International Conference on Energy and Environment Research* (Aveiro, Portugal). ICEER, July 2019, pp. 385–390.

[3] A. Kooy and J. Kroll. "Drive Train Vibrations: Solving the Conflict Between Efficiency and Drivability". In: *Proceedings of the FISITA 2012 World Automotive Congress*. Vol. 193. SAE China, FISITA. Berlin, Heidelberg: Springer, Nov. 2012, pp. 49–61.

[4] K. Ahn and P. Y. Papalambros. "Engine optimal operation lines for power-split hybrid electric vehicles". In: *Journal of Automobile Engineering* 223.9 (2009), pp. 1149–1162.

[5] T. Hofman and M. Steinbuch. "Rule-based energy management strategies for hybrid vehicles". In: *International Journal of Electric and Hybrid Vehicles* 1.1 (2007), pp. 71–94.

[6] Y. Meng and P. Currier. "A system efficiency approach to parallel hybrid control strategies". In: *International Automotive Engineering Congress* (Detroit, Michigan). SAE, Jan. 2016, pp. 1–10.

[7] Y. Kim et al. "Hardware-in-the-loop validation of a power management strategy for hybrid powertrains". In: *Control Engineering Practice* 29.1 (2014), pp. 277–286.

[8] D. Zhang, C. Xiang, and L. Han. "Design and Performance Prediction of a Tri-Mode Power-Split Transmission". In: *Proceedings of the FISITA 2012 World Automotive*

Congress. Vol. 193. SAE China, FISITA. Berlin, Heidelberg: Springer, Nov. 2012, pp. 93–105.

[9] M. Jungen et al. "Analytical Methodology to Derive a Rule-Based Energy Management System Enabling Fuel-Optimal Operation for a Series Hybrid". In: *2020 SAE Powertrains, Fuels and Lubricants Meeting*. SAE, Sept. 2020, pp. 1–11.

[10] S. J. Reinsel. "Drive Quality Improvement and Calibration of a Post-Transmission Parallel Hybrid Electric Vehicle". MA thesis. Virginia Polytechnic Institute and State University, June 2018.

[11] C. Tollefson et al. "Analysis of connected and automated hybrid electric vehicle energy consumption and drive quality". In: *SAE International Journal of Electrified Vehicles* 10.1 (2020), pp. 1–15.

[12] B. Halvorson. "First drive review: 2021 Toyota Venza hybrid reinterprets the marketm iddle at 39 mpg". In: *Green Car Reports* (Aug. 4, 2020). URL: https://www.greencarreports.com/news/1129119_first-drive-review-2021-toyota-venza-hybrid-reinterprets-the-market-middle-at-39-mpg.

[13] B. Halvorson. "2020 Ford Escape revealed: hybrid returns teasing-nearly 40 mpg plug-in with 30 electric miles". In: *Green Car Reports* (Apr. 2, 2019). URL: https://www.greencarreports.com/news/1122398_2020-ford-escape-revealed-hybrid-returns-teasing-nearly-40-mpg-plug-in-with-30-electric-miles.

[14] D. Sherman. "2017 Acura MDX Sport Hybrid". In: *Car and Driver* (May 26, 2017). URL: https://www.caranddriver.com/reviews/a15094505/2017-acura-mdx-sport-hybrid-test-review.

[15] J. Voelcker. "2017 Acura MDX Sport Hybrid SH-AWD first drive review". In: *Motor Authority* (Apr. 8, 2017). URL: https://www.motorauthority.com/news/1109705_2017-acura-mdx-sport-hybrid-sh-awd-first-drive-review.

[16] S. Oldham and M. Sutton. "Tested: 2020 Honda CR-V Hybrid Can't Match the Toyota RAV4 Hybrid's Fuel Economy". In: *Car and Driver* (June 9, 2020). URL: https://www.caranddriver.com/reviews/a31679395/2020-honda-cr-v-hybrid-drive/.

[17] B. Halvorson. "First drive review: 2020 Honda CR-V hybrid teases an EV experience with no charge port". In: *Green Car Reports* (Mar. 17, 2020). URL: https://www.greencarreports.com/news/1127475_first-drive-review-2020-honda-cr-v-hybrid-teases-an-ev-experience-with-no-charge-port.

[18] E. Dyer. "2021 Kia Sorento Is Compelling in Hybrid Form". In: *Car and Driver* (Dec. 29, 2020). URL: https://www.caranddriver.com/reviews/a35086183/2021-kia-sorento-hybrid-drive/.

[19] B. Halvorson. "First drive review: 2021 Kia Sorento Hybrid beats Highlander Hybrid with 37 mpg and better tech, but it's no Telluride". In: *Green Car Reports* (Mar. 1, 2021). URL: https://www.greencarreports.com/news/1131433_first-drive-review-2021-kia-sorento-hybrid-beats-highlander-hybrid-with-37-mpg-and-better-tech-but-it-s-no-telluride.

[20] J. Lorio. "2016 Lexus RX450h F Sport AWD". In: *Car and Driver* (May 4, 2016). URL: https://www.caranddriver.com/reviews/a15101161/2016-lexus-rx450h-hybrid-awd-test-review/.

[21] B. Halvorson. "2016 Lexus RX Hybrid F Sport First Drive". In: *Green Car Reports* (Sept. 9, 2015). URL: https://www.greencarreports.com/news/1099941_2016-lexus-rx-hybrid-f-sport-first-drive.

[22] B. Škugor et al. “Design of a power-split hybrid electric vehicle control system utilizing a rule-based controller and an equivalent consumption minimization strategy”. In: *Journal of Automobile Engineering* 228.6 (2014), pp. 631–648.

[23] B. Škugor, D. Pavković, and J. Deur. “A Series-Parallel Hybrid Electric Vehicle Control Strategy Including Instantaneous Optimization of Equivalent Fuel Consumption”. In: *IEEE Conference on Control Technology and Applications* (Dubrovnik, Croatia). IEEE, Oct. 2012, pp. 310–316.

[24] J. Wu et al. “An optimized real-time energy management strategy for the power-split hybrid electric vehicles”. In: *IEEE Transactions on Control Systems Technology* 27.3 (2018), pp. 1194–1202.

[25] N. Al-Aawar and A. A. Arkadan. “Driveability Optimization of HEV Powertrain”. In: *2019 International Applied Computational Electromagnetics Society Symposium (ACES)* (Miami, Florida). IEEE, Apr. 2019, pp. 1–2.

[26] R. E. Bellman. *Dynamic Programming*. Princeton University Press, 1957.

[27] J. Wang et al. “Hybrid electric vehicle modeling accuracy verification and global optimal control algorithm research”. In: *International Journal of Automotive Technology volume* 16.1 (2015), pp. 513–524.

[28] D. Goerke et al. “Optimal Control based Calibration of Rule-Based Energy Management for Parallel Hybrid Electric Vehicles”. In: *International Automotive Engineering Congress* (Detroit, Michigan). SAE, July 2015, pp. 178–189.

[29] A. Sciarretta, G. De Nunzio, and L. L. Ojeda. “Optimal ecodriving control: energy-efficient driving of road vehicles as an optimal control problem”. In: *IEEE Control Systems Magizine* 10.1 (2015), pp. 71–90.

[30] O. Sundström, D. Ambühl, and L. Guzzella. "On Implementation of Dynamic Programming for Optimal Control Problems with Final State Constraints". In: *Oil and Gas Science and Technology* 65.1 (2010), pp. 91–102.

[31] L. Engbroks et al. "Combined energy and thermal management for plug-in hybrid electric vehicles - analyses based on optimal control theory". In: *IFAC-PapersOnLine* 52.5 (2019), pp. 610–617.

[32] A. Sciarretta, M. Back, and L. Guzzella. "Optimal Control of Parallel Hybrid Electric Vehicles". In: *IEEE Transactions on Control Systems Technology* 12.3 (2004), pp. 352–363.

[33] C. R. Tollefson. "Willans Line Based Equivalent Consumption Minimization Strategy for Charge Sustaining Hybrid Electric Vehicle". MA thesis. Virginia Polytechnic Institute and State University, Sept. 2020.

[34] K. Gökce and A. Ozdemir. "An instantaneous optimization strategy based on efficiency maps for internal combustion engine/battery hybrid vehicles". In: *Energy Conversion and Management* 81.1 (2014), pp. 255–269.

[35] T. Nüesch et al. "Convex Optimization for the Energy Management of Hybrid Electric Vehicles Considering Engine Start and Gearshift Costs". In: *Energies* 7.2 (2014), pp. 834–856.

[36] U.S. Environmental Protection Agency. "U.S. Code of Federal Regulations: Title 40: Chapter I: Subchapter U: Part 1066 - Vehicle Testing Procedures". In: (2021). https://www.ecfr.gov/cgi-bin/text-idx?SID=ba447754d6f766672ab21e5aa4146283&mc=true&node=pt40.33.1066&rgn=div5.

[37] S. International. "Surface Vehicle Recommended Practice: Road Load Measurement Using Onboard Anemometry and Coastdown Techniques". In: (2020).

[38] EPA. *2019 Test Car List Data*. 2020. URL: https://www.epa.gov/compliance-and-fuel-economy-data/data-cars-used-testing-fuel-economy (visited on 01/12/2021).

[39] S. J. Pachernegg. "A closer look at the Willans-Line". In: *International Automotive Engineering Congress* (Detroit, Michigan). SAE, Jan. 1969, pp. 1–12.

[40] EPA. *EPA Engine ALPHA Maps*. 2021. URL: https://www.epa.gov/vehicle-and-fuel-emissions-testing/combining-data-complete-engine-alpha-maps (visited on 02/15/2021).

[41] P. Phlips et al. "Unified Power-Based Vehicle Fuel Consumption Model Covering a Range of Conditions". In: *SAE International Journal of Advances and Current Practices in Mobility* 4.2 (2020), pp. 2320–2336.

[42] L. Doffe and M. Kadiri. "Alternator contribution to CO2 emission reduction policies". In: *XIX International Conference on Electrical Machines* (Rome, Italy). ICEM, Sept. 2010, pp. 1504–1509.

[43] J. Kessels et al. "Energy management for vehicle power net with flexible electric load demand". In: *2005 IEEE Conference on Control Applications* (Toronto, Canada). IEEE, Aug. 2005, pp. 1504–1509.

[44] U.S. Congress. *Public Law 91-6904: Clean Air Amendments of 1970*. 1970.

[45] *EPA-420-R-95-102: Final Technical Report on Aggressive Driving Behavior for the Revised Federal Test Procedure Notice of Proposed Rulemaking*. Tech. rep. Environmental Protection Agency, 1995.

[46] *79 FR 23413: Control of Air Pollution From Motor Vehicles: Tier 3 Motor Vehicle Emission and Fuel Standards; Final Rule*. Regulatory Information. https://www.

govinfo.gov/app/details/FR-2014-04-28/2014-06954. Environmental Protection Agency, 2014.

[47] *SAE J2951: Surface Vehicle Recommended Practice: Drive Quality Evaluation for Chassis Dynamometer Testing*. Standard. SAE International, 1995.

[48] Y. Meng et al. "Test Correlation Framework for Hybrid Electric Vehicle System Model". In: *SAE 2011 World Congress and Exhibition* (Detroit, Michigan). SAE, Jan. 2011, pp. 1–12.

[49] *Certification Summary Information Report*. Tech. rep. EPA, 2020.

[50] J. Larminie and J. Lowry. *Electric Vehicle Technology Explained*. 2nd ed. Wiley, Sept. 2012.

[51] R. A. Kulas, H. Rieland, and J. Pechauer. "A System Safety Perspective into Chevy Bolt's One Pedal Driving". In: *WCX SAE World Congress Experience* (Detroit, Michigan). SAE, Apr. 2019, pp. 1–6.

[52] H. O. List and P. Schoeggl. "Objective Evaluation of Vehicle Driveability". In: *SAE World Congress and Exhibition* (Detroit, Michigan). SAE, Feb. 1998, pp. 1–9.

[53] C. Fang et al. "Driveline Modelling Analysis for Active Driveability Control". In: *2013 IEEE Conference on Systems, Process and Control* (Kuala Lumpur, Malaysia). IEEE, Dec. 2013, pp. 124–128.

[54] A. Albers et al. "Influence of Low-Frequency Powertrain Vibrations on Driveability Assessments". In: *6th International Styrian Noise, Vibration and Harshness Congress - Sustainable NVH solutions inspired by ecology and economy* (Paris, France). SAE International, June 2010, pp. 1–12.

[55] X. Wei and G. Rizzoni. "Objective Metrics of Fuel Economy, Performance and Driveability – A Review". In: *SAE World Congress* (Detroit, Michigan). SAE, Mar. 2004, pp. 1–8.

[56] J. Zehetner et al. "Simulation of Driveability in Real-time". In: *SAE World Congress and Exhibition* (Detroit, Michigan). SAE, Mar. 2009, pp. 1–7.

[57] R. E. Dorey and C. B. Holmes. "Vehicle Driveability - Its Characterisation and Measurement". In: *SAE International Congress and Exposition* (Detroit, Michigan). SAE, Mar. 1999, pp. 1–6.

[58] Q. Huang and H. Wang. "Fundamental Study of Jerk: Evaluation of Shift Quality and Ride Comfort". In: *SAE Automotive Dynamics, Stability and Controls Conference and Exhibition* (Detroit, Michigan). SAE, May 2004, pp. 1–8.

[59] A. Deshmukh et al. "Study of Frequency Characteristics of Vehicle Motions for the Derivation of Inherent Jerk". In: *SAE World Congress and Exhibition* (Detroit, Michigan). SAE, Apr. 2016, pp. 1–7.

[60] J. L. Stout. "Idle Combustion Smoothness". In: *SAE 2009 Noise and Vibration Conference and Exhibition* (St. Charles, Illinois). SAE, May 2009, pp. 1–6.

[61] *ISO 15622:2018 - Intelligent transport systems — Adaptive cruise control systems — Performance requirements and test procedures*. Standard. International Organization for Standardization, 2018.

[62] K. Moriya et al. "Design of the Surge Control Method for the Electric Vehicle Powertrain". In: *2002 Future Car Congress* (Arlington, Virginia). SAE, June 2002, pp. 1–6.

Appendices

Appendix A

Auxiliary load

To model the effect of the added 12 V controllers in the hybrid Blazer on the energy consumption of the vehicle, the stock 12 V system must first be analyzed. The stock alternator electrical load as measured after a hot start is shown in Figure A.1, and the averaged steady-state current is used as the baseline current for the system.

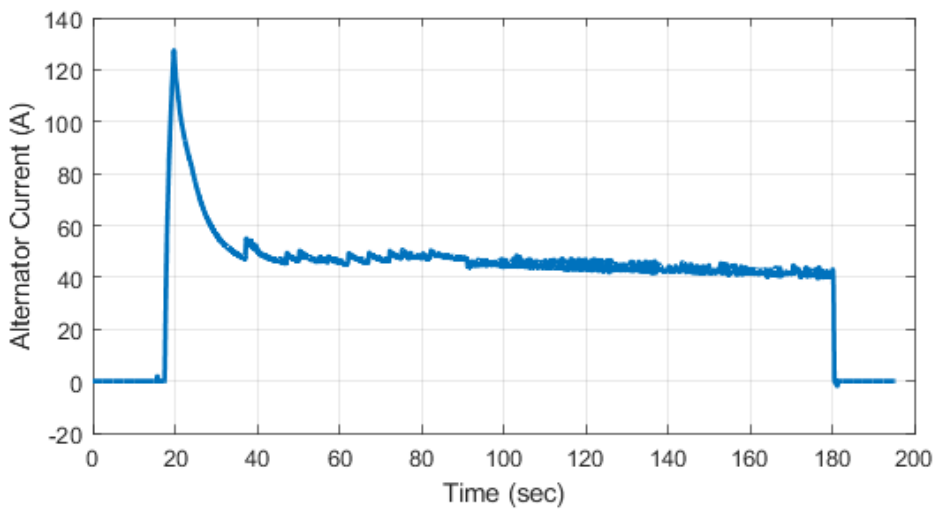

Figure A.1: Stock Blazer RS hot start and idle measured alternator 12 V current

Appendix B

Drive cycle 100 Hz smoothing

In order to accurately simulate the performance of a vehicle, including energy consumption and drive quality, creating a relatively accurate estimate of a human driver is important. While a PI driver model is a favorable solution due to easy tuning and predictable response, a PI driver can react poorly to linearly interpolated input data, as sharp peaks in the input data lead to sharp changes in pedal request output, as shown in Figure B.1. To mitigate the issues with linear interpolation and smooth out the response of the driver model, the MATLAB "pchip" interpolation method is proposed, with minimal error introduced compared to the EPA chosen linear interpolation method, as shown in Figure B.2.

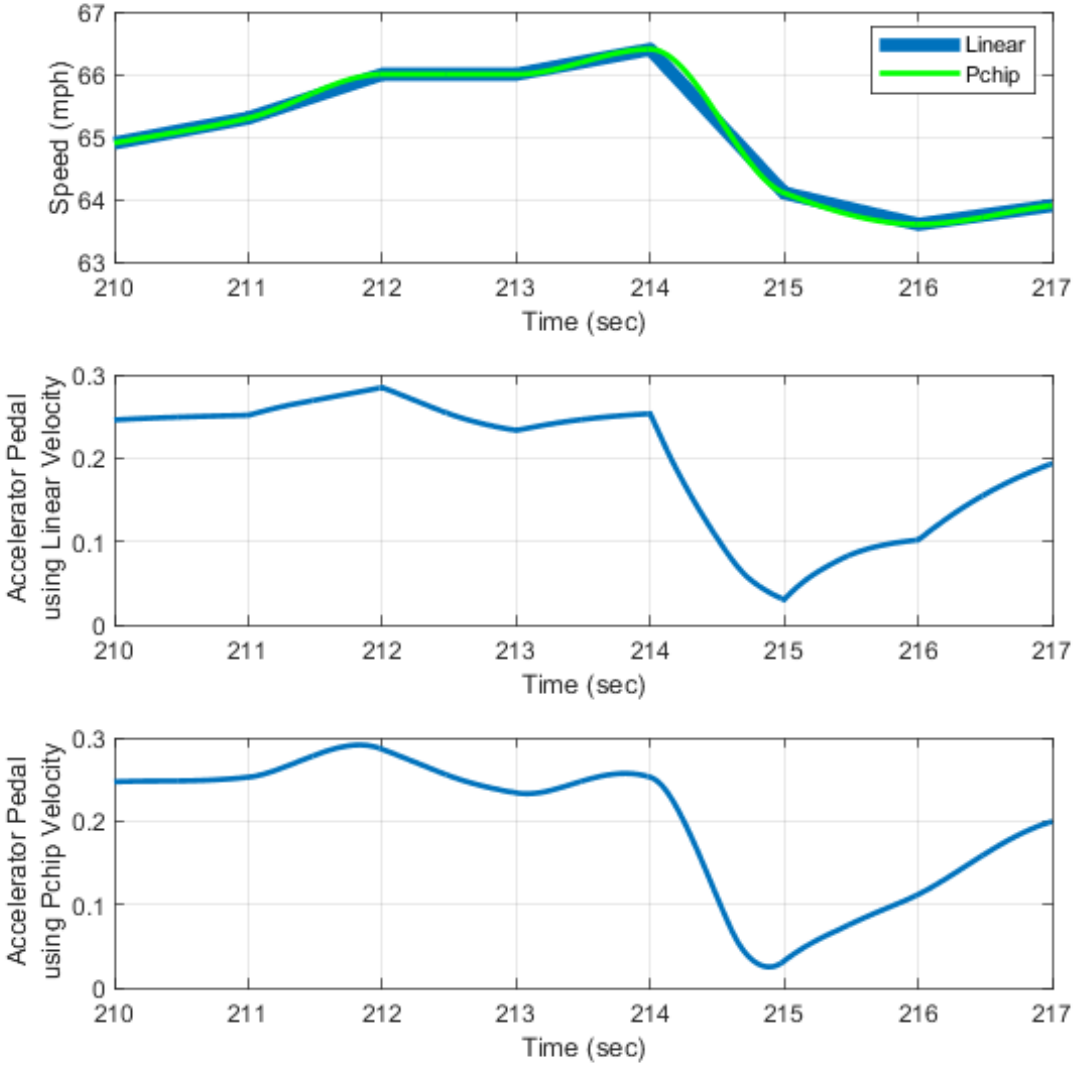

Figure B.1: Comparison of linear and pchip interpolated US06 at 100 Hz

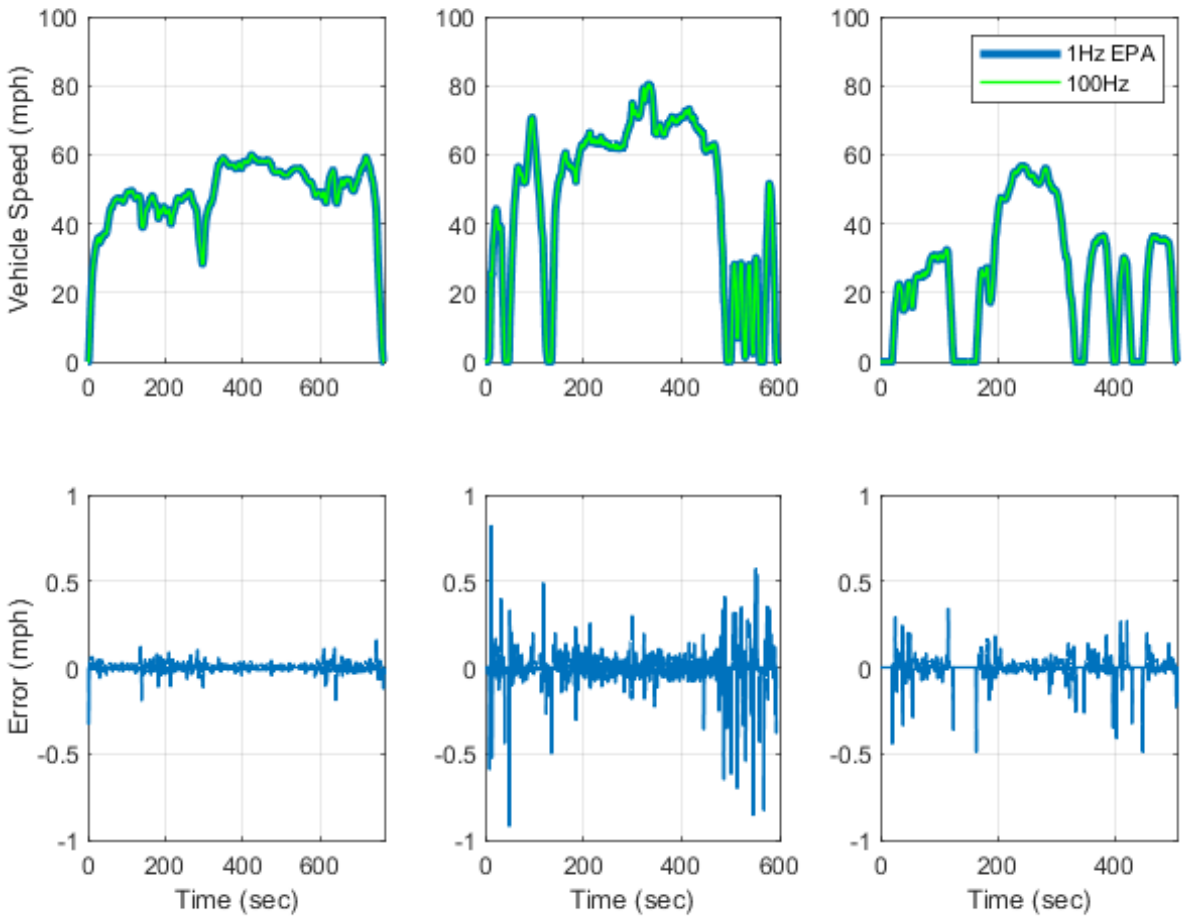

Figure B.2: Error between EPA-defined linear interpolation and pchip interpolation methods

Appendix C

Motor torque rate limit

The code implementation of the second drive quality algorithm is provided in Figure C.1.

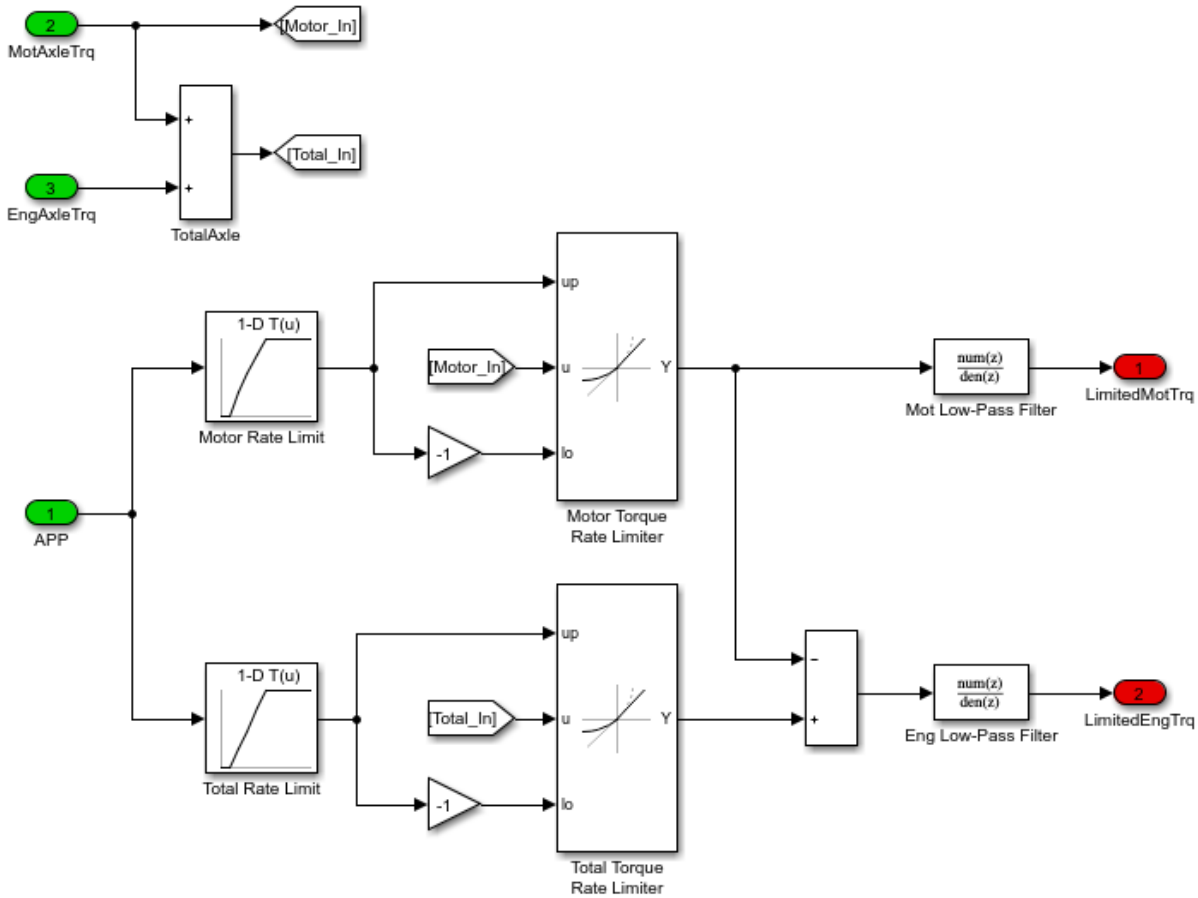

Figure C.1: Simulink code implementation of motor and total axle torque rate limit

Appendix D

Launch scenario speed plot

The speed profile of the drive quality evaluation launch scenario is provided in Figure D.1 for reference. Despite bumps in the acceleration and jerk profiles, the speed of the vehicle during the acceleration event is smooth and free of dips.

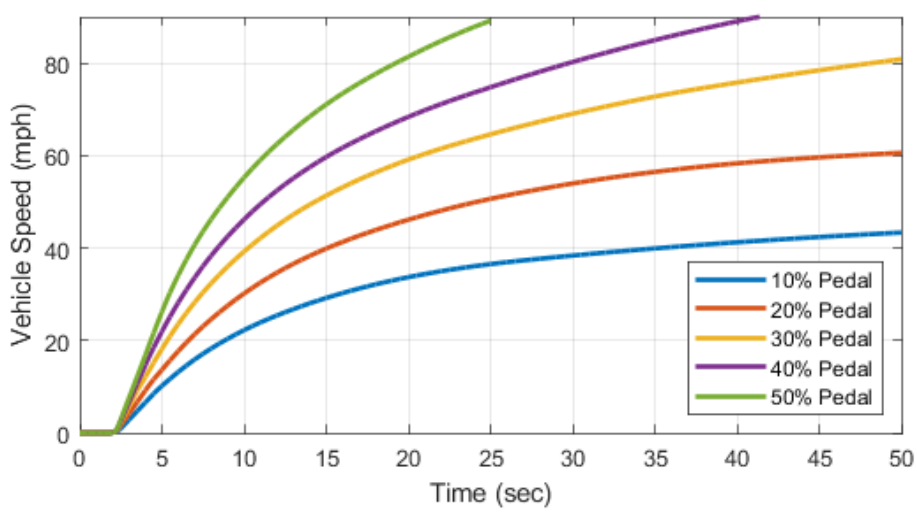

Figure D.1: Speed profile during vehicle launch scenarios

Appendix E

Additional drive quality plots

Each of the test cases for the drive quality evaluation of acceleration into pedal let-off is provided in Figures E.1 through E.4 below. Each test case has a relatively mild response, with maximum jerk around 5 m/s^3 despite the step function accelerator pedal change.

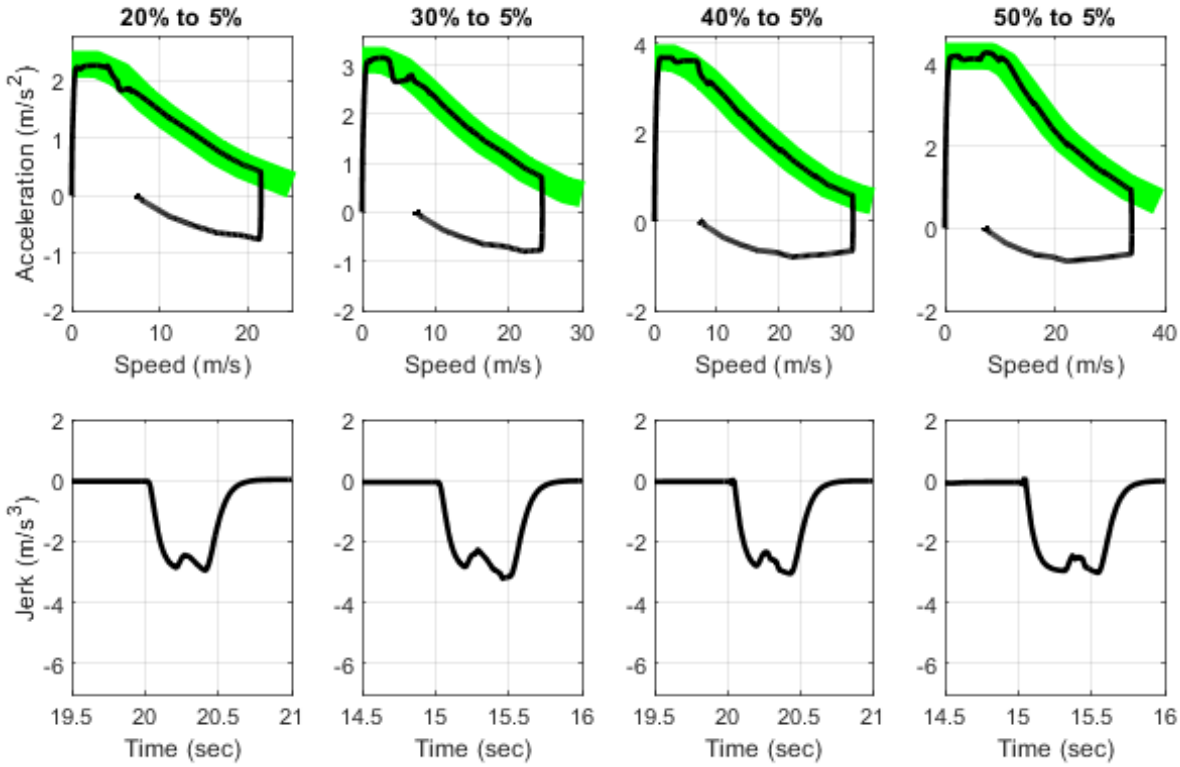

Figure E.1: Accelerator pedal let-off to 5% from a constant pedal acceleration

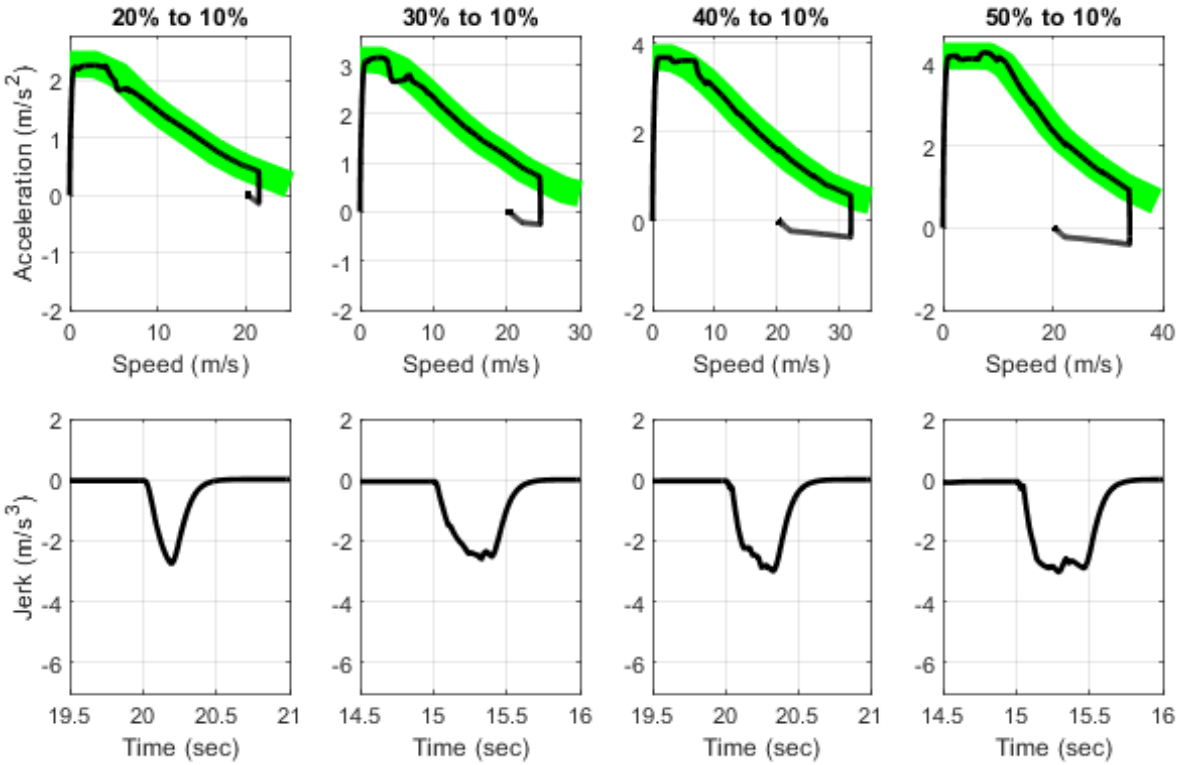

Figure E.2: Accelerator pedal let-off to 10% from a constant pedal acceleration

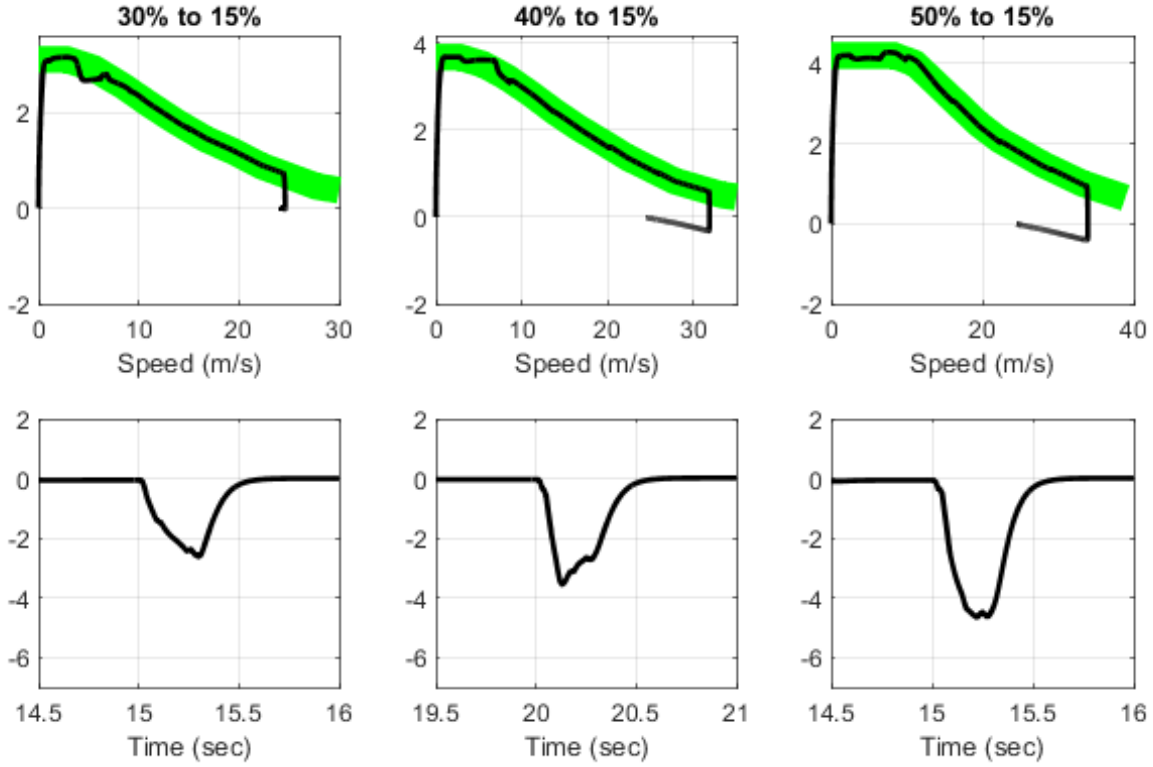

Figure E.3: Accelerator pedal let-off to 15% from a constant pedal acceleration

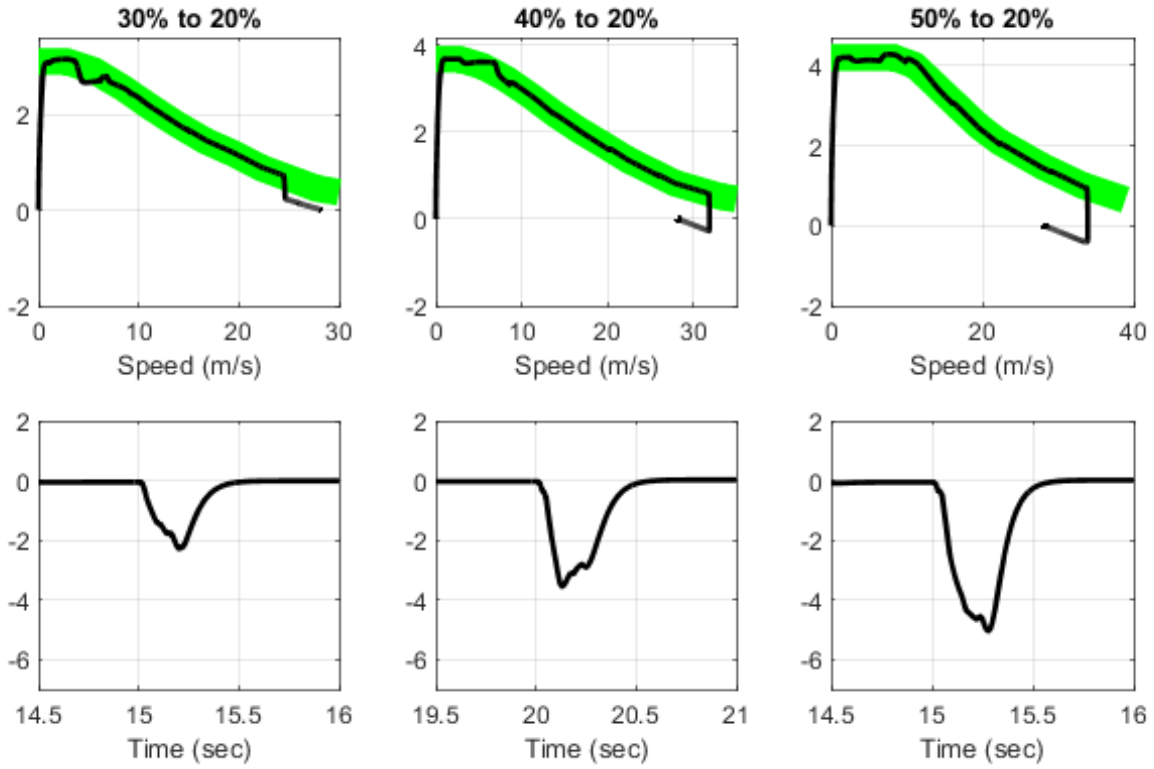

Figure E.4: Accelerator pedal let-off to 20% from a constant pedal acceleration